Investigation of Compression Mechanical Behaviour of Aluminum Foam Filled Metal Tubes

By

Halit KAVİ

A Dissertation Submitted to the
Graduate School in Partial Fulfillment of the
Requirements for the Degree of

MASTER OF SCIENCE

Department : Mechanical Engineering
Major: Mechanical Engineering

İzmir Institute of Technology
İzmir, Turkey

July, 2004

We approve the thesis of **Halit KAVİ**

Date of Signature

--- **14.07.2004**

Assoc. Prof. Dr. Mustafa GÜDEN
Supervisor
Department of Mechanical Engineering

--- **14.07.2004**

Asst. Prof. Dr. Bülent YARDIMOĞLU
Department of Mechanical Engineering

--- **14.07.2004**

Asst. Prof. Dr. Engin AKTAŞ
Department of Civil Engineering

--- **14.07.2004**

Assoc. Prof. Dr. Barış ÖZERDEM
Head of Department

ACKNOWLEDGMENTS

I would like to thank my advisor Assoc. Prof. Dr. Mustafa Güden for his guidance and encouragement. He shared his all knowledge and expertise with me during this research. I would like to thank Mehmet Üzer from Gedik Casting and Valve Inc. for his help in manufacturing steps of the study. Besides, I am also very thankful to IZTECH CMR, IZTECH Atelier staff, my friends A. Kaan Toksoy and Sinan Yüksel because of their helps during the experimental and production steps of the study. I am also grateful to the support provided by TÜBİTAK (Project MİSAG 227). Finally I would like to thank my family for their patience and support.

ABSTRACT

Novel crash element designs, composing of packing of foam-filled multi tubes, were investigated through compression testing at quasi-static deformation rates. Multi-tube designs involved the hexagonal and cubic packing of Al foam-filled deep drawn Al tubes inside rigid cylindrical and rectangular dies. For comparison purposes, empty Al tubes, Al and polystyrene foam-filled single tubes, Al and polystyrene foam-filled bitubular tubes and empty multi-tube designs of hexagonal and cubic packing were also tested under the similar test conditions. The Al-closed cell foams used for the filling of tubes were prepared in house using a patented foaming process. For each tube geometry investigated the average crushing load and specific energy absorption was calculated and the results were compared.

It was shown that although foam filling resulted in higher energy absorption than the sum of the energy absorptions of the tube alone and foam alone, it was not more effective in increasing the specific energy than simply thickening the tube walls. The lower specific energy absorptions of the Al-foam filled single tubes based on the equal mass criterion were due to the relatively lower plateau stresses of the filler material used. The experimental results have further shown that both multi-tube and bitubular geometries exhibited higher specific energy absorption capabilities than those of foam-filled single tubes. The increased strengthening coefficients of the multi-tube geometries with foam filling were solely due to the frictional loads between the adjacent tube walls, tube walls and die wall and constraint effect of die itself. The frictional loads were also found to increase the specific energy absorption of empty multi-tube geometries. The effect of Al foam density was found to increase the specific energy absorption in multi-tube geometries.

ÖZ

Çoklu köpük dolu tüplerin paketlenmesiyle oluşturulan yeni çarpışma elemanı tasarımları düşük deformasyon hızlarında basma testleri uygulanarak araştırılmıştır. Çoklu tüp tasarımları, altıgen ve kübik paketlenmiş alüminyum köpük doldurulmuş derin çekme alüminyum tüplerin silindirik ve kare kalıpların içerisine koyulmasıyla oluşturulmuştur. Boş tekli tüpler, polistren ve alüminyum köpük dolu tekli tüpler, Al ve polistren köpük dolu ikili tüpler, boş altıgen ve kübik çoklu tüplerde karşılaştırma amacıyla aynı test şartları altında test edilmiştir. Dolgu amaçlı kullanılan kapalı hücreli alüminyum köpükler patentlenmiş bir proses kullanılarak hazırlanmıştır. Çalışılan her bir geometri için ortalama ezilme yükleri ve spesifik enerji emme miktarı hesaplanarak sonuçlar karşılaştırılmıştır.

Köpük doldurulması, tek tüp ve köpüğün enerji emme miktarlarının toplamından daha yüksek enerji emilmesine neden olmasına karşın, spesifik enerji emme miktarının artırılmasında tüp et kalınlığının fazlalaştırılmasına göre daha verimsiz olduğu gösterilmiştir. Eşit ağırlığa sahip Al köpük dolu tekli tüplerin düşük spesifik enerji emilimleri oldukça düşük plato gerilimine sahip olan dolgu malzemesinden kaynaklanmaktadır. Ayrıca deneysel sonuçlar ikili ve çoklu tüp geometrilerinin tekli dolu tüplere göre daha fazla spesifik enerji emilimi sağladığını göstermiştir. Çoklu tüp geometrilerindeki kuvvet artışı bitişik tüpler arasındaki, tüp yüzeyleri ve kalıp arasındaki sürtünme kuvvetlerinden ve kalıbın sıkıştırma etkisinden kaynaklanmaktadır. Sürtünme kuvvetleri boş çoklu tüplerdeki spesifik enerji emiliminin artmasına da sebep olmaktadır. Kullanılan köpük yoğunluğunun artırılması çoklu tüp geometrilerinde spesifik enerji emilimi artışı sağlamaktadır.

TABLE OF CONTENTS

LIST OF FIGURES

LIST OF TABLES

NOMENCLATURE

A_E	Crush force efficiency
b	Length of the square cross section
C	Strengthening coefficient of the foam filling
D	Mean diameter
D_C	Deformation capacity
E	Absorbed energy
E^*	Elastic modulus of the foam
E_s	Elastic modulus of the solid material
L	Total length of deformation element
h	Component wall thickness
m	Ratio of inside fold to total fold length
m_{foam}	Mass of deformation element
m_t	Total mass of deformation element
m_{tube}	Mass of deformation element
M_p	Fully plastic bending moment per unit length
N	Number of the circumferential folds
P_a	Average crush load of empty tubes
$P_{a,f}$	Average crush load of foam filed tubes
P_{at}	Atmospheric pressure
P_f	The foam load corresponding to the plateau stress
P_{fp}	The average crushing loads of the foam-filled tube without axial compression of the foam
P_{int}	Interaction load
P_{max}	Maximum deformation load
P_0	Initial gas pressure of the foam cells
R	Anisotropy ratio
r	The ratio of yield stress values of the tube material in compression and tension
SAE	Specific absorbed energy
S_E	Stroke efficiency
t	Thickness of tube
T_E	Total crush efficiency

ε_d	Densification strain of foam
ρ^*	Foam density
ρ_c	Tube material density
ρ_s	Solid material density
σ_c	Collapse stress of the foam
σ_{el}^*	Elastic collapse stress of foam
σ_p	Plateau stress of the foam
σ_{ys}	Yield stress of the solid material
σ_{pl}^*	Plastic collapse stress of foam
σ_U	The ultimate tensile stress of the tube material
σ_0	Mean plastic flow stress of the tube material
$\sigma_{0.2}$	Proof strength of the tube material
υ^*	Poisson ratio
ϕ	Fraction of solid
δ	Displacement
δ_{max}	Maximum total efficiency displacement

Chapter 1

INTRODUCTION AND MOTIVATION

It is a known fact that traffic accidents have been gradually increasing in each year and inevitably causing both physical and spiritual loses. The number of people killed or injured in traffic accidents is probably comparable to those in wars and earthquakes. Just in the year of 1991, for instance, there were 438,338 highway traffic accidents, caused by sleepless, tired and drunk driving, resulting in 4,596 losses, 109,899 injuries and 262 million dollar of physical damage [1].

The protection of passengers in the event of an accident is an important issue mainly in the automotive, railway and aerospace industries. Any generic technology that can provide enhanced levels of protection in these industries is of considerable interest. Most interesting recent developments have however been witnessed in the automotive industry as increasingly stringent crashworthiness legislation coupled with rising consumer awareness of safety issues and cost pressures from insurance companies (damaged cars should be cheap to repair).

The crash protection system in automobiles is solely based on the axial folding of columnar metal structures which has been known for several decades as an excellent energy-absorbing mechanism. Components based upon this principle are also utilized in high-volume industrial products such as trains and any other sector where energy, during a crash situation, needs to be absorbed in a controlled way. Energy absorbers in automobiles, referred as crash boxes, are generally inserted between the bumper cross members and the body. Its predefined shape helps to prevent the costly damages to the supporting parts. The screwed-on crash boxes can also be replaced easily with a relatively low expense.

Steel has been the far most popular structural material applied in automotive energy absorption systems, due to its relatively low price combined with excellent ductility. Hollow box sections constructed by the shaping of sheet metal combined with quick and low-cost assembly, such as spot welding techniques, are well known and applied technology for today's automotive manufacturers. However, aluminum is gaining increased attention due to its low weight, being three times less than that of steel. Owing to this, it is possible to design structural parts of aluminum showing the same stiffness and energy absorbing properties equal to steel, but with significant weight savings.

The crushing behavior of columnar structures including rectangular and circular metal tubes was studied extensively over the 30 years. In the last decade, the scientific interest shifted through filling the columnar structures with light-weight foams because foam-filling results in an increase in the specific energy absorption over the sum of the specific energy absorption of the foam alone and tube alone. This is known as interaction effect and can potentially be used in many diverse engineering applications including main frames of structural parts.

Studies of foam-filled tubes generally were on the single foam-filled tubes and the crushing behavior of multi-tube filled geometries has not been investigated yet. In single filled tubes, the energy absorption simply resulted from the tube folding, foam crushing and interaction between tube wall and filler as will be elaborated in Chapter 3. In order to increase energy absorption of filled tubes additional mechanism should be incorporated or created including friction and constraint imposed by the adjacent deforming tubular structure. These two mechanisms were investigated in this study in hexagonal and cubic packed filled tubes in a large tubular structure. For comparison purposes empty and filled single tube and bitubular geometries were also tested. Present study therefore also provided a broad picture of energy absorptions in various kinds of geometries. Tubes were filled using two different fillers; aluminum closed-cells foams manufacture in house using foaming from powder compact and a commercially available polystyrene foam.

The content of the thesis is as follows: Chapter II summarizes Al foam processing methods, Chapter III gives information on the crushing behavior foams, empty and foam filled tubes and the motivations for the present study, Chapter IV is on the characterization of used filler materials and Chapter V is on the preparation of the single and filled tubes. Results and discussion are given in Chapter VI followed by the conclusions, Chapter VI.

Chapter 2

MANUFACTURING METHODS OF CLOSED CELL AL-FOAMS

Al closed cell foam can be manufactured by 1) foaming of melts by gas injection, 2) foaming of melts with blowing agents, 3) foaming from powder compacts, 4) accumulative roll-bonding technique and 5) laser assisted foaming. The first three methods are currently used to produce commercial Al foam while the others are still in the development stages.

2.1 Foaming of Melts by Gas Injection

Foaming of melts by gas injection is currently used by Alcan N. Hydro (Norway) and Cymat Aluminum Corporation (Canada) [2, 3]. Ceramic particles e.g. SiC, Al_2O_3, or magnesium oxide, are added in order to enhance the viscosity of the liquid metal to be foamed. In the second step, the melt is foamed by injecting gas (air or nitrogen) using rotating air injection shaft which generates fine gas bubbles and distributes them homogeneously in the melt (Figure 2.1) [4]. Since the bubbles are stabilized by ceramic particles, they can be pulled off melt surface using a conveyor belt. Finally, the foam is cooled down below the melting point of metal matrix. Typical volume fraction range of the ceramic particles used in the process is between 10 and 20% with a mean particle size between 5μm and 20 μm as depicted in Figure 2.2 [3, 5]. Typical density, average cell size and cell wall thickness are 0.069- 0.54g/cm3, 3-25 mm, and 50-85 μm, respectively [4]. Average cell size, average cell wall thickness and density can be adjusted by varying processing parameters including gas injection rate and rotating shaft speed.

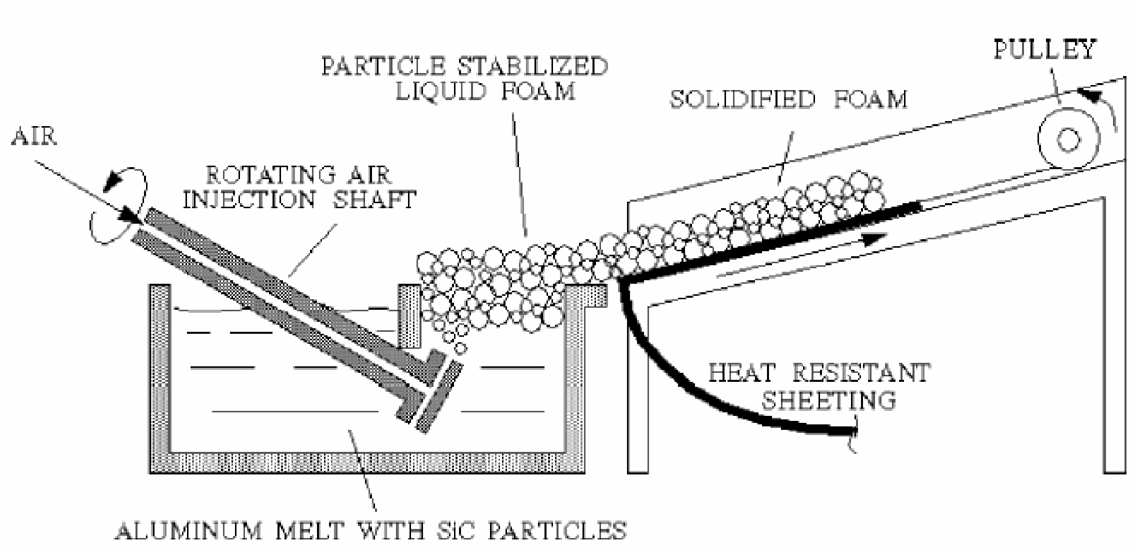

Figure 2.1 Foaming of melt by gas injection.

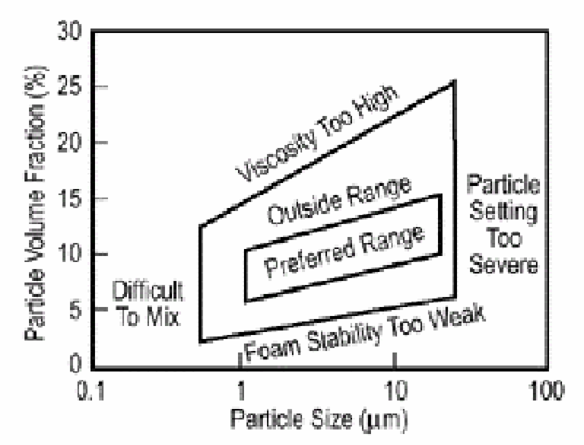

Figure 2.2 Preferable particle volume fraction and particle size range of stabilizing powders.

Drainage is usually observed in the foamed slabs, which causes density and pore size gradients. The conveyor belt also induces shearing forces, leading to the formation of elongated cells [2]. Solidified foams with dense outer surface layers can be directly used or machined into any desired shape. However, machining of these foams may be difficult due to the presence of hard ceramic particles in the metal matrix. The process has the capability for continuous production of large volumes of low density metal matrix composite foams at a relatively lower cost. The disadvantage of direct foaming is the necessity for the secondary processes such as cutting and machining.

2.2 Foaming of Melts with Blowing Agents

The second process of Al closed-cell foam production is to add a foaming agent or blowing agent (e.g. TiH_2) into liquid metal. As the foaming agent decomposes, the released hydrogen gas (H_2) drives the foaming process (Figure 2.3) [6, 7]. Before foaming, 1.5 wt.% calcium metal is added into the liquid Al at 680 ^{o}C and then the melt is stirred quickly (Figure 2.3) [6]. The viscosity of the melt increases with increasing stirring time because of the formation of oxide and/or metallic compounds (calcium oxide, calcium-aluminum oxide, or Al_4Ca intermetallic) which thickens the metallic melt [8]. The effects of calcium volume fraction and stirring time on the viscosity of an Al melt are shown in Figure 2.4 [7]. In a later stage of the process, after adjusting the viscosity of the liquid metal, TiH_2 with an amount of 1.6 wt.% is added into the melt, which releases hydrogen gas in the hot viscous liquid according to the following reaction:

$$TiH_2\,(s) \rightarrow Ti\,(s) + H_2\,(g)$$

Above reaction results in the expansion of the liquid metal and fills the foaming vessel with liquid foam at a constant pressure. Finally, the liquid foam is cooled down below the melting point of the foamed alloy quickly and the solidified Al foam is further processed for specific applications.

Al foams produced by the process, *Alporas™*, is the most homogeneous foams produced currently [7]. Typical densities of the cast foams are between 0.18 g/cm^3 and 0.24 g.cm^{-3} with an average pore size ranging from 2 mm to 10 mm [6, 7]. The viscosity of the molten Al can also be adjusted by injecting oxygen, air and other gas mixtures through the melt which causes the formation of Al_2O_3 particles and by adding viscosity enhancing additives directly such as Al_2O_3 and SiC particles. Complicated temperature cycles, difficulty in the adjustment of variables and the need for secondary processing (machining) are the disadvantages of the process.

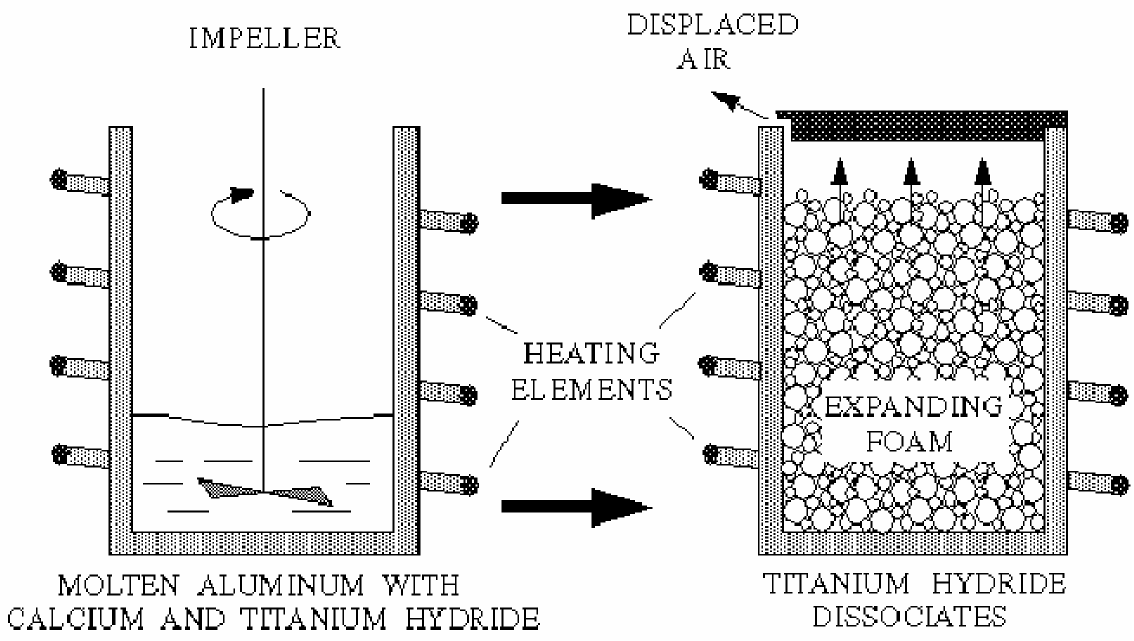

Figure 2.3 Direct foaming of melts by adding gas-releasing agent.

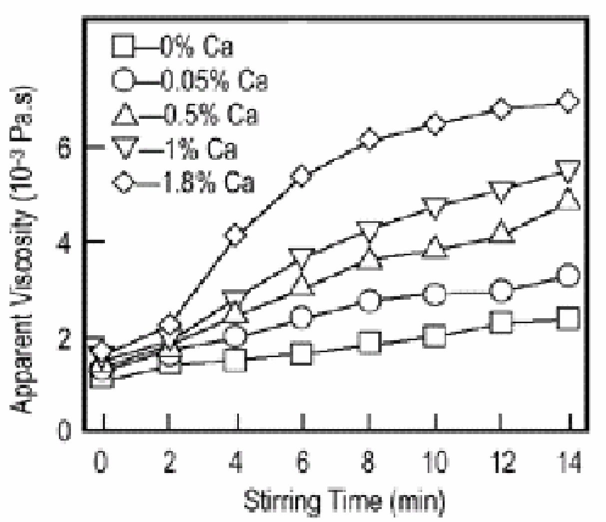

Figure 2.4 Effect of calcium (Ca) fraction and stirring time on the viscosity of Al melt.

2.3 Foaming from Powder Compacts

The process starts with mixing metal powders with a blowing agent which upon heating releases a foaming gas (Figure 2.5) [9]. Metal powder-blowing agent mixture is then compressed to a dense, semi-finished foamable product via metal forming processes such as hot compaction, extrusion and rolling (Figure 2.5). In a final step, the semi-finished product is heated to a temperature near to the melting point of the metal. During heating, the blowing agent decomposes and subsequently releases gas, leading to the expansion of the molten or mushy metal and the formation of a highly porous structure.

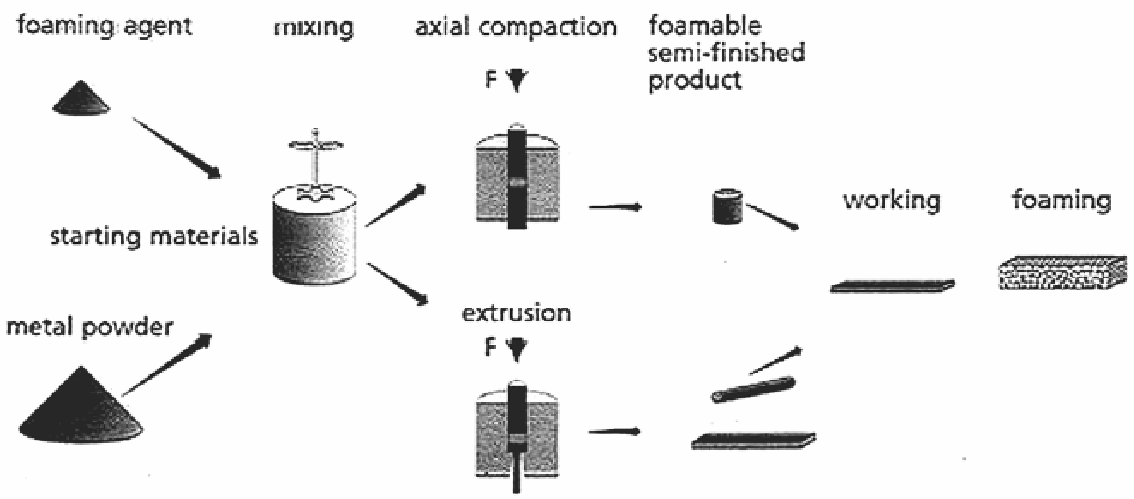

Figure 2.5 Foaming from powder compacts process.

Besides metal hydrides (e.g., TiH_2), carbonates (e.g., calcium carbonate, potassium carbonate, sodium carbonate and sodium bicarbonate), hydrates (e.g., aluminum sulphate hydrate and aluminum hydroxide) or substances that evaporate quickly (e.g., mercury compounds or pulverized organic substances) can also be used as blowing agent.

For an efficient foaming, it is very critical to form a gas-tight semi finished product in which the blowing agent is entrapped fully in the metallic matrix. Therefore the temperature and the pressure of hot compaction must be high enough to bond the individual metal powder particles and form a gas-tight seal around the blowing agent particles so that early decomposition of the blowing agent and the escape of H_2 gas before the melting of semi-finished product are avoided. In compaction by rolling, a temperature range between 350 ^{o}C and 400 ^{o}C is sufficient for the diffusion between the particles [9].

The amount of blowing agent for foaming of Al and its alloys has been found to be small. Calculations have shown that 0.6 wt. % TiH_2 in a foamable Al compact would give an expansion factor of 17, a value almost 4 times higher than the experimentally found expansion factor (4-5) [10]. This indicates that, only small portion of the released hydrogen (25%) is effective in forming pores and the rest is lost during foaming.

The time needed for full expansion of the semi-finished product depends on the temperature and size of the precursor and ranges from a few seconds to several minutes. The process is not only restricted to Al and its alloys, but also tin, zinc, brass, lead, gold, and some other metals and alloys can also be foamed using appropriate blowing agents and process parameters [11].

If a piece of foamable product is foamed in a furnace, the result will be a lump of metal foam with an undefined shape unless the expansion is limited. This is done by inserting the semi-finished foamable material into a hollow mold and expanding it by heating (Figure 2.6). This process results in near-net shaped parts with a closed and dense outer skin and a highly porous cellular core. Complicated parts can be manufactured by pouring the expanding liquid foam into a mold (Figure 2.7 (a)). Sandwich panels consisting of a foamed metal core and two metal face sheets can be manufactured by bonding the face sheets to a piece of foam with adhesives. Another way is to roll clad Al or steel sheets into a sheet of foamable material and allow the foamable core to expand while the face sheets remain dense (Figure 2.7 (b)) [12]. By this method, Al foam structures can be combined with steel or titanium face sheets as well as with Al face sheets. In the latter case, Al sheets with melting points that are higher than the core material must be used to avoid melting of the face sheets during foaming.

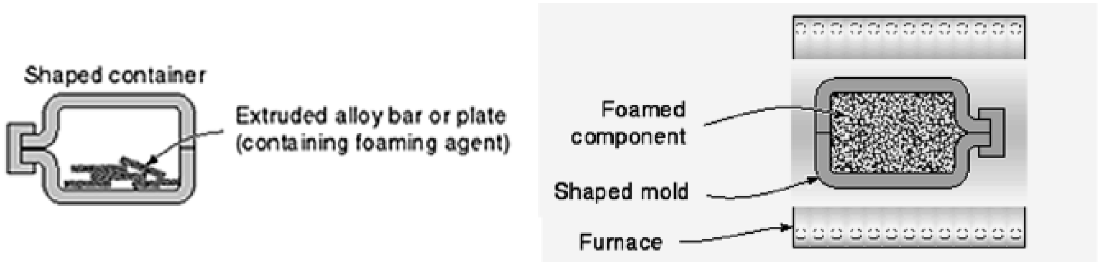

(a) (b)

Figure 2.6 Foaming inside a mould (a) inserting precursor material (b) foaming in the mould.

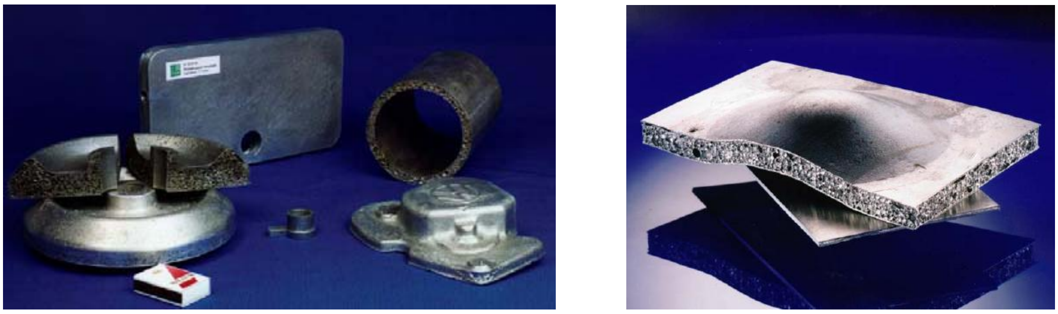

(a) (b)

Figure 2.7 (a) complicated foam parts (b) sandwich foam panel.

It is also possible, with this process by applying suitable heating, to produce bodies that have continuously or discontinuously changing densities over the cross section. If the foaming process is interrupted after a certain time at a constant temperature, a certain density will be obtained and if the foaming process is continued further, a higher density value will result. For example, structures having higher foam densities on the locations exposed to higher external loads could be manufactured by this method. If the hot compaction process is performed inside a mold, the powder mixture will be surrounded completely or partially by a blowing agent free metal powder. Upon foaming, this forms a dense or less porous cover layer and a highly porous foam core. This offers advantages for the joining similar or different structures and for the production of foam core structures that require a dense cover such as car doors and frames.

Foaming from powder compacts process has been recently modified by incorporating TiH_2 particles directly into an Al melt instead of using powders to prepare a foamable precursor material. To avoid premature H_2 evolution, the melt should be quickly cooled down below its melting point after mixing or the blowing agent has to be passivated to prevent it from releasing gas before solidification. The former technique, called *Foamcast* is carried out in a die-casting machine and the TiH_2 is injected into the die simultaneously with the melt [13]. The resulting cast part is virtually dense and could be foamed by remelting in analogy to foaming from powder compacts; however, achieving a homogeneous distribution of TiH_2 powders in the die is difficult. The latter route requires that TiH_2 powders be subjected to a heat treatment cycle that forms an oxide layer on each particle, which delays the decomposition of TiH_2. TiH_2 is then added to the melt and the melt can be cooled at comparatively slow rates after stirring. Melts containing SiC particles are used to obtain stable foams. The name *Formgrip* has been given to this process which is an acronym of foaming of reinforced metals by gas release in precursors. [14]

2.4. Accumulative roll-bonding technique (ARB)

This process is recently proposed by Kitazono [15] and based on the dispersion of foaming agent into bulk metal sheets through sequential rolling. The stages of process are schematically illustrated in Figure 2.8 (a). Two metal strips are stacked together with blowing agent powder (TiH_2) in between them. The stacked strips are then roll-bonded by the reduction of thickness. The bonded strips are then cut and after surface treatment, they are stacked again and roll-bonded. After several roll-bonding cycles, rolled foamable precursor composite in which the blowing agent particles dispersed in a metal matrix is obtained (Figure 2.8 (b)). The composite is used as the starting material for the following high temperature foaming process.

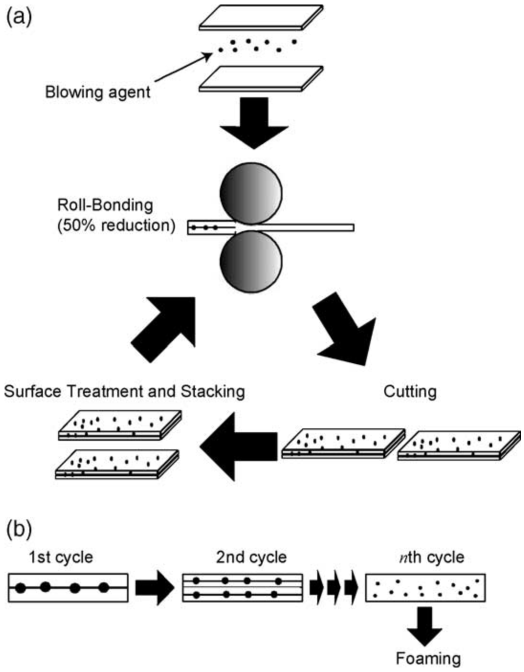

Figure 2.8 (a) schematic of the manufacturing process of a perform sheet through ARB process (b) prediction of gradual distribution of added blowing agent particles [15].

The microstructure of the manufactured preform using ARB method is the same as the precursor produced by P/M process. Closed-cell aluminum foams with about 40% porosity were successfully produced through the ARB process. This process has the potential to produce a large scale sandwich structure comprising a foam core and skin plates using conventional cladding techniques.

2.5. Laser assisted aluminum foaming

This process is recently proposed by Kathuria [16]. The basic principle of laser assisted foaming is shown schematically in Figure 2.9. The precursor material with blowing agent, prepared by P/M process, is foamed by heating it up to its melting point by a high power laser beam irradiation. The uni-directional expansion of the foamable precursor material can be observed during the entire foaming process in the irradiation direction. The expansion in the other directions is relatively negligibly small.

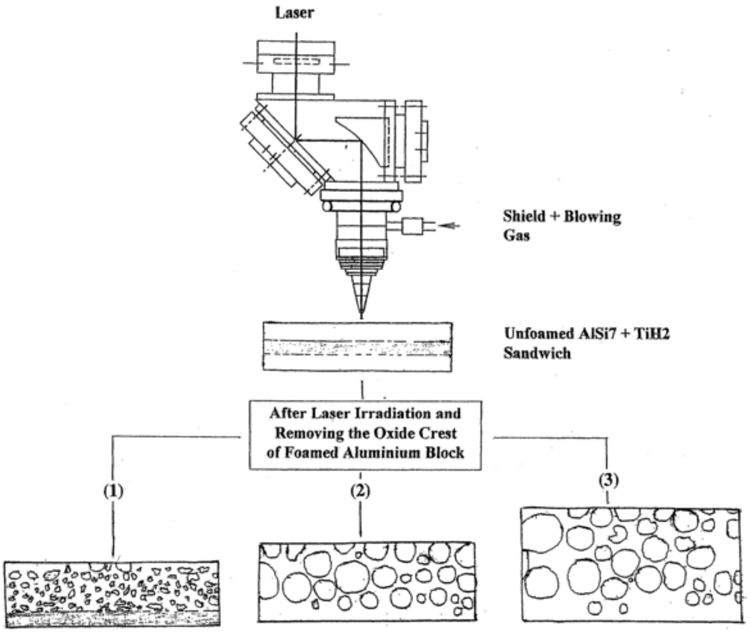

Figure 2.9 The block diagram of laser assisted AlSi7 foaming for three processing speeds, in decreasing order (1) > (2) > (3) [16].

Besides H_2 evolution and foaming, the shield gas Ar is an additional help for the formation of the porosity and may also become trapped inside the solidified foam. In the conventional thermal melting process, the average temperature gradient of the interface varies as the bulk temperature is lower. This is accompanied by a slow cooling rate and hence a long time for the stabilization of the pores to occur. However, in the case of laser process the average temperature gradient of the interface is much higher, thus, a faster cooling rate results in the pore stabilization. Figure 2.9 also illustrates, as to how the processing speed could affect the cell morphology and the expansion ratio of the buildup foam.

The foamable Al-alloy sandwich samples fabricated according to the P/M procedure are used in this technique. Porous structures with relative densities of 0.33-0.39 and porosity of (61-67%) can be fabricated by using this method.

Chapter 3

CRUSHING BEHAVIOR OF Al-FOAMS, EMPTY TUBES AND FOAM FILLED TUBES

3.1 Foams: Structure and Compression Deformation Behavior

Foams are the light-weight materials made of groups of cells. Nature uses these materials in many applications. The cellular structure of the wood is mechanical; that is to support the tree and cancellous bone is to give human a light and stiff frame. Among many other purposes, the nature’s choice of foams is also for the optimization of fluid transport and thermal insulation.

Synthetic man made foams are usually inspired from nature and they may be considered in two groups in terms of cell structure; open and closed-cell foams (Figure 3.1) and in three groups in terms of mechanical behavior: elastomeric, elastic-plastic and elastic-brittle foams (Figures 3.2(a), (b) and (c)).

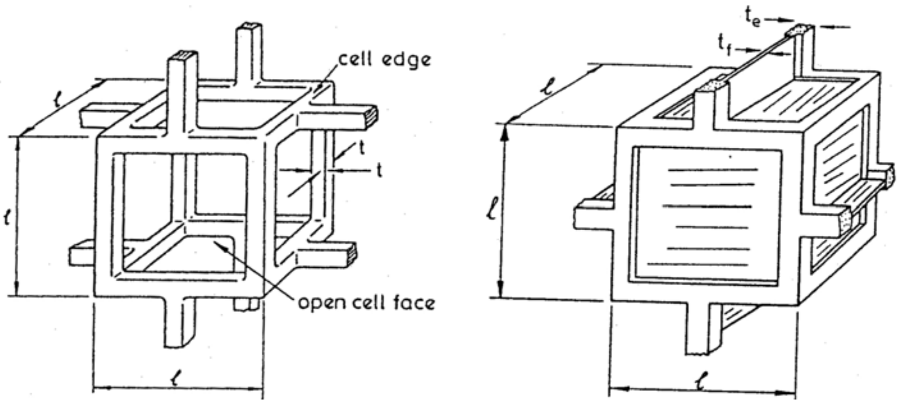

(a) (b)

Figure 3.1 Cubic models of a) open-cell and b) closed-cell foams [17].

Under compressive loads, foams show characteristic stress-strain behavior. Compressive stress-strain curve consists of three consecutive regions: linear elastic, plateau or collapse and densification (Figure 3.2) [17, 18].

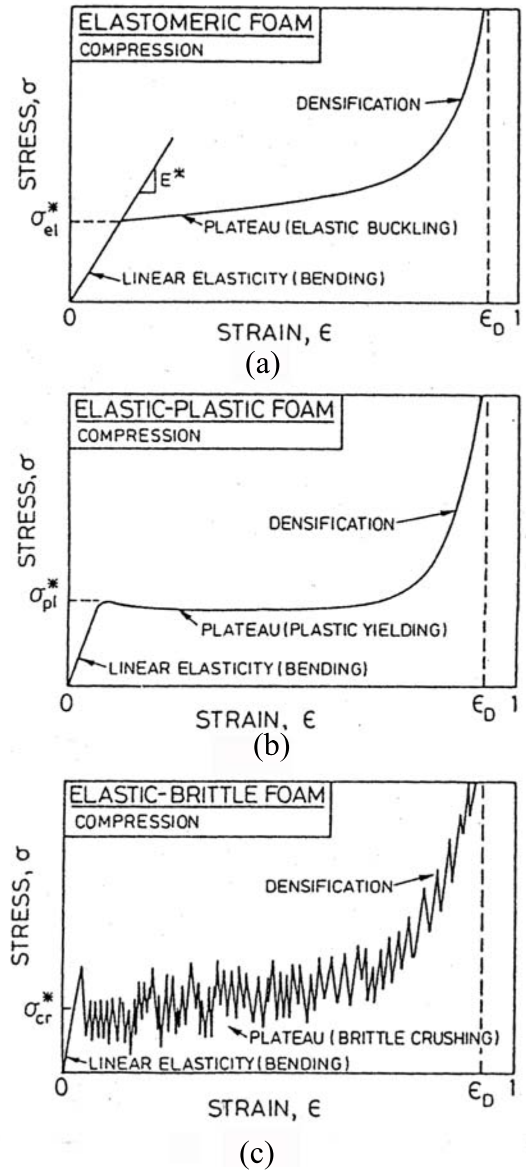

Figure 3.2 Compressive stress-strain curves of a) elastomeric, b) elastic-plastic and c) elastic-brittle foam [17].

3.1.1 Linear Elasticity

Open cell foam of low relative densities (the ratio between foam density and solid foam material density (ρ^*/ρ_s)), deforms primarily by cell wall bending [19]. With increasing relative density ($\rho^*/\rho_s > 0.1$), cell edge compression plays a significant role. Fluid flow through open-cell foam contributes to the elastic module if the fluid has a high viscosity or the strain rate is exceptionally high. Besides cell edge deformation, the thin membranes of the closed cell foams, which form the cell faces, stretch normal to the compression axis and therefore contribute to the modulus. If the membranes do not rapture, the compression of the cell fluid trapped within the cells also increases the modulus. Each of these mechanisms contributing to the linear-elastic response of the foams is shown schematically in Figures 3.3(a) and (b) for open and closed-cell foams, respectively.

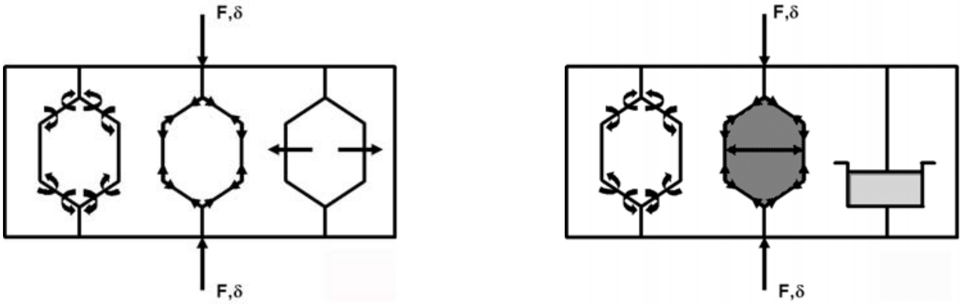

(a) (b)

Figure 3.3 The mechanisms of foam deformation: a) open-cell foam, sequentially cell wall bending, cell wall axial deformation and fluid flow between cells and b) closed-cell foams, sequentially cell wall bending and contraction, membrane stretching and enclosed gas pressure [17].

The simplest model of foam structure is the cubic model, which encompasses cubic array of members of length l and square cross-section of side t (Figures 3.1(a) and (b)). The structure and shape of the cells are actually more complex than those of the cubic model. The deformation and failure mechanisms of the cubic model are however quite similar to those of real foams and therefore it is very useful in predicting mechanical properties.

The elastic modulus of the open cell foams (E^*), which is calculated from the linear-elastic deflection of a beam of length l loaded at its mid point by a load F, is given as [17];

$$\frac{E^*}{E_s} = C_1\left(\frac{\rho^*}{\rho_s}\right) \tag{3.1}$$

where s refers to the solid material from which the foam is made and C_1 is a constant. The experimental elastic modulus of open-cell foams showed that C_1 is nearly equal to unity. The experimental results have further showed that the Poisson ratio (υ^*) was around 0.3 [17].

In closed-cell foams, a fraction of the solid, represented by ϕ, is contained in the cell edges having a thickness of t_e and the remaining fraction, $(1-\phi)$, is in the cell faces of a thickness of t_f. By including enclosed gas pressure, the Elastic modulus of closed-cell foams of the cubic model is expressed as [17],

$$\frac{E^*}{E_s} = C_1\varphi^2\left(\frac{\rho^*}{\rho_s}\right) + C_1'(1-\varphi)\frac{\rho^*}{\rho_s} + \frac{P_0(1-2\nu^*)}{E_s\left(1-\rho^*/\rho_s\right)} \tag{3.2}$$

where P_o is the initial pressure of the cell fluid and C_1 and C_1' are the constants. The first, second and third terms of Equation 3.2 are the contribution of cell wall bending, membrane stretching and enclosed gas pressure, respectively.

3.1.2 Elastic and Plastic Collapse

Linear elasticity is generally limited to small strains, 5% or less. Elastomeric foams can be compressed much larger strains. Deformation is still recoverable, but non-linear. In compression the stress-strain curve shows an extensive plateau at the elastic collapse stress (σ^*_{el}), see Figure 3.2(a). The elastic collapse stress of cubic cell model is given as [17];

$$\frac{\sigma^*_{el}}{E_s} = 0.05\left(\frac{\rho^*}{\rho_s}\right) \tag{3.3}$$

for open cell and,

$$\frac{\sigma^*_{el}}{E_s} = 0.05\left(\frac{\rho^*}{\rho_s}\right) + \frac{(P_0 - P_{at})}{E_s} \tag{3.4}$$

for closed-cell foams, respectively. P_{at} is atmospheric pressure (100 KPa).

Foams made from material that have a plastic yield point such as rigid polymers and ductile metals collapse plastically when loaded beyond the linear-elastic region. Plastic collapse gives a long horizontal plateau in the stress-strain curve similar to the elastic buckling, but the strain is no longer recoverable. Both elastic buckling and plastic failure are localized; a deformation band is usually formed transverse to the loading axis and propagates through undeformed sections of the foam with increasing strain until all the foam section is filled with the band [17].

The plastic collapse stress is predicted as [17],

$$\frac{\sigma^*_{pl}}{\sigma_{ys}} = 0.3\left(\frac{\rho^*}{\rho_s}\right)^{3/2} \tag{3.5}$$

for open-cell foams and ,

$$\frac{\sigma^*_{pl}}{\sigma_{ys}} = 0.3\left(\varphi\frac{\rho^*}{\rho_s}\right)^{3/2} + (1-\varphi)\frac{\rho^*}{\rho_s} + \frac{P_0 - P_{at}}{\sigma_{ys}} \tag{3.6}$$

for closed-cell foams. σ_{ys} is the yield stress of solid material.

3.1.3 Densification

Following the plateau region, at a critical strain, the cell walls start to touch each other and, as a result the foam densifies. The stress in this region increases rapidly and approaches to the strength of the solid foam material. The densification strain (ε_D) is related to relative density with following equation [17];

$$\varepsilon_D = 1 - 1.4\left(\frac{\rho^*}{\rho_s}\right) \tag{3.7}$$

3.1.4 Anisotropy

The anisotropy in cell shape measured by the ratio of the largest cell dimension to the smallest is called the shape-anisotropy ratio (R). The value of R varies from 1 for isotropic foam to 10 for very anisotropic foams [17]. The relation between the plateau stress and R is calculated using cubic cell model as,

$$\frac{(\sigma_{pl})_3}{(\sigma_{pl})_1} = \frac{2R}{1 + \frac{1}{R}} \tag{3.8}$$

where 3 and 1 refer to the strongest and weakest directions, respectively. The strongest direction in polymeric foams is usually the rise direction in the foam expansion process and the transverse directions are relatively weaker. Cells are relatively longer in the rise direction, giving rise to higher modulus and plateau stress in this direction. Figures 3.4 (a) and (b) show the effect of foam directions on the load-displacement curves of elastomeric and rigid plastic foams, respectively.

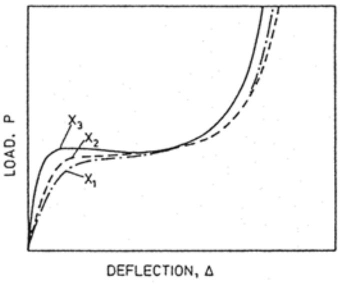

(a)

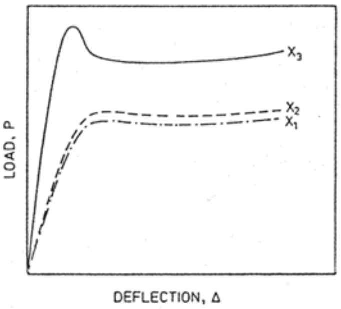

(b)

Figure 3.4 Load-deflection curves measured parallel to the three principal axes a) an elastomeric foam and b) a rigid plastic foam [17].

3.2 Tubes

The crushing behavior of thin (mean diameter (D)/ thickness (t) > 20 [20]) and thick-walled tubes has been experimentally studied since 1960. In parallel with experimental investigations, numeric and finite element analysis methods have been implemented and experimental results were compared with those of numerical studies. The filling of tubes with light-weight polymeric and metallic foam has shown to be one of the effective way of increasing energy absorption of the columnar structures on the specific energy basis [21-26].

3.2.1. Terminologies Used In Crush Analysis

In any crushing event of columnar structure (Figure 3.5), the total absorbed energy (E) is the area under the load-displacement curve and is,

$$E(\delta) = \int_0^{\delta} P \, d\delta \tag{3.9}$$

where δ and P are the displacement and the load, respectively. The corresponding average crushing load (P_a) is calculated dividing the absorbed energy by the displacement,

$$P_a(\delta) = \frac{E(\delta)}{\delta} \tag{3.10}$$

The specific absorbed energy (SAE) shows the capability of a structure to absorb the deformation energy. SAE can be formulated in several bases including per unit mass and volume. SAE per unit mass is expressed as,

$$SAE = \frac{\int_0^{\delta} P \, d\delta}{m_t} \tag{3.11}$$

where m_t is the total mass of the deformation element.

The ratio between the average load P_a and maximum load P_{max}, both calculated in the interval of $\{0,\delta\}$, is defined as the crush force efficiency (A_E):

$$A_E = \frac{P_a(\delta)}{P_{max}(\delta)} = \frac{E(\delta)}{P_{max}(\delta)\,\delta} \tag{3.12}$$

Total efficiency (T_E) is the total absorbed energy divided by the products of $P_{max}(\delta)$ and total length of deformation element (l):

$$T_E = \frac{E(\delta)}{P_{max}(\delta)\,l} \tag{3.13}$$

The stroke efficiency is defined as the ratio between the point at which the total efficiency has its maximum value (δ_{max}) and total length of the crushing element,

$$S_E = \frac{\delta_{max}}{l} \tag{3.14}$$

The efficiency terms are directly related to the deformation capacity (D_C), which is the displacement divided by the initial length of the element:

$$D_C = \frac{\delta}{l} \tag{3.15}$$

$$E(\delta) = \int_0^{\delta} P \, d\delta$$

$$P_a(\delta) = \frac{E(\delta)}{\delta}$$

$$SAE = \frac{\int_0^{\delta} P \, d\delta}{m_t}$$

$$A_E = \frac{P_a(\delta)}{P_{max}(\delta)} = \frac{E(\delta)}{P_{max}(\delta)\,\delta}$$

$$T_E = \frac{E(\delta)}{P_{max}(\delta)\,l}$$

$$S_E = \frac{\delta_{max}}{l}$$

$$D_C = \frac{\delta}{l}$$

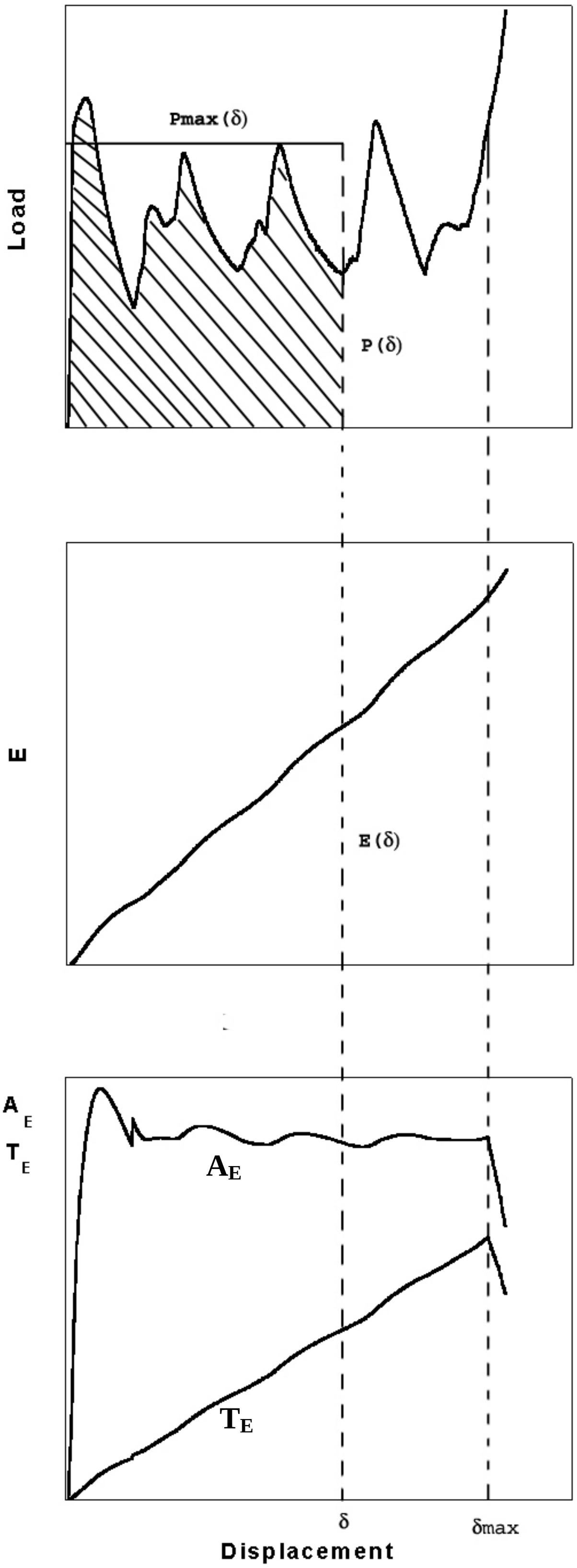

Figure 3.5 Terminologies used in the crush analysis of tubes.

3.2.2 Crushing Behavior of Empty Tubes

The crushing behavior of collapsible structures has been recently reviewed in [20] and briefly explained in this section. To our knowledge, the first analytical study on the crushing behavior of circular tubes was due to Alexander [27]. He modeled the concertina mode of deformation basing on the plastic work required for bending and stretching of extensible thin cylinder. Alexander's model of concertina mode of deformation (Figure 3.6) gives the average crushing load as;

$$P_a \cong 6\sigma_0 t(Dt)^{1/2} \tag{3.16}$$

σ_0 is the mean plastic flow stress;

$$\sigma_0 = \left(\frac{\sigma_{0.2} + \sigma_U}{2} \right) \tag{3.17}$$

where $\sigma_{0.2}$ is proof stress and σ_U is the ultimate tensile stress of tube material.

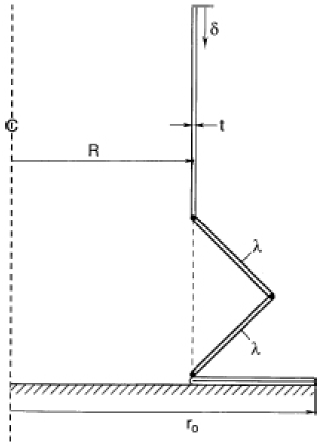

Figure 3.6 Alexander's concertina mode of deformation model.

Early studies were on the classification of the deformation modes as function of tube material properties, geometry and geometrical parameters of the tubes and the first systematic investigation on the classification of crushing types was due to Andrews *et al.* in 1983 [28]. They performed crushing tests on tubes having large ranges of t/D and L/D ratios and classified the crushing modes of cylindrical tubes in 7 groups. These are;

1. *Concertina*: axisymmetric and sequential or progressive folding starting at the end of the tube (Figures 3.7(a) and (b)).
2. *Diamond:* asymmetric but sequential folding accompanying a change in the cross-section shape of the tube (Figure 3.8(a) and (b)).
3. *Euler*: bending of tube as a strut.
4. *Concertina and 2 lobe and/or 3-lobe diamond (Mixed)*: Folding first in the concertina mode changing to diamond configuration (Figure 3.9(a) and (b))
5. *Axisymmetric/concertina*: simultaneous collapse along the length of the tube, axisymmetric single or multiple barreling of the tube (Figure 3.10(a) and (b) and Figure 3.11(a) and (b)).
6. *2-lobe diamond:* Simultaneous collapse along the tube in the form of the 2-lobe diamond configuration.
7. *Tilting of tube axis*: Shearing of tube on the platen surface in the form of the 2-lobe diamond configuration.

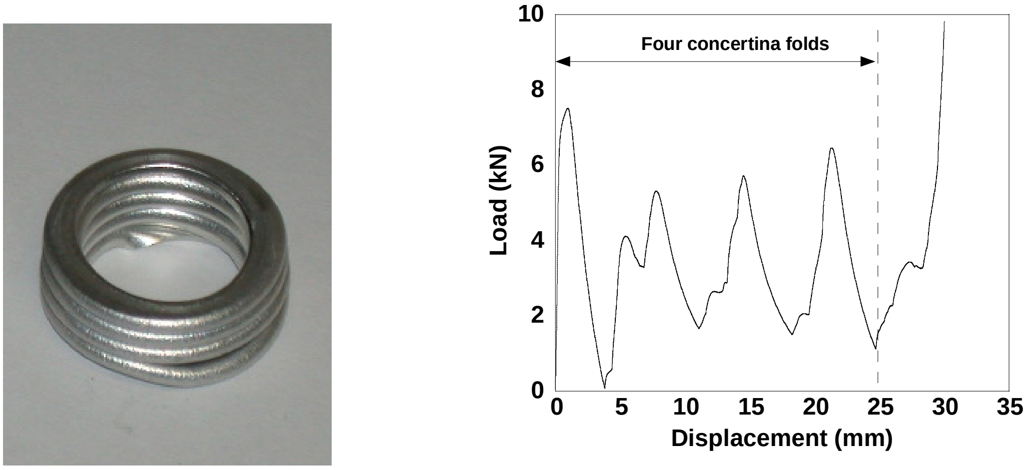

(a) (b)

Figure 3.7 (a) Concertina mode of deformation in 6063 Al tube (D=19.16 mm and t= 0.84 mm) and (b) corresponding load-displacement curve with 4-fold.

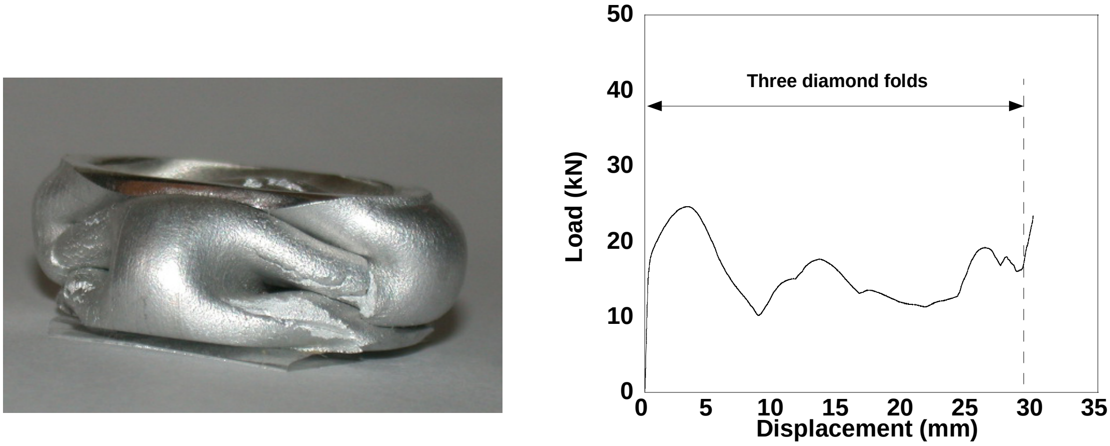

(a) (b)

Figure 3.8 (a) Diamond deformation mode in 6063 Al tube (D=17.5 mm and t=1.31 mm) and b) corresponding load-displacement curve with 3-fold.

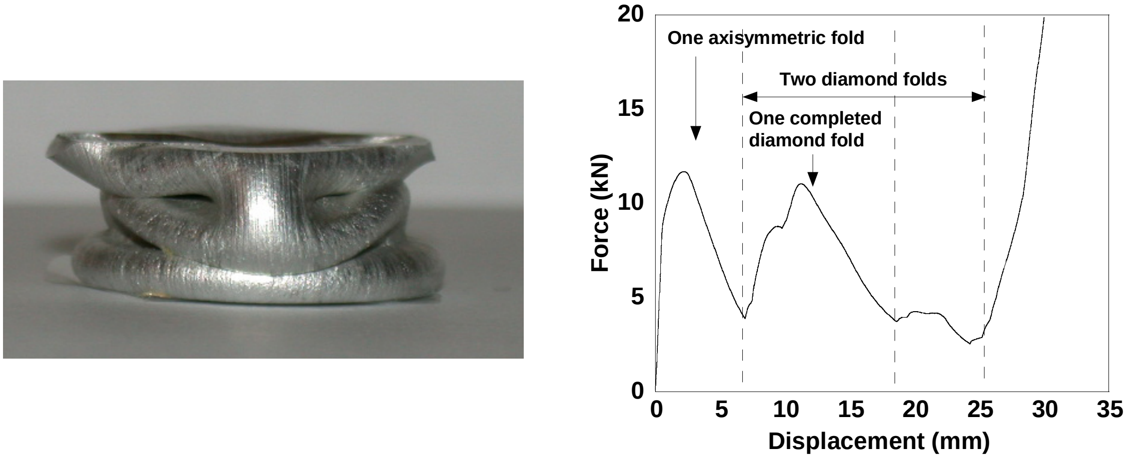

(a) (b)

Figure 3.9 (a) Mixed mode of deformation in 6063 Al tube (D=20.63 mm and t=1.48 mm) and (b) corresponding load-displacement curve with 3-fold.

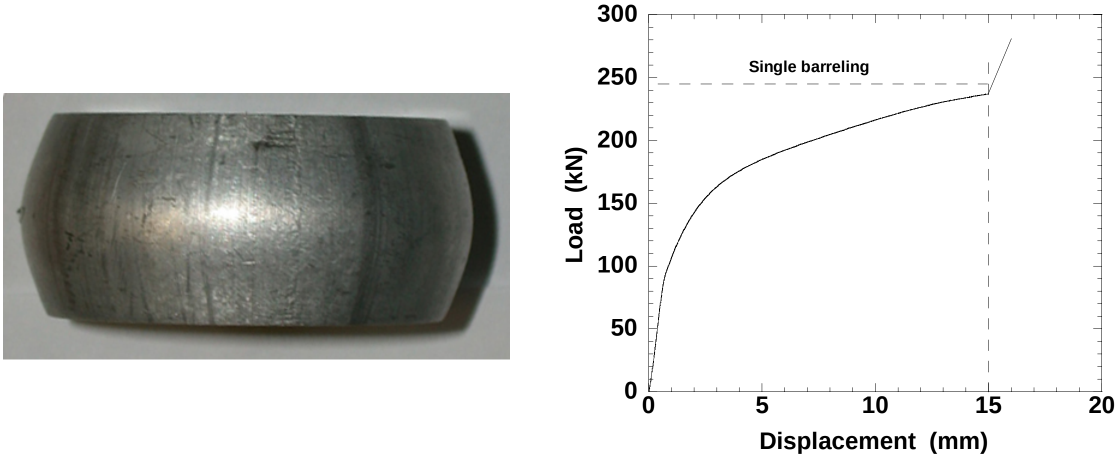

(a) (b)

Figure 3.10 (a) Single barreling in 6063 Al tube (D=42.5 mm and t=7.5 mm) and (b) corresponding load-displacement curve.

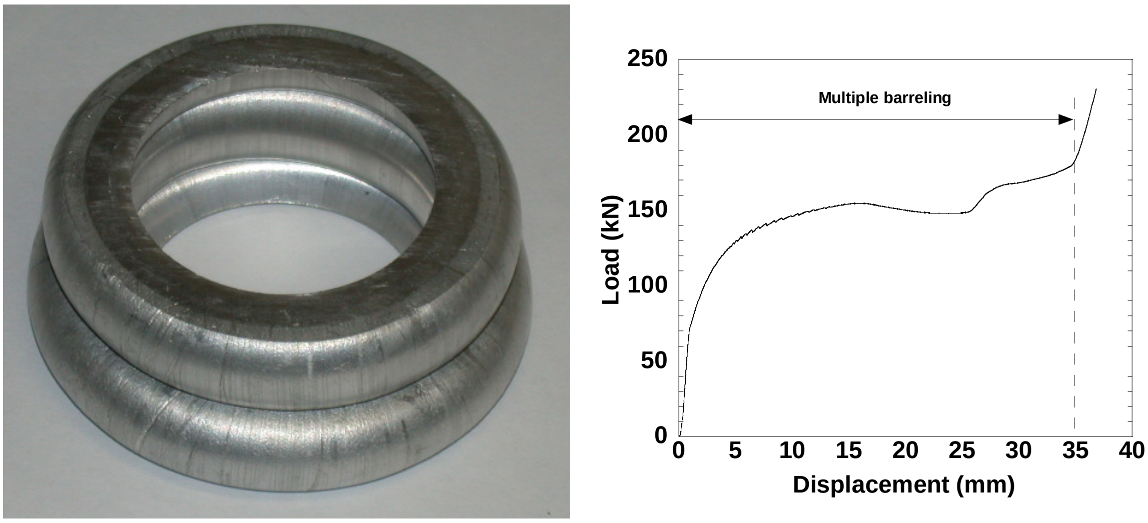

(a) (b)

Figure 3.11 (a) Multiple barreling in 6063 Al tube (D=44.88mm and t=5.12mm) and (b) corresponding load-displacement curve.

Andrews *et al.* also formed a chart that indicated the dominant deformation modes of HT30 Al alloy tube as functions of L/D and t/D (Figure 3.12). For the thin-walled tubes with t/D ratio smaller than 0.013, the deformation mode was found to be diamond and the number of folds increased with decreasing t/D ratio. It was also shown in this study that although the average crushing load and absorbed energy were higher in the concertina mode, the absorbed energy in the development of one complete fold was higher in diamond mode [28].

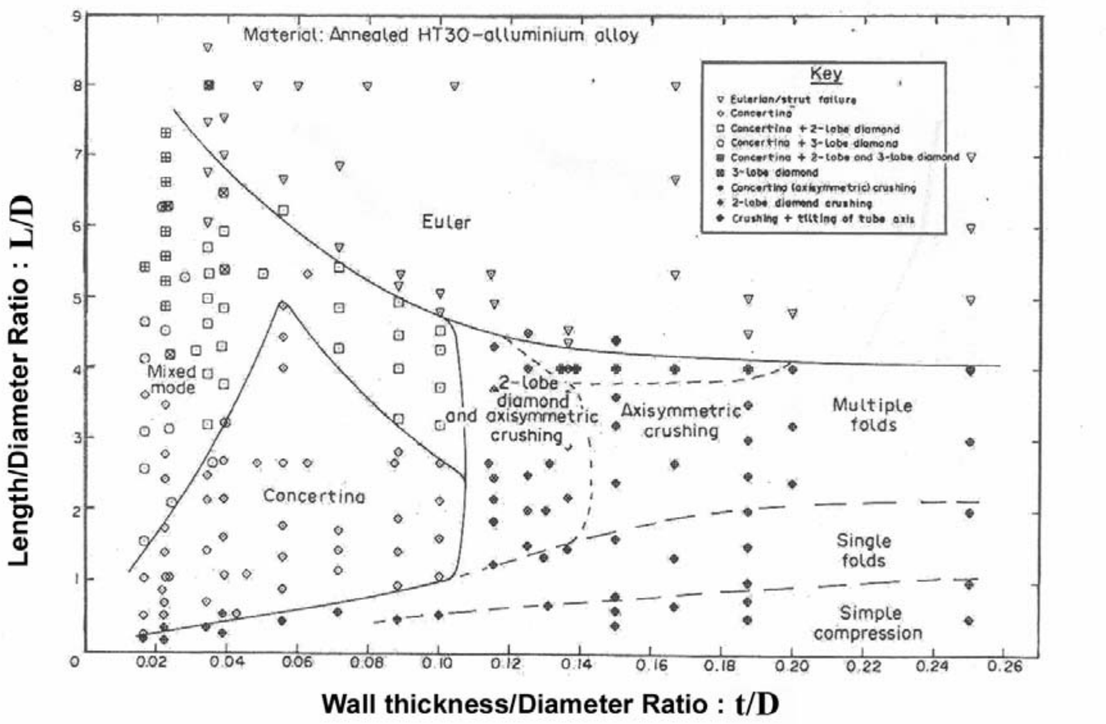

Figure 3.12 Classification of crushing mode of HT30 Al tubes as functions of D/t and L/t [28].

Abramowicz and Jones modified Alexander's model and proposed the average crushing load equations in 1984 and 1985 for the concertina mode of deformation

[29, 30, 31] as,

$$P_a \cong \sigma_0 t\left(6(Dt)^{1/2} + 3.44t\right) \tag{3.18}$$

and

$$P_a \cong \sigma_0 t \frac{6\sqrt{Dt} + 3.44t}{0.86 - 0.57\sqrt{t/D}} \tag{3.19}$$

Wierzbicki *et al.* proposed an expression for the concertina mode of deformation as [32];

$$P_a = 7.933\,\sigma_0 t^2 \left(\frac{D}{t}\right)^{1/2} \tag{3.20}$$

Singace and Elbosky experimentally studied concertina mode of deformation [33]. They showed that concertina mode was composed of two characteristic movements: outward and inward folding (Figure 3.13). During the axial deformation, tube will be laid down partly to the inside and partly to the outside of the tube generator, the total of which is defined by the folding length in concertina deformation mode [34].

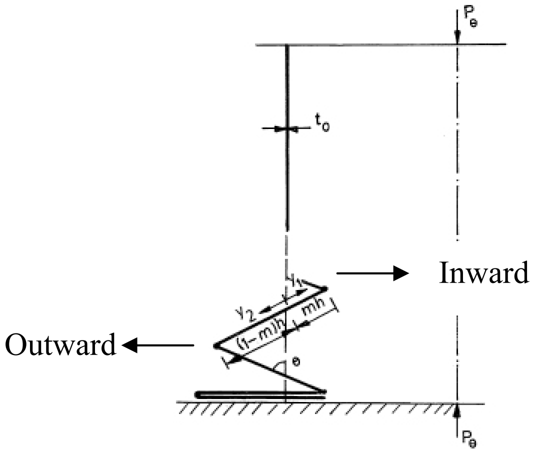

Figure 3.13 Concertina mode of circular tube deformation; inward and outward folding [33].

Outward fold length over total length of deformation fold is called eccentricity. The eccentricity factor was proposed to be 0.65, but experimentally determined values of the eccentricity factor was shown to be less than this value [34]. It was proposed that if continuous zone or curved elements were used to represent the folding elements, a better agreement between the theory and the experimental results was expected [34]. Singace's analytical approach of mean crushing force is,

$$\frac{P_a}{M_P} \cong 22.27\left(\frac{D}{t}\right)^{1/2} + 5.632 \qquad (3.21)$$

where $M_P = \sigma_0\, t^2 / 2\sqrt{3}$ is the fully plastic bending moment per unit length [34].

By minimizing the total external work which is done by the total bending and membrane energy during the deformation, Singace proposed following equation for the mean crush load of diamond mode of deformation [35],

$$\frac{P_a}{M_P} \cong -\frac{\pi}{3}N + \frac{2\pi^2}{N}\tan\left(\frac{\pi}{2N}\right)\frac{D}{t} \qquad (3.22)$$

where N is the number of the circumferential folds.

Alexander, assuming the energy was dissipated at the plastic hinges during the folding process of diamond mode of deformation, proposed following equation [27],

$$P_a \cong 2.286 n^2 \sigma_0 t^2 \qquad (3.23)$$

where n is the number of diamonds formed.

Pugsley and Macaulay investigated the diamond mode of deformation of thin cylindrical columns having large D/t ratios [36]. The deformation energy was assumed to be absorbed by plastic bending and shear of the diamond pattern and following equation was proposed for the average crushing load of diamond mode of deformation,

$$P_a \cong \sigma_0 t(10.05t + 0.38D) \qquad (3.24)$$

Wierzbicki gives an approximate expression for diamond mode of deformation as [23];

$$P_a \cong 18.15\sigma_0 t^2 (D/t)^{1/3} \qquad (3.25)$$

For diamond mode of deformation, Abramowicz and Jones developed an expression for the mean crush force as [29]

$$\frac{P_a}{M_p} = 86.14\left(\frac{D}{t}\right)^{0.33} \tag{3.26}$$

In a recent study of Bardi *et al.* [37] the concertina mode of deformation in circular tubes was experimentally and numerically analyzed. Results of numeric model using ABAQUS were found to be close to those of experiments. The experimental results were also compared with the plastic hinge models of Alexander (Equation 3.16), Singace *et al.* (Equation 3.21) and Wierzbicki *et al.* (Equation 3.20). Although Wierzbicki *et al.* plastic hinge model predicted the load values in the range 81-91% of the measured values, predictions of the wavelength of the folds were generally poor for all three models.

H. Abbas *et al.* used the curved fold model for the analysis of concertina mode of deformation [38]. The curved fold model used was different from the previous studies of plastic hinge models of Alexander [27], Singace *et al.* [33] and Wierzbicki *et al.* [32] in a way that the straight portion of the fold was also included in the analysis. Three cases inside, outside and partly inside-outside folding, were investigated. It was found that when the accepted length of straight portion decreased, analytical load deformation curve become closer to the experimental curve in all cases. Analytical results of mean crushing load values and size of folds were also found to decrease with increasing the accepted length of straight portion but the results were still far from those of the experiments. The aim of their study was to show how mean crushing and energy absorption changed with folding parameter; m (ratio of inside fold to total fold length), as well with the parameter r (the ratio of yield stress values of the tube material in compression and tension).

Grupta and Abbas investigated the effect of thickness change in concertina folding of metallic round tubes [39]. They showed that by including thickness change, the calculated m values come closer to experimental values. Calculated average crushing loads, however, for different values of r (the ratio of the yield stress values of the tube material in compression and tension) were found to be lower than those of experiments. This was explained as fallows: since the next fold started even before the complete crushing of previous fold, the crushing load observed in experiments started to rise before vertical crushing reached two times the size of the fold. The average crushing load was also found to increase with the increasing the value of r and reached to the experimental values [38]. They concluded that thickness change had no significant effect on the average crushing load.

Wierzbicki and Abramowicz [40, 41] developed average crushing load equations for square and hexagonal cross-sections as,

$$\frac{P_a}{M_0} \cong 48.64\left(b/t\right)^{0.37} \tag{3.27}$$

for square column and

$$\frac{P_a}{M_0} \cong 80.92\left(b/t\right)^{0.4} \tag{3.28}$$

for hexagonal column, where b is the length of the cross-section.

3.2.3. Crushing Behavior of Foam-Filled Tubes

The filling of tubular structures with lightweight foams for a goal of increasing specific energy absorption (SEA) has also taken considerable interest. One of the earliest investigations on the crushing behavior of thin-walled sections filled with lightweight polyurethane foam was conducted by Thornton [42], who pointed out that although noticeable increase in SEA was possible with foam filling, it was not weight effective when compared with the thickening of empty tube wall. Lampinen and Jeryan [43] investigated the crushing of sheet metal tubes filled with low density polyurethane foams and concluded that foam filling stabilizes the deformation of thin-walled tubes. The crushing behavior of polyurethane foam-filled thin-walled metal tubes was also investigated by Reid *et al.* [44], at quasi-static and dynamic deformation rates. It was concluded that tube wall interacts with the foam filler deformation resulting in a more tendency for the axisymmetric mode of deformation. They also concluded that the simple addition of the uniaxial foam contribution gave the total average crushing load of filled tube. Guillow *et al.* [45] have recently pointed out that the average crushing loads of polyurethane foam-filled aluminum (Al) thin-walled tubes were greater than the sum of the average crushing loads of empty tube (alone) and foam (alone), a result which contrasted with those of Reid *et al.* [44] and Reddy and Wall [26].

Seitzberger *et al.* [46] investigated the crushing behavior of Al closed-cell foam-filled monotubal and bitubal arrangements of square, hexagonal and orthogonal cross-sections and concluded that mass related average load level can be improved by filling tubular members with aluminum foam. It was also pointed out in the same study that suitable foam *vs.* tube selection was important for the designing of efficient crush elements. Santosa and Wierzbicki [47] investigated the crushing behavior of Al honeycomb and foam-filled box columns both numerically and experimentally and showed that the effect of filler on the tube crushing load was similar when the strong axis of the honeycomb through and normal to the compression axis, proving that both axial and lateral strength of the filler were effective in increasing the crushing load of the tube. Further, Santosa *et al.* [48] noted that the bonding between filler and tube wall increased the average crushing load of filled tube over the unbounded filled tube when appropriate tube geometry and foam density were chosen.

Santosa and Wierzbicki [48], based on FEM study, proposed following empirical equation for the average crushing load of foam-filled square tubes of length b,

$$P_{a,f} = P_a + C\sigma_p b^2 \tag{3.29}$$

where $P_{a,f}$, P_a and σ_p are the average crushing loads of the filled and empty tubes and plateau stress of the filler, respectively. The constant C in Equation 3.29 is considered strengthening coefficient of the foam filling. The values of C were numerically and experimentally shown to be 1.8 and 2.8 for foam filled square tubes with and without adhesive, respectively [48]. It was also shown by the same authors that there was a critical mass of the foam filled tube (or foam density) above which the foam filling was more efficient than tube wall thickening based on specific absorbed energy per unit mass.

Hannsen *et al.* [49, 50] studied static and dynamic crushing behavior of aluminum foam filled square aluminum extrusions. They showed that foam filled tubes formed more deformation folds as compared with empty tubes in both static and dynamic tests. This was explained as the stiffness effect of aluminum foam on sidewalls of deformation element, which decreased the buckling length of the sidewalls. It was also found that the average crush load of the filled tubes was higher than that of the sum of the crushing loads of the tube alone and foam alone, which is known as interaction effect. They also modeled average crushing load of foam filled columns by including contributions of the average crushing force of empty tube, foam plateau stress and interaction effect. The model was found to be well agreed with experimental results and is given as

$$P_{a,f} = P_a + \sigma_p b^2 + C_{avg}\sqrt{\sigma_f \sigma_0}\, bh \tag{3.30}$$

where C_{avg} is a dimensionless constant which is directly related to the interaction effect.

Chapter 4

FILLER MATERIALS

4.1. Aluminum closed-cell foam

4.1.1. Aluminum closed-cell foam preparation

Aluminum closed cell foam investigated in this study was manufactured at İzmir Institute of Technology using a patented powder metallurgical technique known as foaming from powder compacts [9]. The method consists of mixing aluminum or aluminum alloy powders with an appropriate blowing agent and compacting the mixture to a dense product called foamable precursor. Heating the precursor to its melting point turns the metal compact into a semi-liquid viscous mass and simultaneously causes the blowing agent to decompose. The associated release of gas first leads to the formation of pores and then, in a later stage, causes the metal to expand into a low-density foam structure.

A foam production line composing of mixing and compaction of powder blends for foamable precursor material and foaming of precursor has been constructed in our laboratory for the aluminum foam manufacture (Figure 4.1). Production line includes a hydraulic press for compaction of powder (100 tons) (Figure 4.2), a box-furnace for foaming of powder compacts and a specially designed carrier for handling and moving the hot foaming molds (Figure 4.3).

The selection of appropriate raw powder materials with respect to purity, particle size and distribution and alloying elements is essential for a successful foam manufacturing. Commercial air-atomized aluminum powders were proved to be of sufficient quality. The specifications of materials, Al powder and TiH_2, used to prepare foams are tabulated in Table 4.1. The content of blowing agent in all precursor materials was chosen to be 1 wt%. This amount was found to be sufficient to form foaming in Al compacts.

Al powder

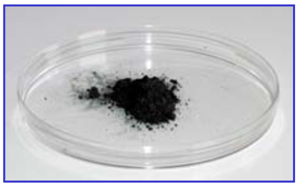

TiH$_2$

Mixing of the powders

Pressing of the blend

Thinning of the precursor

Processing of the precursors

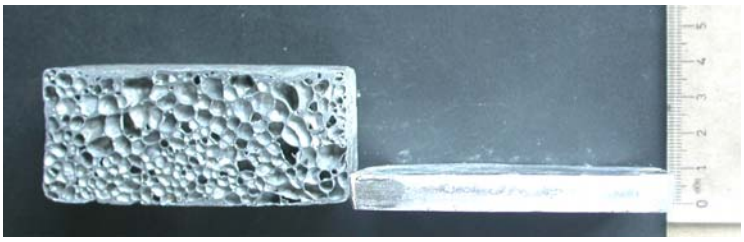

Foaming

Figure 4.1 Schematic of foam preparation process.

Figure 4.1 Hydraulic press (100 tons) used for compact preparation.

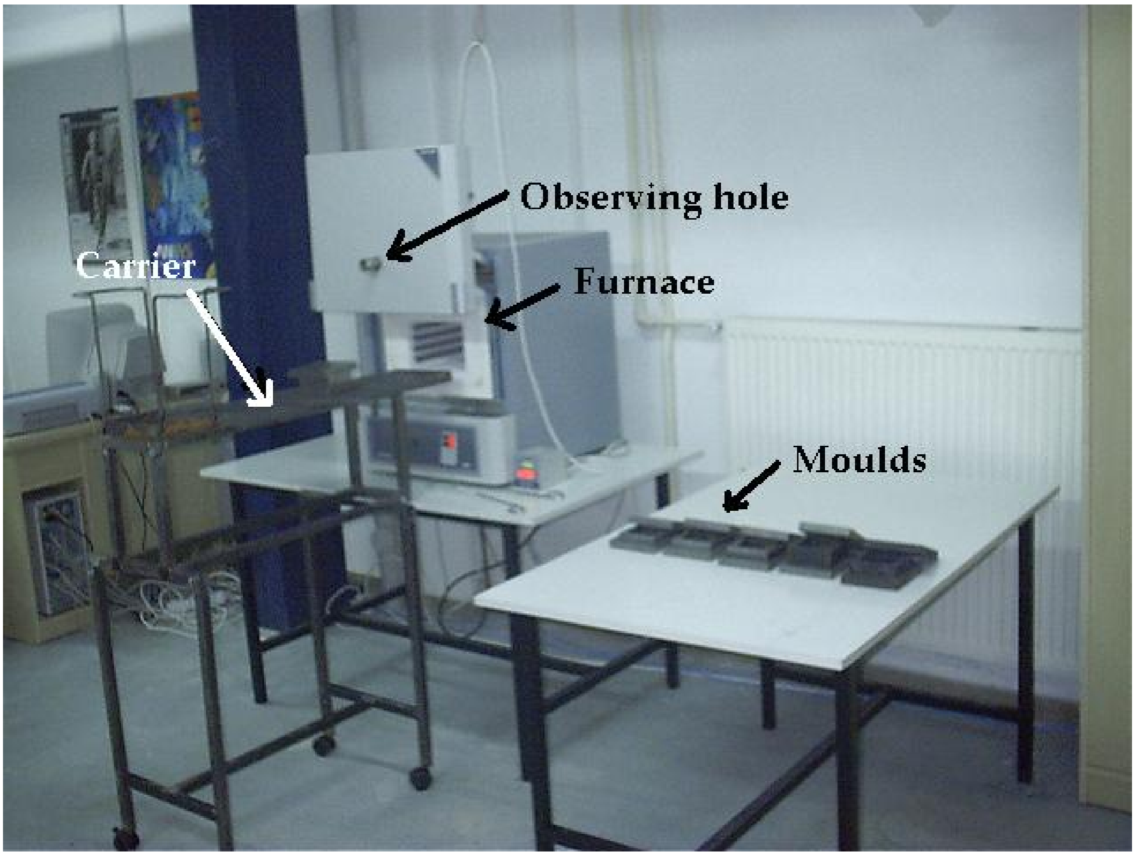

Figure 4.3 Foaming furnace, mould carrier and moulds.

Table 4.1 Specifications of powders used in foam manufacturing.

Material	**Density**	**Molar mass**	**Size**	**Purity**
Al powder (Aldrich)	2.702 g/cm^3	26.98 g/mol	$<$ 74μ	99 %
TiH_2 (Merck)	3.76 g/cm^3	49.92 g/mol	$<$ 37μ	>98 %

The mixing procedure should yield a homogeneous distribution of Al powder and the blowing agent to ensure that high-quality foams with uniform pore size distributions are obtained. Powders were mixed in batches of 129 g blends in a commercial tumbling mixer (Figure 4.1). Basic ingredients were mixed inside a plastic container which was rotated on a rotary mill to form a homogeneous powder mixture.

Preliminary investigation was conducted in order to determine the effect of compaction pressure on the final relative densities of powder compacts for an ultimate goal of producing precursor material in which the blowing agent (TiH_2) was fully embedded into metal matrix. For this purpose the mixture (Al and TiH_2) was cold compacted in the hydraulic press under various compaction pressures in a rectangular ST 37 steel die (Figure 4.4(a)), having a cross-section of 7x7 cm, see Figure 4.4(b) for the technical drawing of the die used. Initially 51 dense precursor materials were prepared at various compaction pressures at room temperature ranging between 100 and 400 MPa. The details of the precursor preparation are tabulated in Table 4.2.

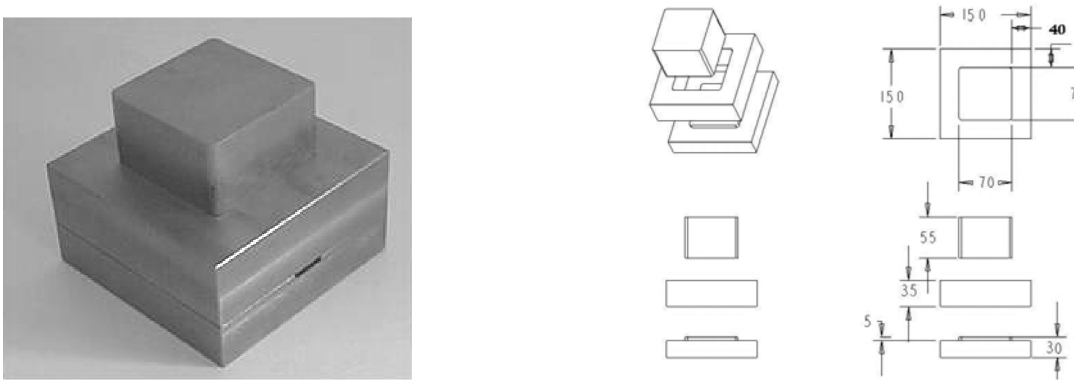

(a) (b)

Figure 4.4 (a) Compaction die (b) technical drawing (dimensions are in millimeters).

Table 4.2 Specifications of the initially prepared cold compacted precursors.

Precursor Number	**Dimensions (mm)**	**Mass (g)**	**Applied Pressure (MPa)**	**Relative Density (%)**
1	11.8 x 70.08 x 70.08	129.532	100.1	82.24
2	11.09 x 70.10 x 70.16	129.944	150.1	88.13
3	10.56 x 70.14 x 70.10	129.278	200.2	92.10
4	10.21 x 70.14 x 70.18	129	300.2	94.94
5	10.15 x 70.13 x 70.16	128.746	300.2	95.30
6	9.58 x 70.07 x 70.08	123.817	400	97.30

The maximum relative density obtained in these compacts was 97% at the highest pressure applied (400 MPa). Initial foaming experiments conducted on the precursors listed in Table 4.2 resulted in poor foaming. Because of the relatively low density of compacts used the released H_2 escaped before the melting of precursor. In order to increase the final relative densities further, the partially compressed precursor materials were hot forged at 350 ^oC. The compacts for hot forging were prepared in the hydraulic press under a pressure of 200 MPa, with a relative density of 92% (Figure 4.5(a)) and a thickness of 10 mm. The thickness of the compact was reduced to 7 mm after the hot forging (Figure 4.5(b)) and the relative density of the precursor materials was increased to ~99%.

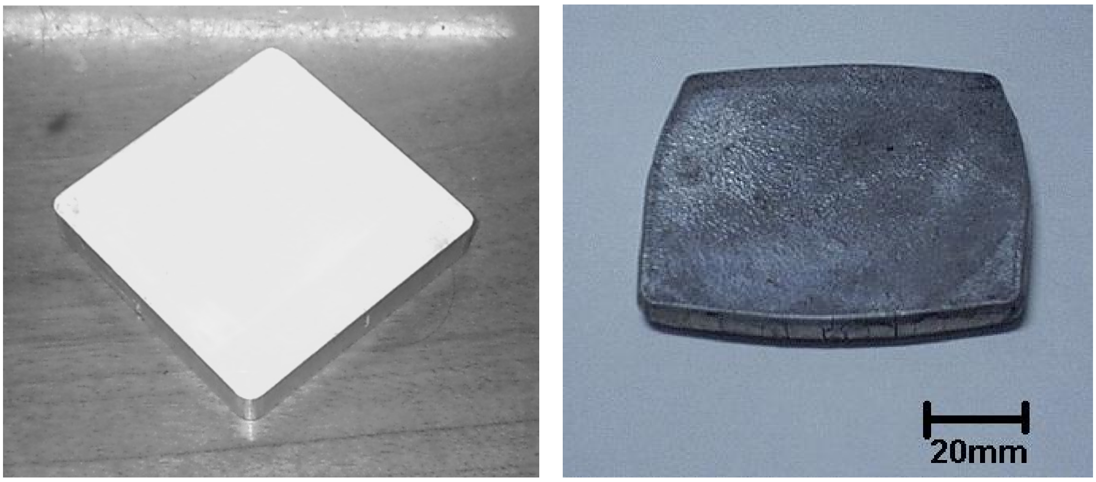

(a) (b)

Figure 4.5 (a) Cold compacted precursor (92% dense) and (b) hot forged precursor (99% dense).

As a result of open die forging as seen in Figure 4.5(b), the cross-sectional area of the precursor increased and cracks formed at the edges. In order to remove the cracks, cross-sectional area of hot-forged precursor was machined into rectangular cross-section (Figure 4.6(a)), same with the cross-sectional dimensions of the foaming molds (Figure 4.6(b)). Flat side surfaces also provided good thermal contact with the foaming mold.

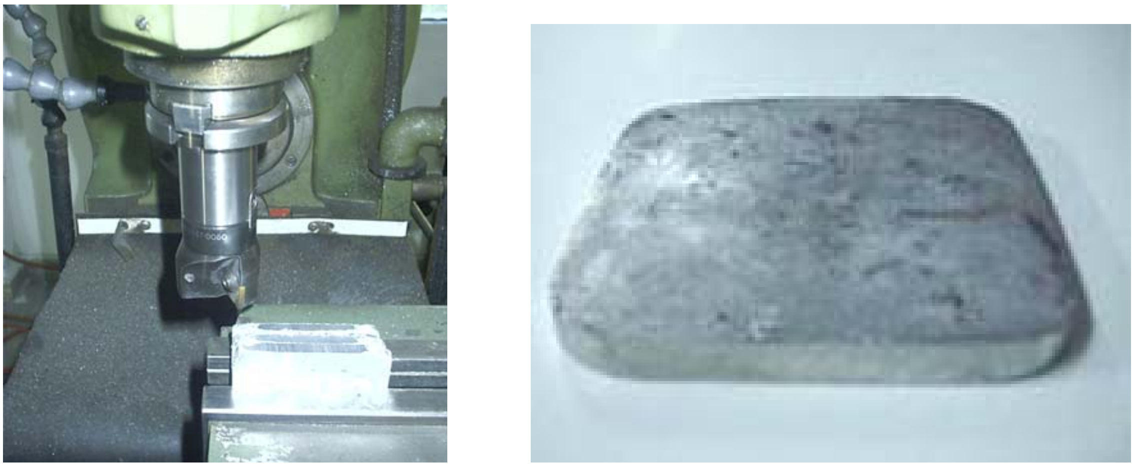

(a) (b)

Figure 4.6 (a) Machining of the forged precursor material and (b) machined precursor.

In a final step the machined hot forged precursor material was foamed by heating it above its melting point in a foaming mold, having a cross-sectional area of 8x8 cm and a height of 3.5 cm. The precursor was inserted into the heated foaming mold at 750^oC. The preheated foaming mold also provided heat for the foaming process. During foam insertion the furnace temperature dropped about 50^oC for 2 minutes then the temperature increased again to 750^oC. Since the inner dimensions of the foaming mold was the same with the precursor cross-section, after a certain furnace holding time it expanded vertically and filled the mold. Initial foaming experiments were conducted in order to find out an optimum furnace holding time that would completely fill the mold. It was found that at a furnace holding time of about 5 minutes precursors completely filled the mold (Figure 4.7). The final expansion obtained about the 4 times the initial thickness of the precursor, see Figure 4.8. After the specified furnace holding time the foaming mold containing the liquid foam was taken from the furnace. In order prevent the collapse of liquid foam the liquid foam was quickly cooled together with foaming mold. Following cooling methods were applied: 1) plunging the mould into large water filled reservoir 2) slow cooling by spraying water on foaming mold 3) cooling by air without any intervention. It was found that plunging the mould into a large water filled reservoir resulted in solidification of the liquid foam nearly with same dimensions of liquid foam. In other methods it was found that foam collapse was substantial. By simply changing the furnace holding time, foam plates having 3 different densities; 0.27, 0.35 and 0.43 g.cm^{-3}, were obtained and used in filling of thin-walled Al tubes as will be explained in following sections. Cell sizes of al foams decreases with increasing density. Cell wall thickness also increases with increasing density (Figure 4.9(a), (b), (c)).

Figure 4.7 Liquid Al foam taken from the furnace after filling the mold.

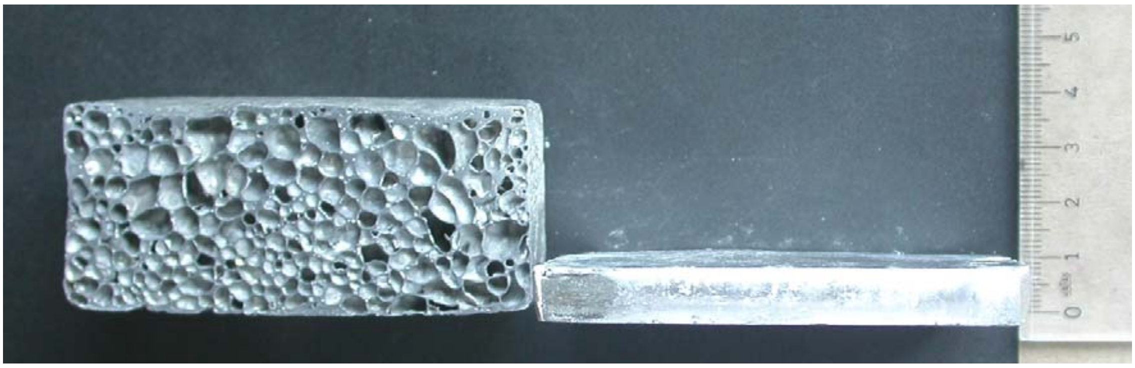

Figure 4.8 Pictures of Al foam and precursor material, showing 4 times expansion of initial thickness of the precursor.

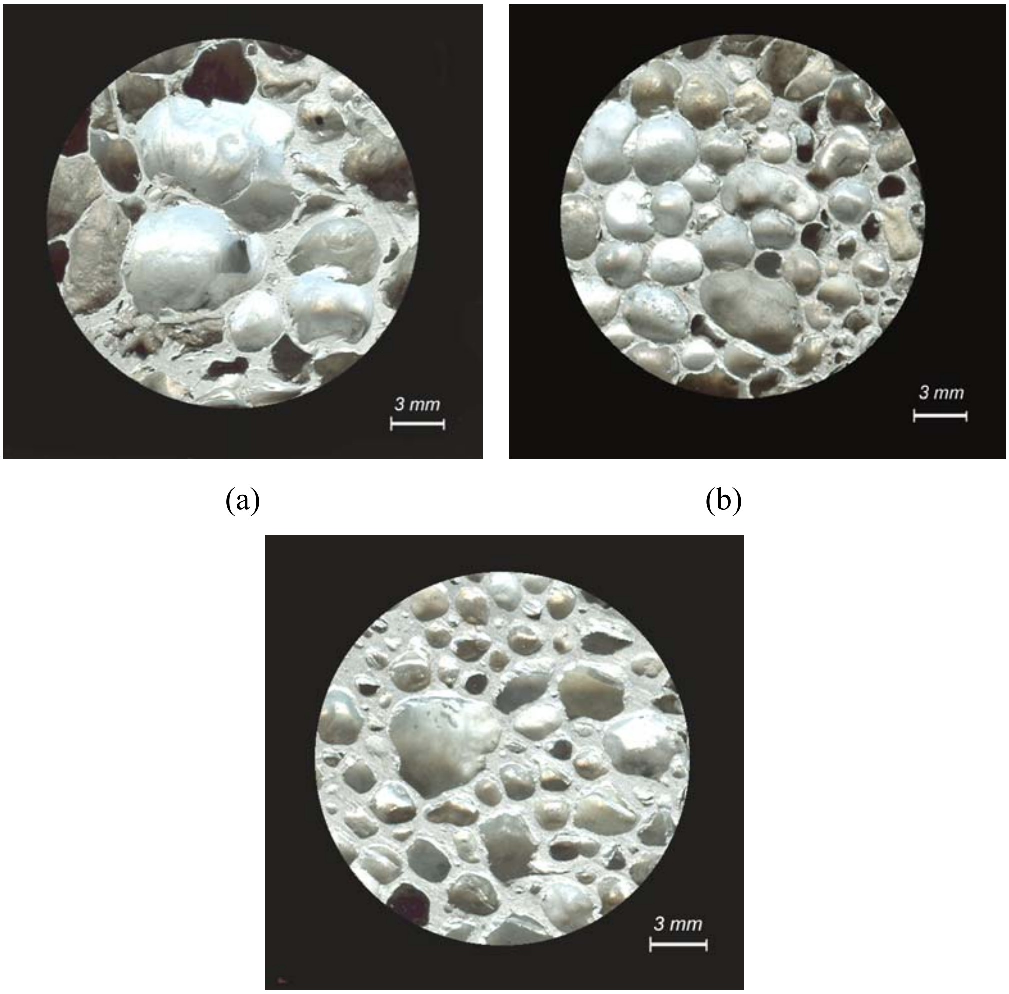

(a) (b)

(c)

Figure 4.9 Views taken from aluminum foams at different densities (a) 0.27 g.cm^{-3} (b) 0.35 g.cm^{-3} (c) 0.43 g.cm^{-3}.

4.1.2 Aluminum foam filler sample preparation

The X-ray radiography inspections of cell structure has shown that the regions near to the skins contained denser Al metal layer as compared with the interior sections (Figure 4.10 (a)). Further, a dense foam layer formed near the bottom of the foam sample (Figure 4.10 (b))) mainly due to the liquid foam drainage. More homogenous cell structure was therefore found interior of the foam plate and therefore for the foam-filling of Al tubes, cylindrical foam samples were core-drilled normal to the thickness of the plate or normal to the foam expansion direction. In each foam plate four foam-filler, having the diameter and length of 25mm and 27mm respectively, were core drilled (Figure 4.11). During core-drilling the pressure was kept as low as possible in order not to induce plastic deformation in the foam specimens. In order to prevent excessive heating of foam plate during core-drilling technical grade alcohol was used as coolant. A typical compression sample prepared by core-drilling of the foamed sample is shown in Figure 4.12. All drilled foam fillers were dried for 2 hours at 180^{o}C. The density of fillers was measured after drying by simply dividing the weight to the volume of the sample.

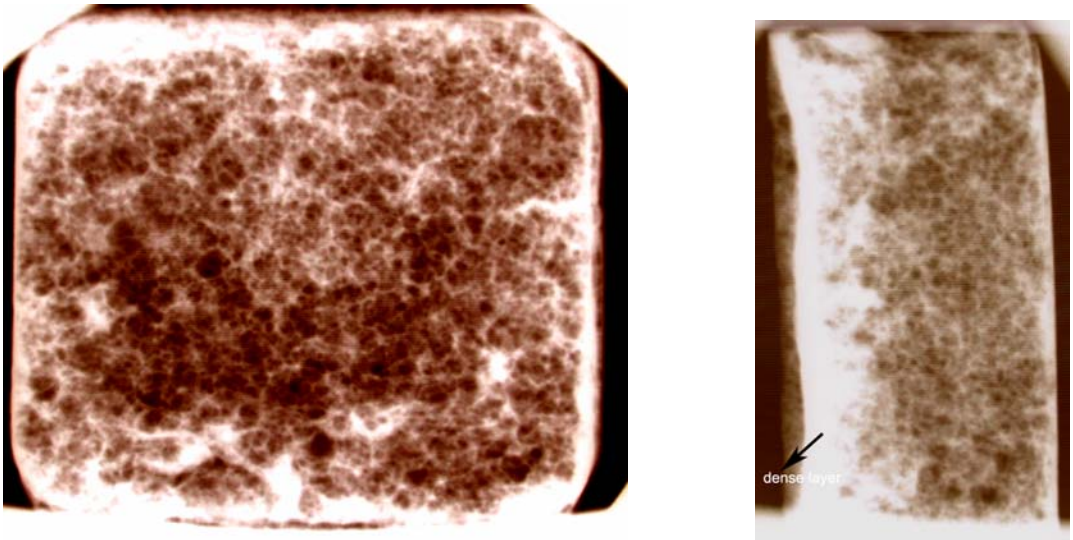

(a) (b)

Figure 4.10 Radiography views of Al foam (a) cross-section and (b) thickness.

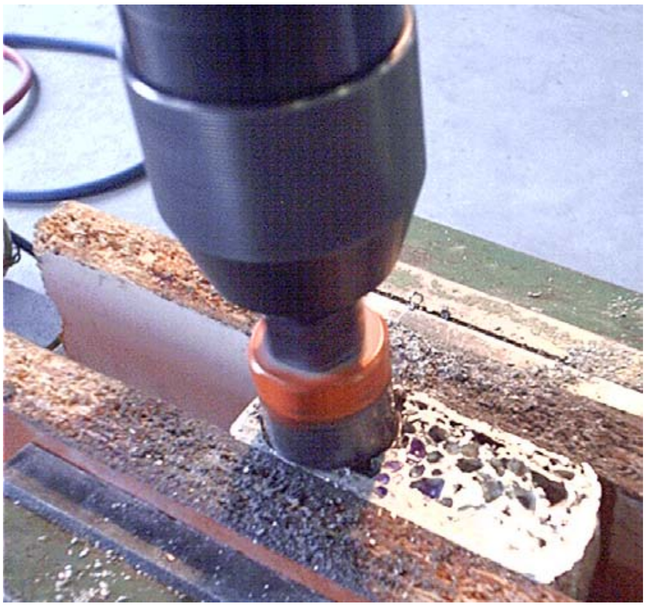

Figure 4.11 Core-drilling normal to foaming direction.

Figure 4.12 Cylindrical Al foam sample for tube filling.

The quasi-static compression testing of prepared foams were carried out using a fully computerized SHIMADZU testing device with cross head speed of 0.04 mm s^{-1}. Compression tests results were digitally recorded as load *vs.* displacement data, which were then converted into nominal stress *vs.* strain data. In few tests, the deformation sequence was also recorded using a video camera.

4.2. Polystyrene Foam Filler

As-received extruded polystyrene foam sheets with dimensions of 5x60x120 cm were manufactured by Izocam Company of Turkey using a process that produces partly oriented closed-cell foams with smooth continuous skins (Figure 4.13). The foam sheets investigated were supplied with a trade name “Foamboard® 3500”. The density of the polystyrene foam was determined by dividing the mass of the cubic foam sample (5x5x5 cm) by its volume and found to be 0.0321 g cm^{-3}. The corresponding mean relative density, 0.0305, was calculated by dividing the foam density to the dense polystyrene density (1050 kg m^{-3}).

Figure 4.13 Polystyrene Foamboard 3500 panels.

The cell distribution in each as-received foam sheet was examined through Rise-Width (R-W) plane (Figure 4.14). The foam samples show typical closed cell foam structure composing of 14-sided (tetrakaidecahedral) closed cells and each cell is composed of cell faces, edges and vertices (Figure 4.15 (a) and (b)). Cell faces are the thin membranes that separate two adjacent cells; cell edges are relatively thick struts of intersection of three neighboring cells and cell vertices are the intersection of four neighboring cell edges. In a tetrakaidecahedral cell, there are 14 faces, 36 edges and 24 vertices and of 14 of cell faces are 8 regular hexagons and 4 squares [51]. Figure 4.15(c) shows the SEM (Scanning Electron Microscopy) micrographs of cross-sections of the cells and Figure 4.15 (d) is a magnified SEM micrograph near to the cell edge [51].

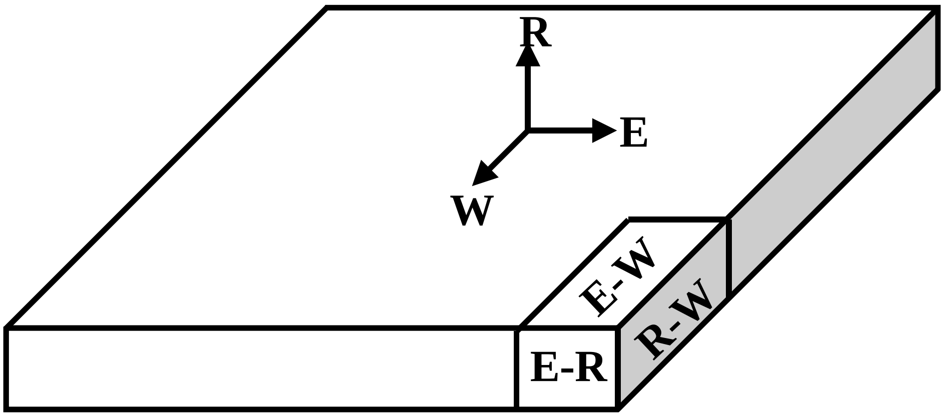

Figure 4.14 Schematic of as-received foam sheet showing R, W and E-directions and planes. [51]

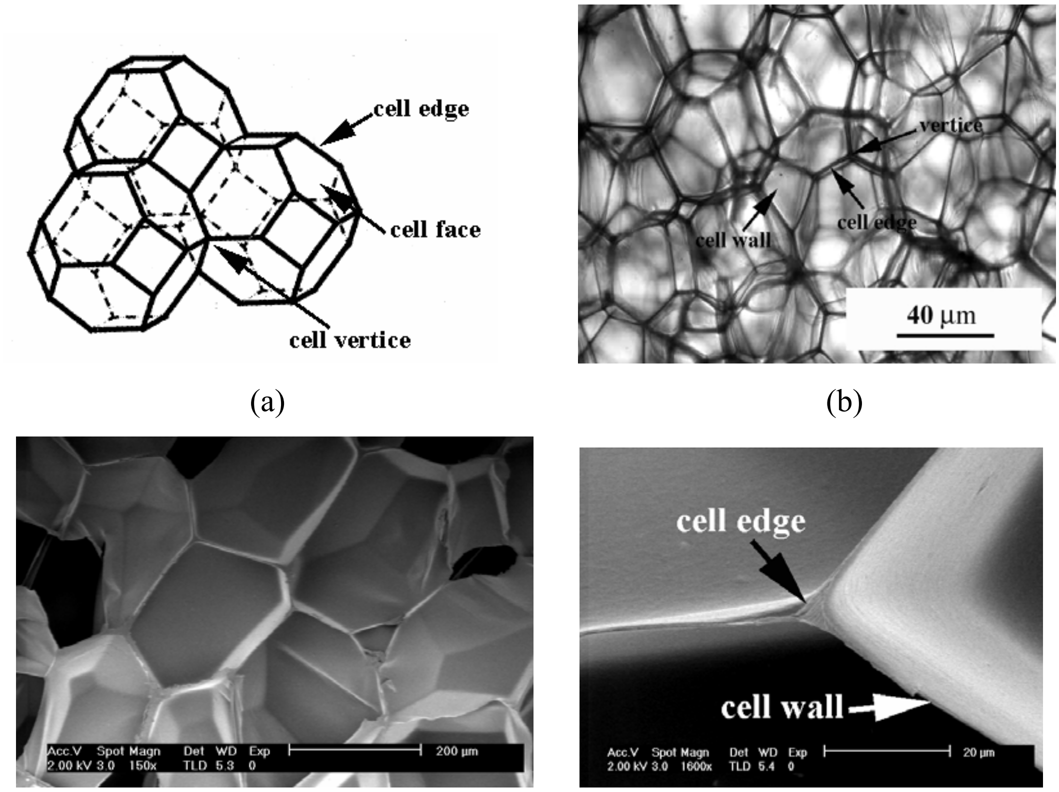

(a) (b)

(c) (d)

Figure 4.15 (a) tetrakaidecahedral polystyrene foam model, (b) transmitted optic and (c) SEM micrographs of the cell wall and edges and vertices and (d) SEM micrograph of the cell wall and edge [51].

In order to determine polystyrene foam crushing behavior, compression tests were conducted on cylindrical tube filler samples, 25 mm in diameter and 27 mm in length. Compression tests were conducted through (parallel) R-direction with cross-head speed of 0.04 mm s^{-1}, corresponding to the strain rate of $8.33x10^{-4}$ s^{-1}, using a computer controlled SHIMADZU AG-I testing machine.

Chapter 5

PREPARATION AND CHARACTERIZATION OF EMPTY AND FILLED TUBES

5.1 Single empty tubes

Deep-drawn Al tubes were produced by METALUM Company of Turkey and received in two diameters, 25 and 35 mm, having wall thickness of 0.29 and 0.35 mm respectively. The yield and ultimate strength of the tube material was previously determined by Toksoy [51] at a quasi-static strain rate of ~$1x10^{-3}s^{-1}$ and is shown in Figure 5.1. The ultimate tensile stress (σ_U), 0.2%, proof strength ($\sigma_{0.2}$) and Vickers hardness number of the tube materials are listed in Table 5.1. Tubes were machined to 27 mm in length using a diamond saw for compression testing. Geometric and material parameters of tested empty tubes are listed in Table 5.2.

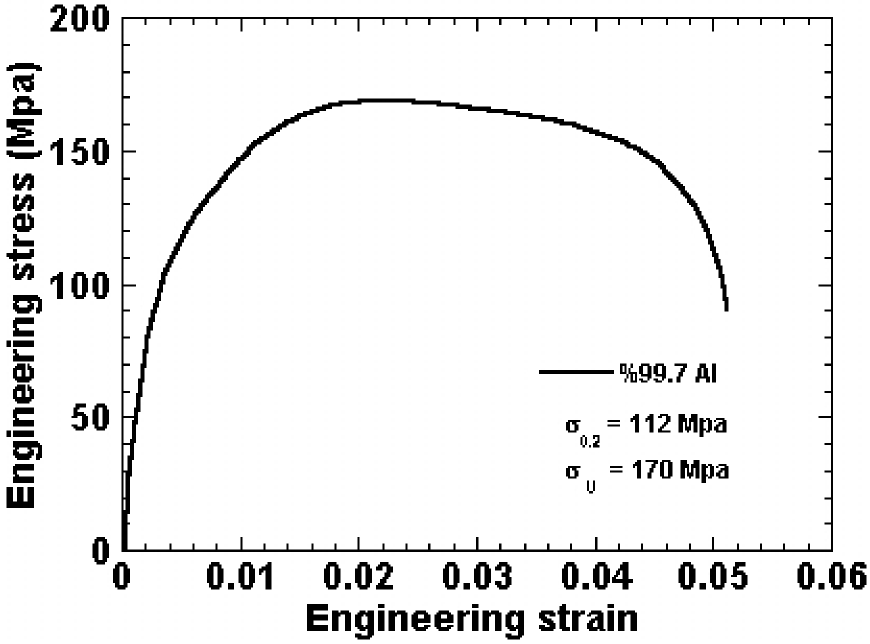

Figure 5.1 Tensile stress-strain curve of 99.7% Al tube material [51].

Table 5.1 Mechanical properties of Al tube material [51].

Materials	**σ_U ($\pm$ 10 MPa)**	**$\sigma_{0.2}$ ($\pm$ 10 MPa)**	**Σ_0 $(\frac{\sigma_{0.2}+\sigma_U}{2})$**	**Vickers hardness number**
99.7% Al	170	112	141	58

Table 5.2 Geometric parameters of tested empty tubes.

Tube Material	**Outer Diameter (mm)**	**Thickness (mm)**	**Length (mm)**	**Mass (g)**	**D/t ratio**
%99.7 Al	25	0.29	27	1.72	86.2
%99.7 Al	35	0.35	27	2.61	100

All the tubes, empty and foam-filled, were compressed at a cross-head speed of 2.5 mm min^{-1}. The corresponding deformation rate, which is defined as the cross-head speed divided by the initial length of the tube, were $1.54\text{x}10^{-3}$ s^{-1}. The compression tests were conducted between the compression plates as depicted in Figure 5.2.

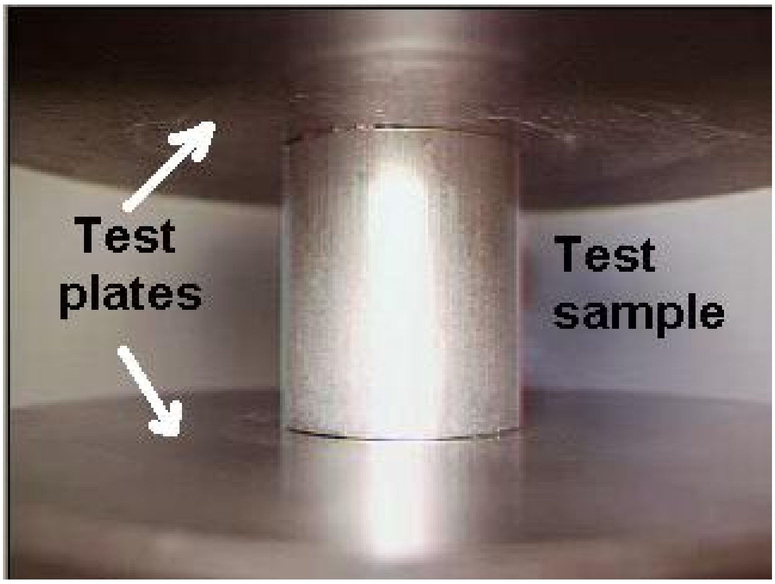

Figure 5.2 View of an empty tube between the compression test plates.

5.2 Single and bitubular filled tubes

The geometric parameters of filled single tubes are listed in Table 5.3. The nomenclature used for describing the single filled tubes is as follows: the first letter in the name of each sample refers to the filling material (Polystyrene ‘P’ and Aluminum ‘A’), followed by “FF” which means “foam-filled” and the number is the specimen group. At least four compression tests were conducted for each group. It should also be noted in Table 5.3 Al foam filling was only applied to 25 mm Al tube.

Table 5.3 Geometric parameters of single filled tubes.

Group	**Length (mm)**	**Diameter (mm)**	**Wall thickness (mm)**	**Foam density ($g.cm^{-3}$)**	**Average mass (g)**
PFF1	27	25	0.29	0.0321	2.106
PFF2	27	35	0.35	0.0321	3.3983
AFF1	27	25	0.29	0.27	5.3168
AFF2	27	25	0.29	0.35	6.0325
AFF3	27	25	0.29	0.43	7.5219

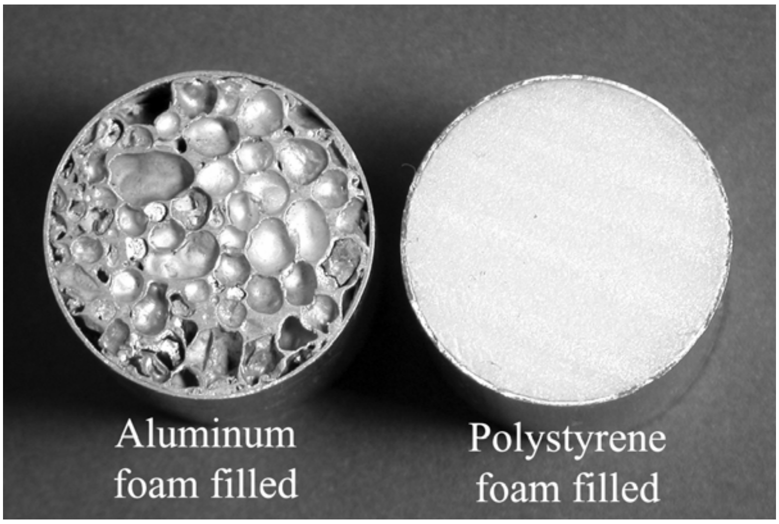

Figure 5.3 Top views of Al and polystyrene foam-filled Al tubes (25 mm diameter).

Three different bitubular configurations were investigated. These are:

i- *Series BPH*; interior: 25 mm diameter empty tubes and exterior: 35 mm polystyrene foam filled tube (Figure 5.4(a)).

ii- *Series BPP*; interior: 25 mm diameter polystyrene foam-filled tube and exterior: 35 mm polystyrene foam-filled tube (Figure 5.4(b)).

iii- *Series BPA*; interior: 25 mm diameter aluminum foam-filled tubes, exterior: 35 mm polystyrene foam-filled tube (Figure 5.4(c)).

In Table 5.4 the dimensions of the investigated tubular geometries are listed together with filling foam densities. The nomenclature used for describing the tested specimens is as follows: “B” means bitubal, second letter in the name of each sample refers to the exterior filling material (Polystyrene “P”), followed by second letter for the interior filling material (Aluminum “A”, Polystyrene “P” and hollow “H”) and the last number is the specimen number. Again at least four compression tests were conducted for each group.

(a) (b) (c)

Figure 5.4 Bitubal arrangements (a) series BPH, (b) series BPP and (c) series BPA.

Table 5.4 Geometric parameters of bitubular filled tubes.

Test Code	Length (mm)	Wall thickness (in / out) (mm)	Foam density (exterior/interior) (gr.cm^{-3})	Average mass (g)
BPH	27	0.29 / 0.35	0.0321	4.6411
BPP	27	0.29 / 0.35	0.0321/ 0.0321	5.1799
BPA4	27	0.29 / 0.35	0.0321/ 0.3301	8.9985
BPA1	27	0.29 / 0.35	0.0321/ 0.3541	9.1125
BPA2	27	0.29 / 0.35	0.0321/ 0.2596	8.0389
BPA3	27	0.29 / 0.35	0.0321/ 0.3104	8.5833

5.3. Multiple empty and filled tubes

Multiple tube geometries tested are the empty and Al foam-filled hexagonal packed 25 mm tube bundles (Figure 5.5(a) and (b)) and the empty and Al foam filled cubic packed 25 mm tube bundles (Figure 5.6(a) and (b)). Hexagonal packed bundles composed of seven tubes (Figures 5.5) while 4 tubes were used for cubic packing (Figure 5.6). A special compression test apparatus (Figure 5.7(a)) that fits inside the circular lateral constraint tube (Figure 5.7(b)) was used in crushing tests of hexoganal packed bundles. The constraint aluminum tube was 75 mm in inner diameter, 2.5 mm in wall thickness and 35 mm in length.

(a) (b)

Figure 5.5 Hexagonal multi tube design (a) empty and (b) aluminum foam filled.

(a) (b)

Figure 5.6 Cubic multi tube design (a) empty and (b) aluminum foam filled.

(a) (b)

Figure 5.7 (a) Compression test apparatus for hexagonal packed tube bundles and (b) Al circular lateral constraint tube.

For hexagonal packed tube bundles, three different Al foam-filled tube groups were tested according to their Al foam filler density as tabulated in Table 5.5. The first group was constructed from the tubes filled with foam densities between 0.4 and 0.47 g cm^{-3}. The second and third groups of tubes were filled with foam densities ranging between 0.34 and 0.4 g cm^{-3} and 0.51 and 0.6 g cm^{-3}, respectively.

Table 5.5 Al foam filled single tube specifications used in hexagonal multi-tube design.

Test Group	Single tube code	Length (mm)	Diameter (mm)	Wall thickness (mm)	Foam density (g.cm^{-3})	Mass (g)
MHF1	AFF31	27	25	0.29	0.472	7.6292
	AFF32	27	25	0.29	0.454	7.3468
	AFF34	27	25	0.29	0.415	6.9025
	AFF39	27	25	0.29	0.4219	7.0220
	AFF46	27	25	0.29	0.40	6.70
	AFF48	27	25	0.29	0.458	7.4802
	AFF49	27	25	0.29	0.446	7.29
MHF2	AFF22	27	25	0.29	0.3668	6.29
	AFF25	27	25	0.29	0.385	6.52
	AFF28	27	25	0.29	0.382	6.45
	AFF29	27	25	0.29	0.35	6.03
	AFF33	27	25	0.29	0.391	6.61
	AFF41	27	25	0.29	0.359	6.249
	AFF45	27	25	0.29	0.40	6.70
MHF3	AFF21	27	25	0.29	0.6	9.3103
	AFF27	27	25	0.29	0.535	8.3767
	AFF36	27	25	0.29	0.546	8.5225
	AFF37	27	25	0.29	0.5152	8.1544
	AFF38	27	25	0.29	0.567	8.7620
	AFF42	27	25	0.29	0.58	8.9736
	AFF43	27	25	0.29	0.51	8.1237

The cubic packed bundles were tested inside a rectangular die using a machined compression test plate as shown in Figure 5.8(a) and (b). Figure 5.8(c) shows a scene from the compression testing. The compression test apparatus for cubic packing had the dimensions of 50 mm x 50 mm cross-section. For this design two different groups of tests were conducted. These groups are listed in Table 5.6 and composed of foam densities ranging between 0.30 and 0.33 g cm $^{-3}$ for the first group and 0.26 and 0.29 g cm $^{-3}$ for the second group. Finally, in both multi tube arrangements the compression test plates moved inside the lateral constraint tube freely without imposing any friction.

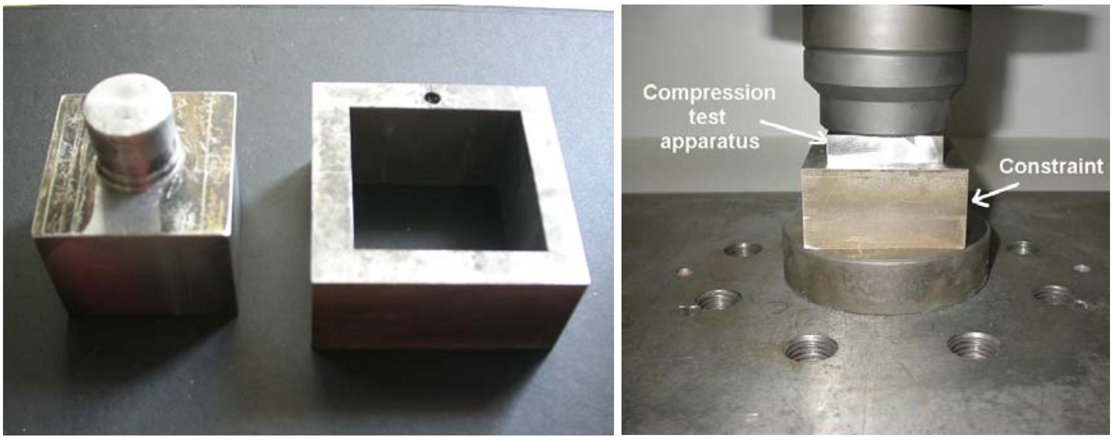

(a) (b) (c)

Figure 5.8 (a) Compression test apparatus (b) square lateral constraint and (c) compression testing.

Table 5.6 Al foam filled single tube specifications used in cubic multi-tube design.

Test Group	**Single tube code**	**Length (mm)**	**Diameter (mm)**	**Wall thickness (mm)**	**Foam density (g.cm^{-3})**	**Average mass (g)**
MCF1	AFF23	27	25	0.29	0.331	5.80
	AFF24	27	25	0.29	0.312	5.64
	AFF35	27	25	0.29	0.30	5.45
	AFF44	27	25	0.29	0.31	5.64
MCF2	AFF20	27	25	0.29	0.26	4.95
	AFF26	27	25	0.29	0.30	5.46
	AFF40	27	25	0.29	0.285	5.17
	AFF47	27	25	0.29	0.289	5.26

Chapter 6

RESULTS AND DISCUSSIONS

6.1. Foaming Experiments

The effect of cold compaction pressure on the relative density of the compacts, which were initially prepared for a goal of investigating precursor preparation with suitable relative densities for efficient foaming (at least 4 times expansion) without a hot compaction stage applied, is shown in Fig. 6.1. Even at the highest compaction pressure applied, 400 MPa, the relative density of the compact was less than 98% and therefore a hot forging stage was required in order to increase the precursor material relative density above 99%.

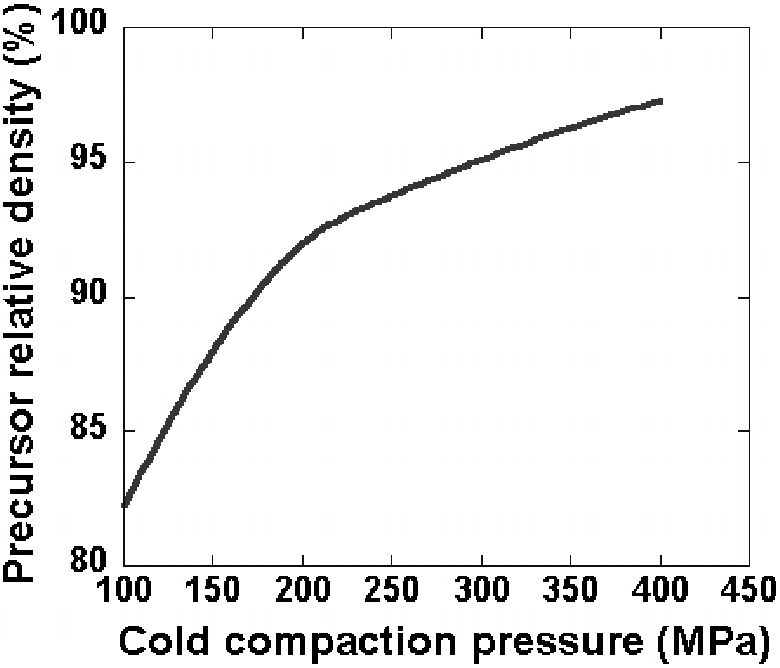

Figure 6.1 Precursor relative density *vs.* cold compaction pressure.

Foaming in a box furnace at 750 ^{o}C, above the melting point of the foamable precursor material, was previously shown to be sufficient for the foaming of Al compacts [52]. The temperature-time history of a precursor material in the furnace shown in Fig. 6.2 also represents several important stages of foaming. Since the precursor material was inserted at room temperature into the preheated foaming mold, foaming started after some time: initially the precursor temperature increases to 700 ^{o}C (over heating) and this is followed by the melting of the precursor at 663 ^{o}C as depicted in Fig.6.2. For the studied hot forged precursors and the foaming set-up used including foaming mold and furnace, foaming started only after 4 min 45 seconds and precursor material filled foaming mould completely at 5 min 25 seconds. Figs. 7(a) through (d) show the foamed precursor material at various furnace holding times.

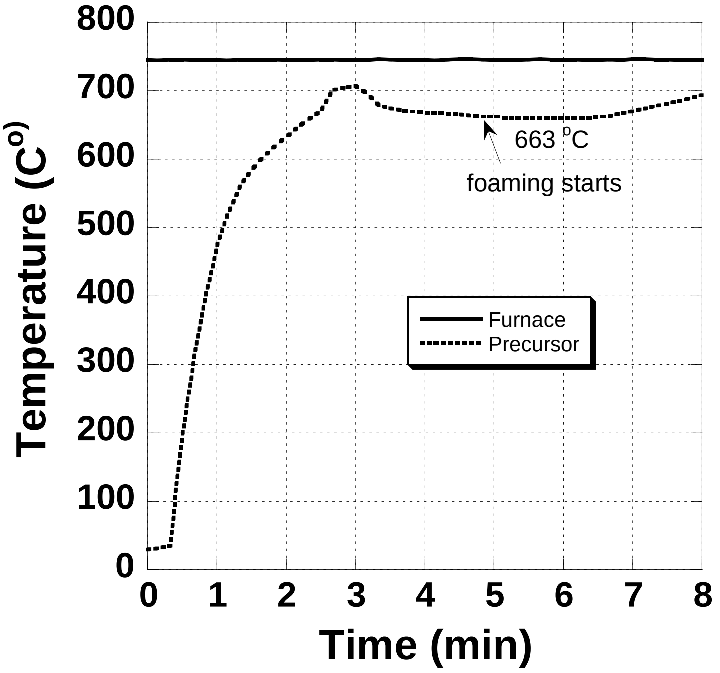

Figure 6.2 Furnace and precursor temperature-time histories.

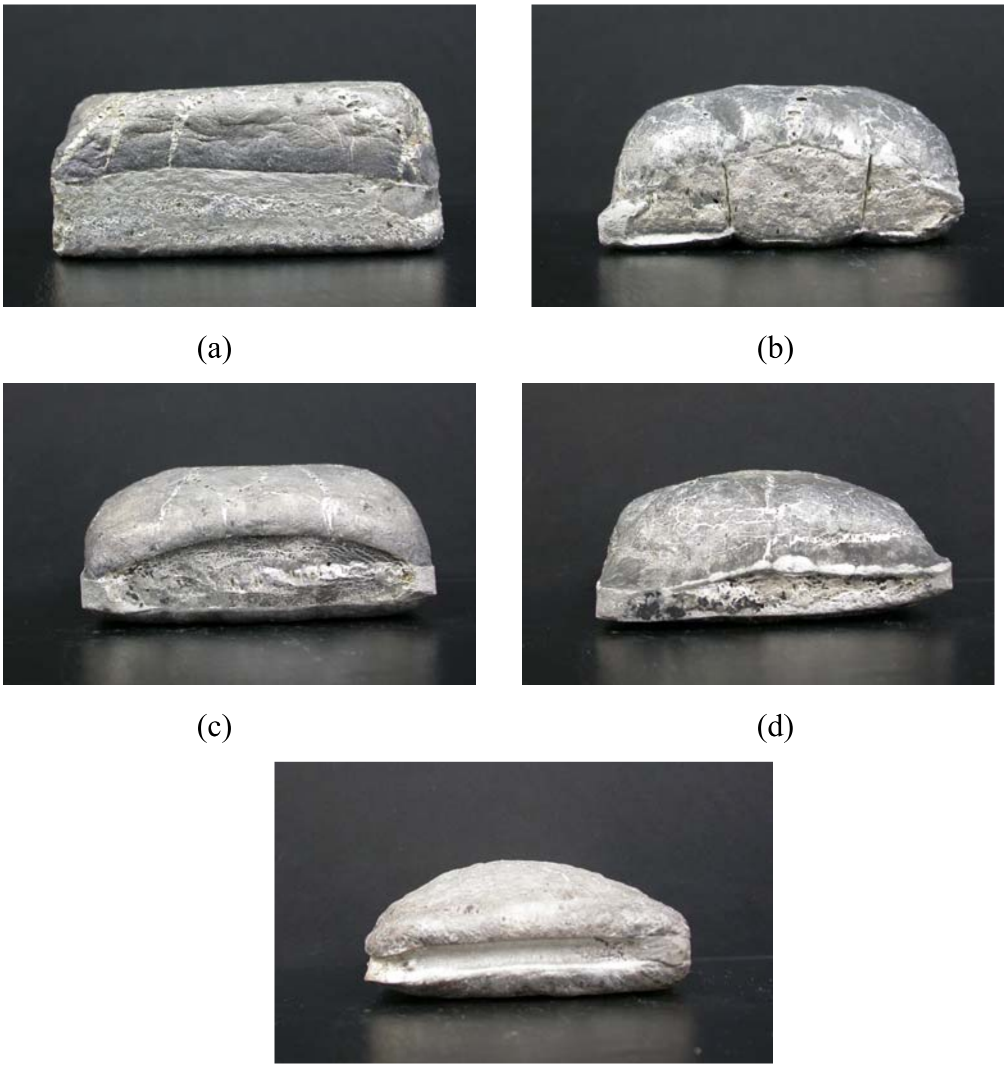

(a) (b)

(c) (d)

(e)

Figure 6.3 Foamed precursors at different furnace holding times (a) 5 minutes 25 seconds (b) 5 minutes 15 seconds (c) 5 minutes 10 seconds (d) 5 minutes 5 seconds (e) 5 minutes.

The material and geometry of the foaming mold and the type and size of the furnace used are naturally expected to have substantial influences on the heating rate of the precursor; therefore, their effects should be taken into account for designing an efficient foaming process. In this study, the same foaming mold made from the same material (st37 steel) was used in all foaming experiments. Therefore, the expansions at various furnace holding times given-above were found to be quite repeatable as long as the foaming and heating conditions were carefully adjusted and controlled, e.g. preheating temperature, the time for inserting into and removing the precursor from the mold. One of the difficulties in the preparation foamed metals is that the liquid foam is thermodynamically unstable and conditions change constantly during foaming. It should also be noted that the precursor material was heated indirectly via heat conduction from the preheated foaming mold. Any interruption in the heat conduction mainly caused by the loose contact between precursor and foaming mold resulted in delays in expansion at prescribed furnace holding times.

When the expansion of precursor reaches to a prescribed level the liquid foam should be solidified quickly in order to retain its shape and cell structure in the solid state. Otherwise, the molten aluminum flows downwards, a natural process known as drainage, at longer foaming durations and forms a dense metal layer at the bottom of the precursor. Longer furnace holding times also results in collapse of cell walls leading to nonuniform and very large cell sizes. It should also be noted that the phenomena occurring during solidification of liquid foam are also quite complex and difficult to describe for the reasons similar to those mentioned for the heating phase. In the cooling stage, geometrical defects mostly arising from the inhomogenuous cooling rates were also found. Fig. 6.4 shows such a large defect formed at the bottom of a foamed precursor material. The foamed precursors that contained defects were discarded.

Figure 6.4 A typical geometrical defect in foamed precursor.

6.2. Compression Behavior of Al Foams

Closed-cell metal foams show a characteristic compressive stress-strain curve composing of three distinct regions; linear elastic, collapse and densification (Fig. 6.5) [53]. At low strains, the foam deforms elastically and deformation is controlled by cell wall bending and/or stretching. This region is followed by a collapse region occurring by several different mechanisms, i.e. elastic buckling and brittle crushing of cell walls and formation of plastic hinges. Deformation in this region is highly localized and proceeds with the spreading of deformation from localized to undeformed regions of the sample. Since the deformation is localized, large oscillations in stress occur due to the repetitive nature of the process of cell collapse and densification. Collapse region is characterized by a stress plateau either with a constant value or increasing slightly with strain, see Fig. 6.5. At a critical strain, ε_d, cell walls start to touch each other and, as a result of this, the material densifies (densification region). The stress in this region increases sharply and approaches to the strength of the bulk Al metal. The extent of each region is a function of relative density. The prepared Al foams in this study also show above-mentioned deformation mechanisms. Fig. 6.6 shows the compressive stress–strain curves of the prepared Al foams of three different densities, 0.27, 0.35 and 0.43 g cm^{-3}. In order to see the repeatability of compression stress-strain behavior of foams with the same density, two tests results are shown in Fig. 6.6. It is also noted in Fig. 6.6, the plateau stresses of foams are not constant and increase with increasing strain. It is supposed that foams having homogeneous cell size and cell size distribution show steady plateau stress in collapse region. But in reality, differences in cell size and cell distribution cause the collapse of weak cells before the collapse of strong cells. This leads to increase in the stress values in the collapse region. Figs. 6.7 (a-d) show the compression deformation images of 0.27 g cm^{-3} foam at 0, 25, 50 and 75% strains, respectively. As shown in Fig. 6.7(a) localized deformation of the tested foam started near the upper compression test plate (Fig. 6.7(b)) and proceeded down to the denser sections.

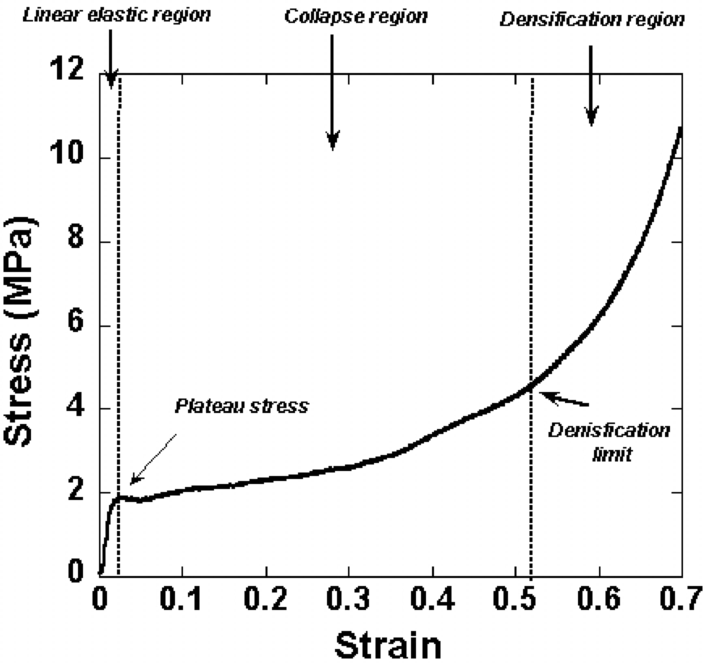

Figure 6.5 Typical compressive stress-strain curve of Al foams [53].

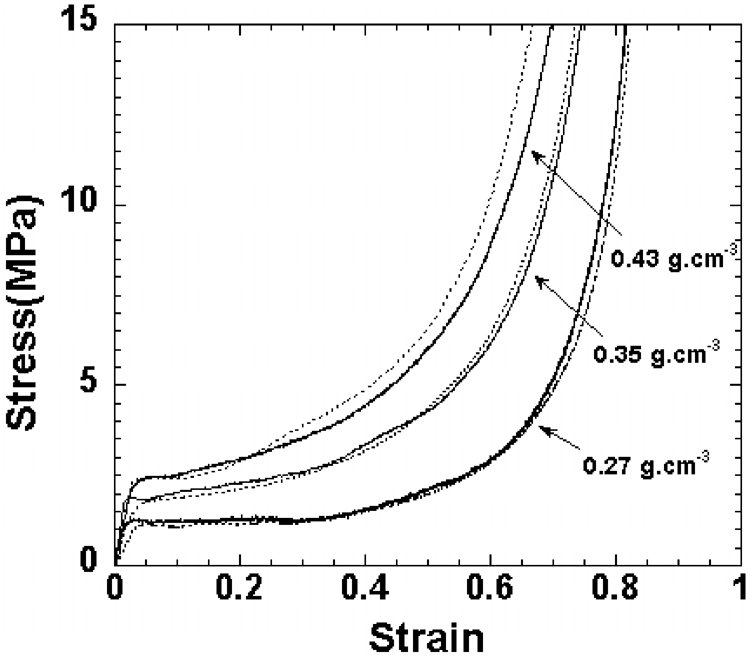

Figure 6.6 Compressive stress-strain curves of the prepared Al foams at various densities [53].

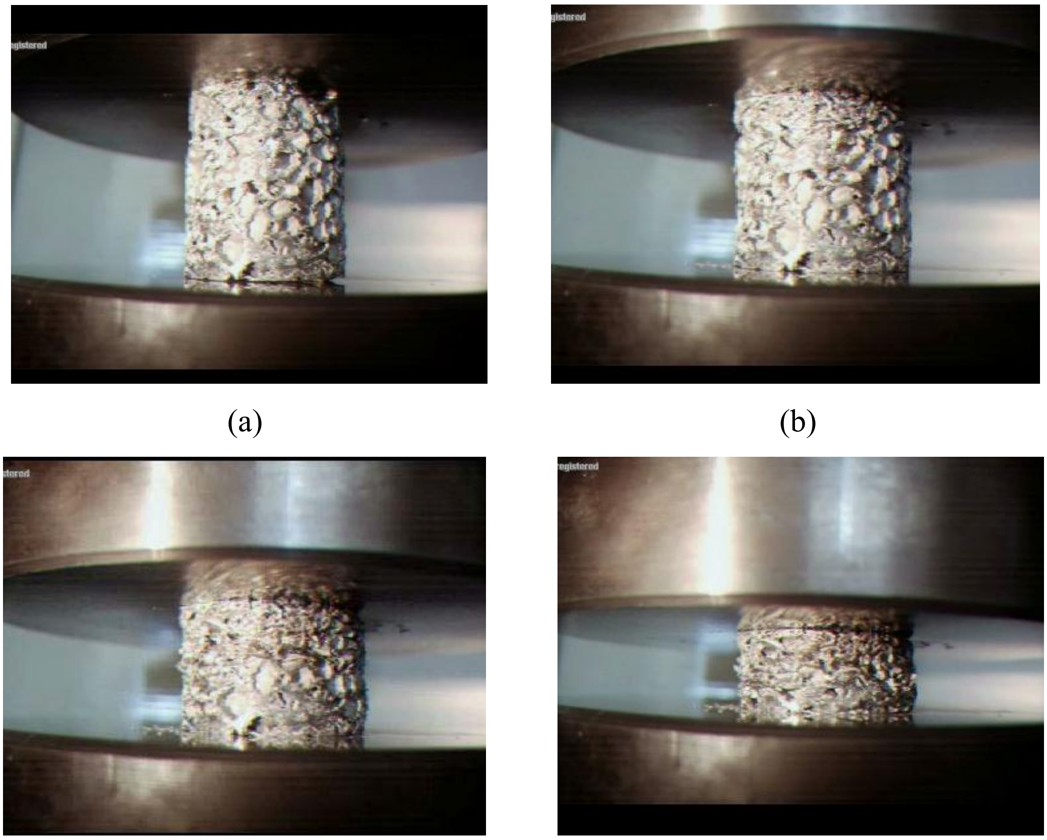

(a) (b)

(c) (d)

Figure 6.7 Images of Al foam (0.27 g cm^{-3}) deformed at (a) 0% (b) 25% (c) 50% (d) 75% strains.

The plateau stress varied with the foam density as depicted in Fig. 6.8; as the relative density increased the plateau stress increased. It is of great advantage to be able to describe the strain hardening properties of the aluminum foams by a simple model. Such model has been proposed by Hannsen *et al.* [54] for the compression stress-strain behavior of Al foams and the constitutive model was also validated by using non linear finite element code LS-DYNA. The strain-hardening model proposed is given by the following equation:

$$\sigma = \sigma_P + \gamma \frac{e}{e_D} + \alpha \ln\left[1/(1-(\frac{e}{e_D})^{\beta} \right] \tag{6.1}$$

where σ_P, e, e_D, γ, α and β are the plateau stress, strain, compaction strain, linear strain hardening coefficient, scale factor and shape factor respectively.

$$e_D = 1 - \frac{\rho_f}{\rho_b} \tag{6.2}$$

Because of its simplicity, the above-given model was also used to construct the stress-strain relation of the prepared Al foams. Experimental stress-strain curves corresponding to a specific density were witted with Equation 6.1. The coefficients of Equation 6.1 are also listed for each density in Table 6.1. The constructed stress-strain curves are presented in Fig. 6.9 together with experimental curves. Generally satisfactory agreements are found.

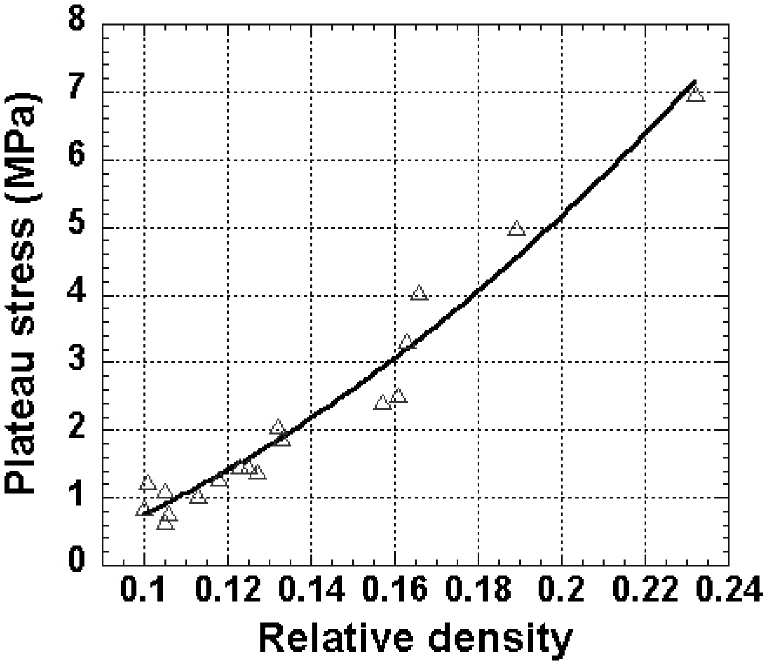

Figure 6.8 Typical plateau stress *vs*. relative density curves of the Al foams [53].

Table 6.1 Coefficients of Equation 6.1 for each foam density studied.

Foam denisty (g.cm^{-3})	σ_P **(MPa)**	**γ**	**α**	**β**
0.27	1.24	0.2	17	6
0.35	1.96	1.7	17	5
0.43	2.44	1.7	18	4

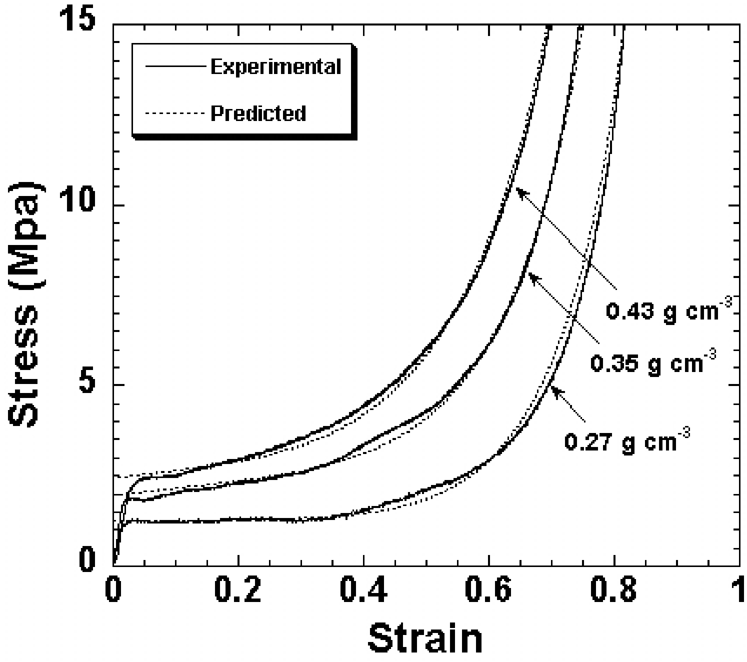

Figure 6.9 Experimental and fitted stress strain curves of foams [53].

6.3. Compression Behavior of Empty Tubes

Empty Al tubes, both 25 and 35 mm, deformed in diamond mode. Typical load-displacement curves of the tubes are shown in Fig. 6.10. The deformation was progressive as shown for 25 mm Al tube at displacements of 0, 5.4, 9.45 and 16.2 mm in Figs.6.11 (a), (b), (c) and (d), respectively. In both tubes the eight-corner diamond folding geometry was found (Fig. 6.12). The distances between the peaks loads shown in Fig. 6.10 correspond to the fold length and accordingly the total number of load peaks corresponds to the number of the folds formed in the tubes. Totally 4-5 folds formed in both tubes. The densification of tubes, the sudden rise in load values, further starts after 21 mm displacement, corresponding to about 80% deformation of the initial tube length. It is also noted in Fig.6.11 that the initial peak-loads are greater than the following peak-loads. This is a phenomenon commonly observed in thin-wall tube crushing, which simply arises from the constraining effect imposed by the compression test plates. The initial peak-load is further interpreted as the maximum load of the tube crushing.

Average crushing load-displacement curves of empty tubes are also shown in Fig. 6.13. 25 mm tube crushes nearly at 1 kN while 35 mm tube at about 1.25 kN as seen in the same figure. Table 6.2 lists the compression test results of empty tubes.

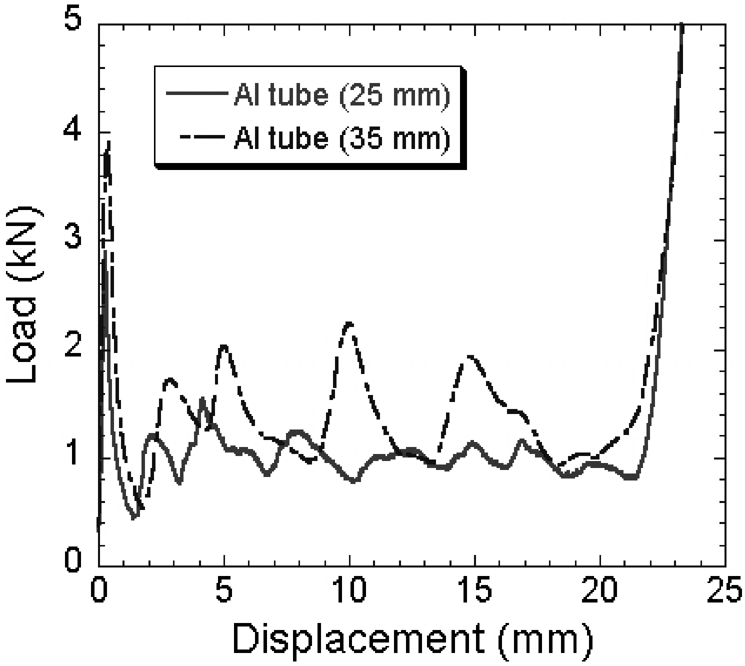

Figure 6.10 Typical load *vs.* displacement curves of the empty Al tubes at 2.5 mm min^{-1}.

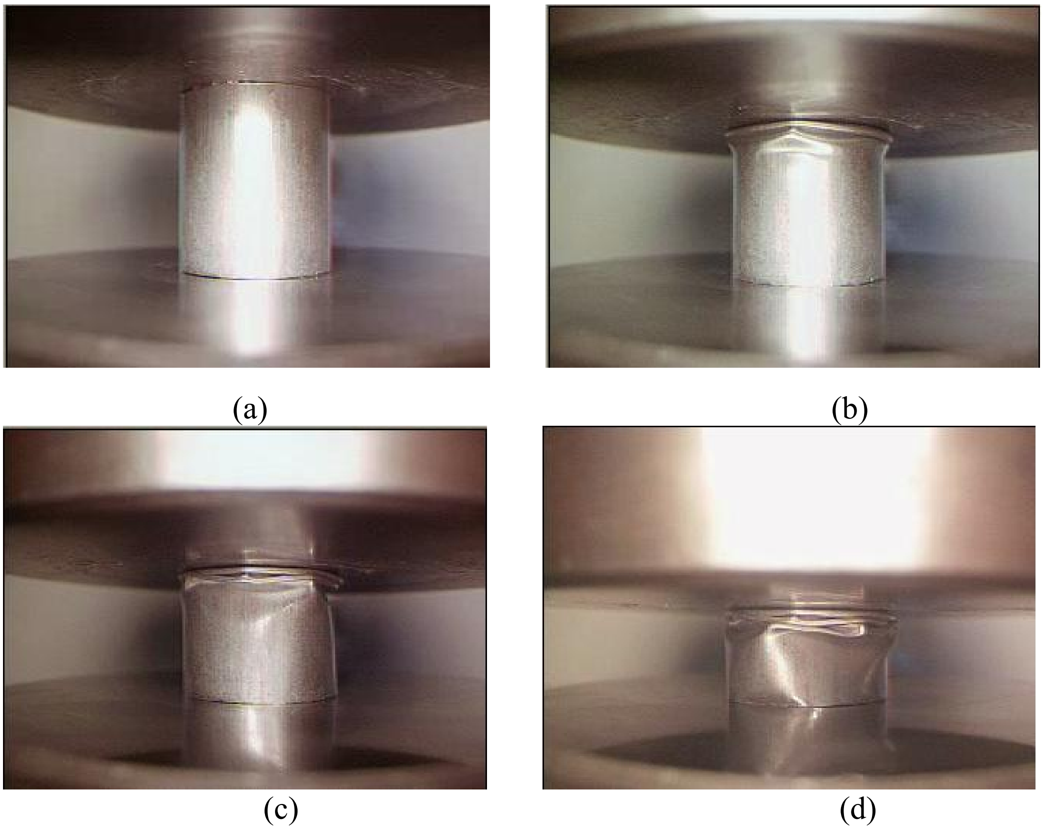
(a) (b) (c) (d)

Figure 6.11 Images of crushed 25 mm diameter Al tube at (a) 0% (b) 20% (c) 35% (d) 60% strains.

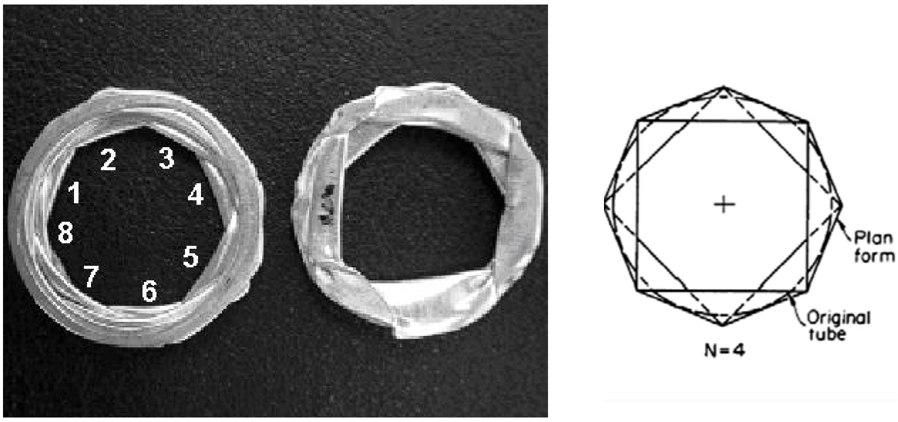

(a) (b) (c)

Figure 6.12 a) Top and b) bottom views of the crushed 25 mm Al tube and c) schematic of the diamond collapse mode with 4 circumferential lobes (only figure (c),[55]).

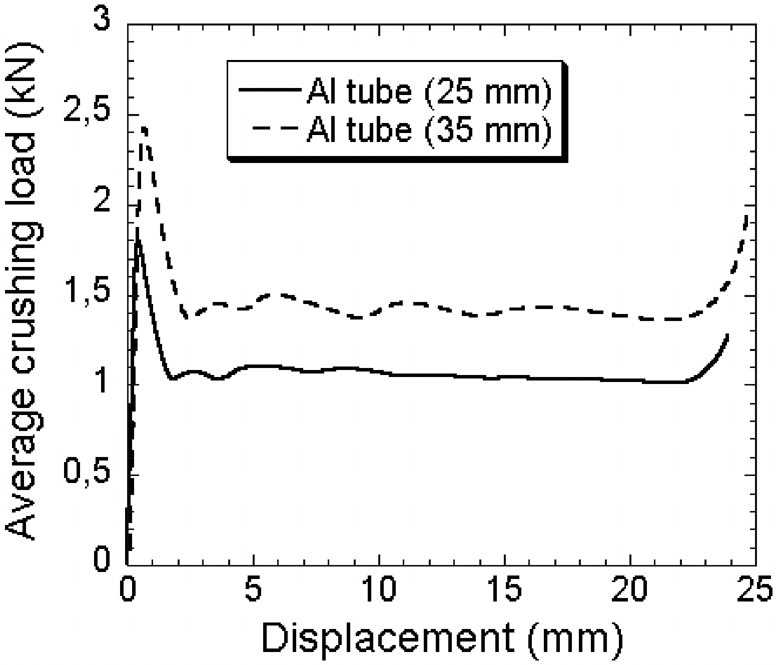

Figure 6.13 Average crushing load *vs.* displacement of empty tubes.

Table 6.2 Compression test results of empty tubes

Extrusion			Empty tube response parameters			
Test Code	Tube diameter (mm)	Tube thickness (mm)	Max force F_{max} (kN)	Mean force at %50 strain F_{avg} (kN)	Total number of folds	Crushing mode
E1-1	25	0.29	1.5313	0.999	4	Diamond
E2-1	25	0.29	1.4844	1.0299	4-5	Diamond
E3-1	25	0.29	1.5547	1.0192	4-5	Diamond
E4-1	25	0.29	1.4219	0.9439	4	Diamond
E5-1	25	0.29	1.5156	1.039	5	Diamond
E6-1	25	0.29	1.3516	0.9416	5	Diamond
E7-1	25	0.29	1.375	1.085	5	Diamond
E8-1	25	0.29	1.3438	0.9265	4	Diamond
E9-1	25	0.29	1.3516	0.9534	5	Diamond
E1-2	35	0.35	1.6406	1.1378	4	Diamond
E2-2	35	0.35	1.8141	1.2812	4	Diamond
E3-2	35	0.35	2.2438	1.3609	4	Diamond

6.4. Compression Behavior of Single Al and Polystyrene Foam Filled Tubes

Fig. 6.14 (a) shows the crushing load-displacement response 0.27 g cm^{-3} Al-foam-filled 25 mm tube together with that of empty tube, Al-foam and empty tube+Al foam. Empty+Al foam is the sum of loads of empty tube (alone) and foam(alone). On the same figure, the average crushing loads are shown by dotted lines. The average crushing loads of Al foam-filled tubes were calculated between the displacements 2 and 10 mm since at higher displacements, >10 mm, Al foam filler crushing load increases sharply above the plateau load, which makes the calculation of the strengthening effect of foam filler difficult. As is seen in Fig. 6.14(a) the crushing and average crushing loads of filled tube are higher than those of empty and tube+Al foam. This is known as interaction effect. The interaction effect was also found in 0.35 and 0.43 g cm^{-3} foam-filled tubes as shown sequentially in Figs. 6.14(b) and (c).

Regardless the Al foam density used, foam-filling shifted the deformation mode from diamond to progressive axisymmetric (concertina) mode of deformation. Figs. 6.15(a-d) show the progression of concertina mode of deformation in 0.35 g cm^{-3} foam-filled 25 mm tube at various deformation ratios. The folding started at the one of the ends of the tube as seen in Fig. 6.16. The number of folds formed also increased with foam filling from 4 to 6 and hence the fold length decreased accordingly.

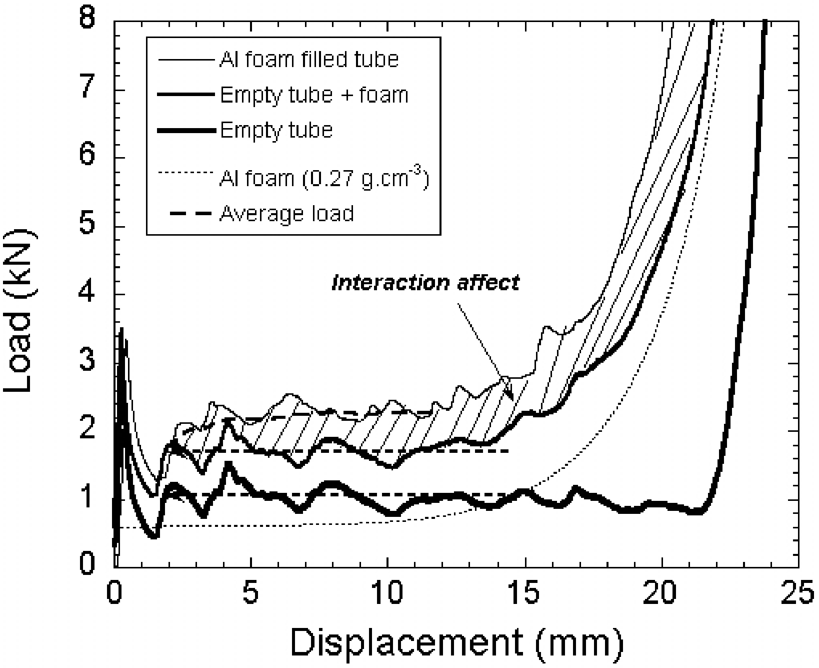

(a)

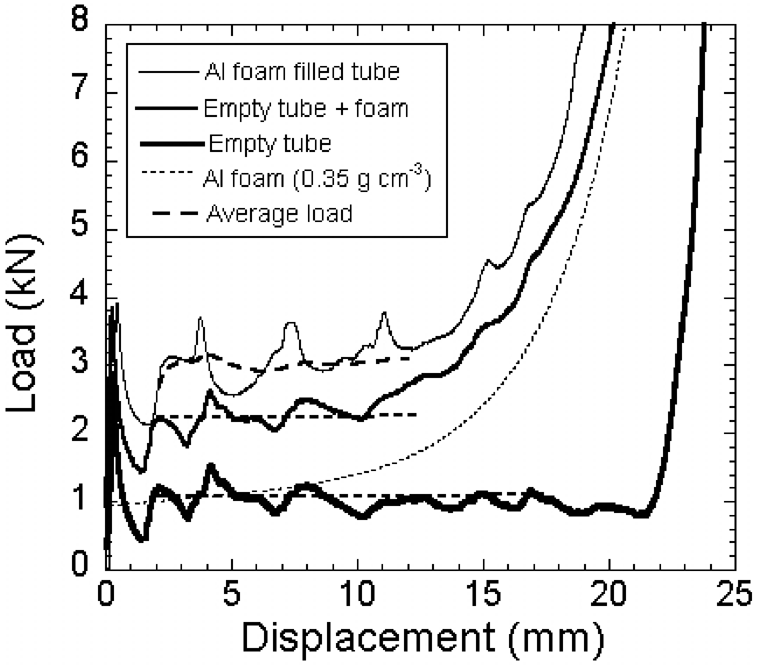

(b)

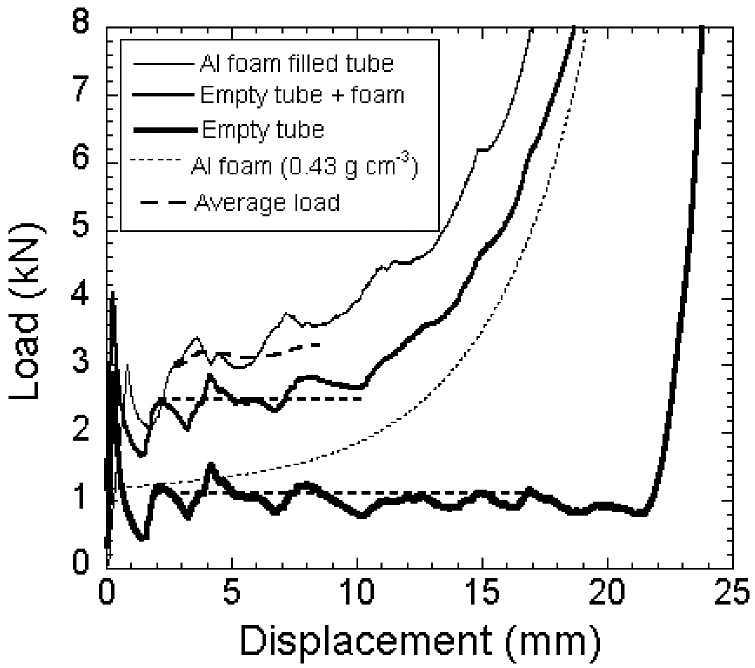

(c)

Figure 6.14 Load and average crushing load-displacement curves of foam-filled 25 mm Al tube, empty tube, empty tube+foam and foam; (a) 0.27 g cm^{-3} Al-foam-filled (b) 0.35 g cm^{-3} Al-foam-filled and (c) 0.43 g cm^{-3} Al-foam filled tube [53].

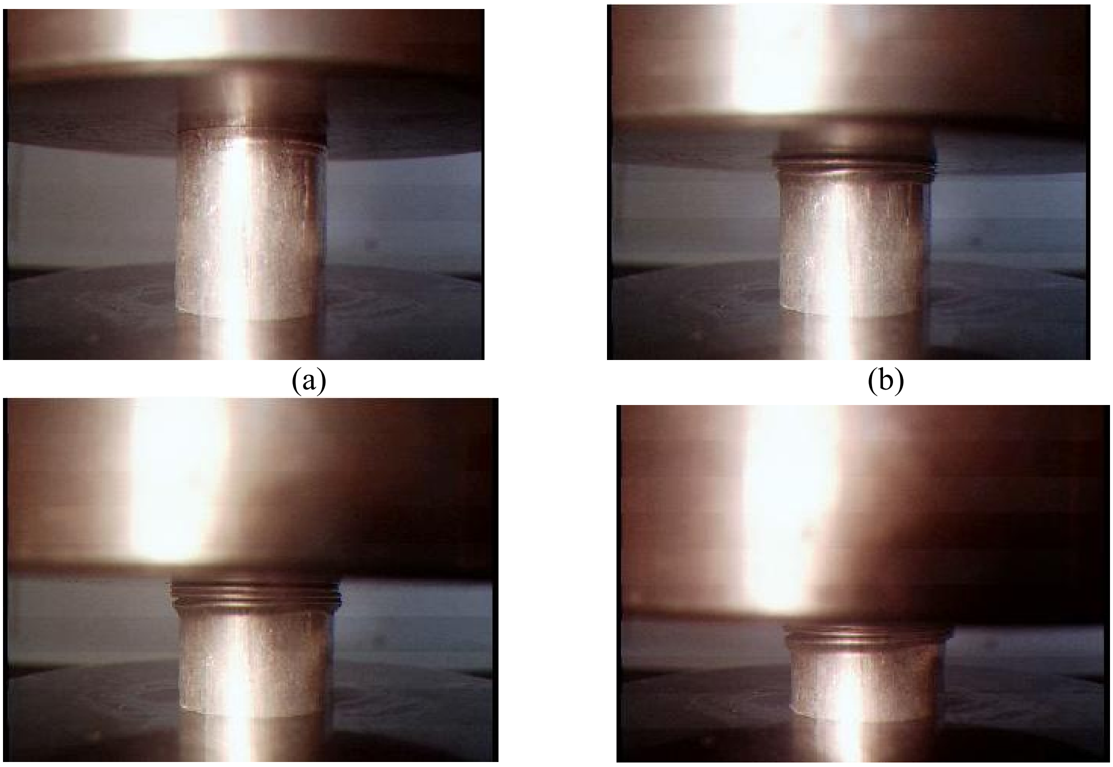

(a) (b)

(c) (d)

Figure 6.15 Progression of concertina mode of deformation in 0.35 $g.cm^{-3}$ Al-foam filled 25 mm tube at (a) 0%, (b) 20%, (c) 35% and (d) 50% deformation ratios.

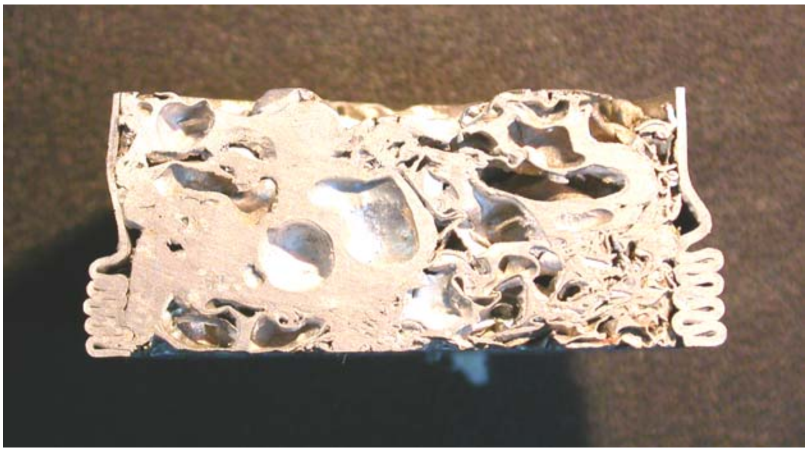

Figure 6.16 Interior view of axisymmetric deformation of Al foam-filled Al tube.

In both polystyrene foam-filled 25 mm and 35 mm tubes, the deformation mode shifted from diamond to mixed mode (Fig. 6.17(a-d)). The axial crushing of cylindrical columns is known to produce two distinctive deformation modes, namely the concertina and diamond and a blend between the two modes is also commonly encountered as in the case of polystyrene foam-filled tubes in this study.

Fig. 6.18(a) and (b) show the typical load-displacement curves of the polystyrene foam-filled 25 mm and 35 mm tubes, respectively. On the same figures load-displacement curves of empty and empty tube+foam are also shown. For both filled tubes again foam filling increased the average crushing load values above those of foam+empty tube (Fig. 19(a) and (b)), confirming again the afore-mentioned interaction effect. Similar to Al-foam filled tubes, foam filling reduced the fold length; hence, increased the number of folds formed, resulting in shifting of the densification region to lower values of the displacement.

Table 6.3 lists the geometrical and crushing parameters of foam-filled tubes. As noted in Table 6.3 concertina mode of deformation induced more fold formation as compared with mixed mode of deformation.

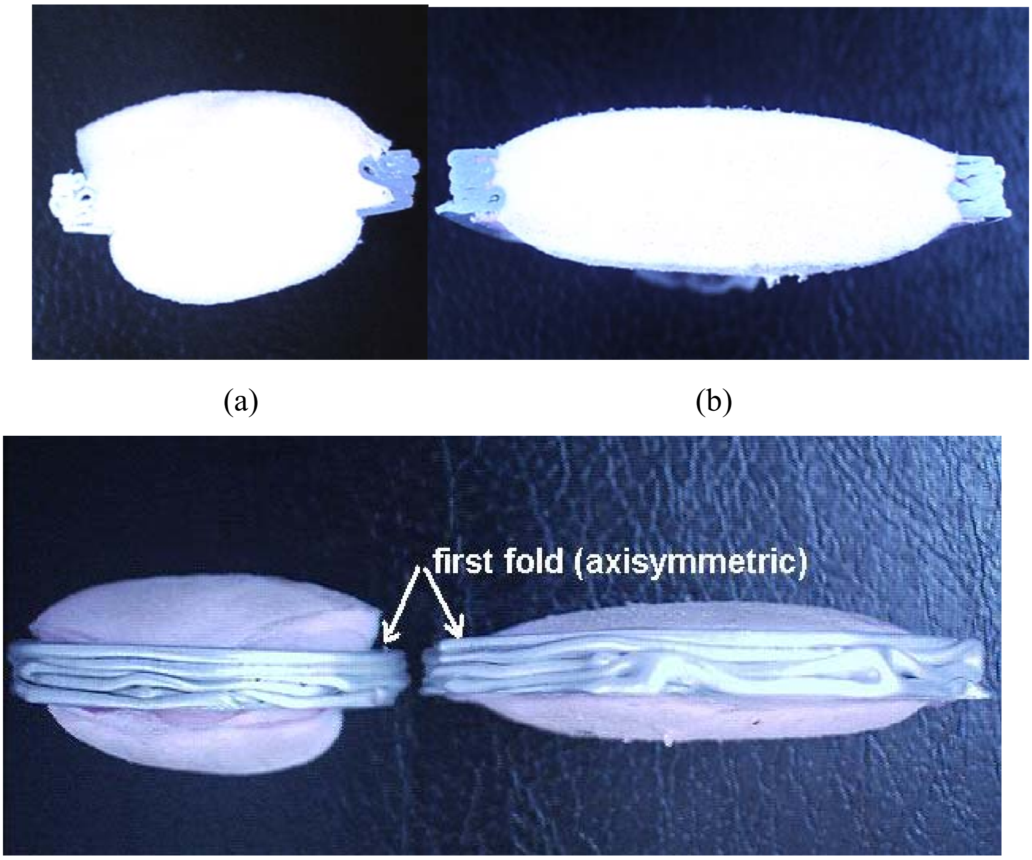

(a) (b)

(c) (d)

Figure 6.17 Mixed deformation mode of polystyrene foam filled tubes (a) interior view of 25 mm polystyrene foam filled tube (b) interior view of 35 mm polystyrene foam filled tube (c) exterior view of 25 mm polystyrene foam filled tube (d) exterior view of 35 mm polystyrene foam filled tube.

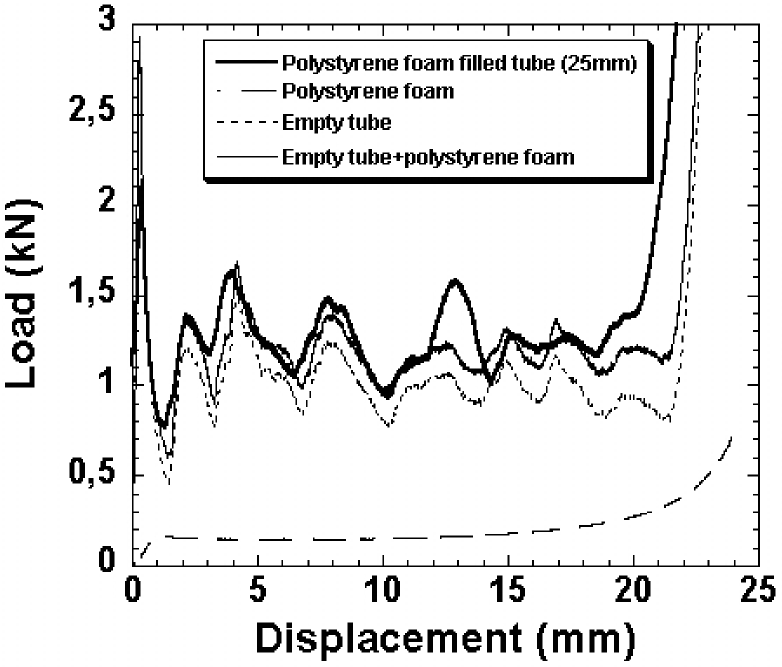

(a)

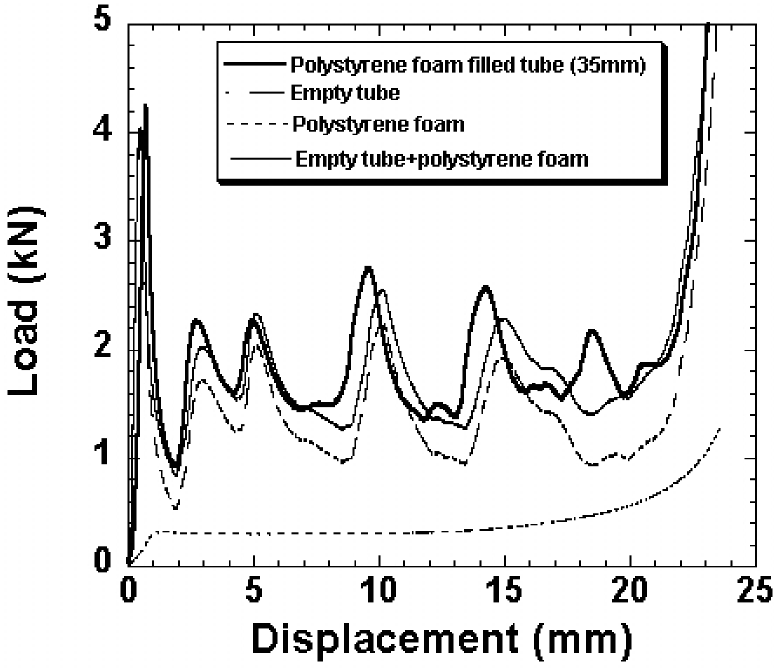

(b)

Figure 6.18 Load displacement curves of polystyrene foam (0.0321 g cm^{-3}) filled, empty and empty tube+foam a) 25 mm and b) 35 mm Al tube.

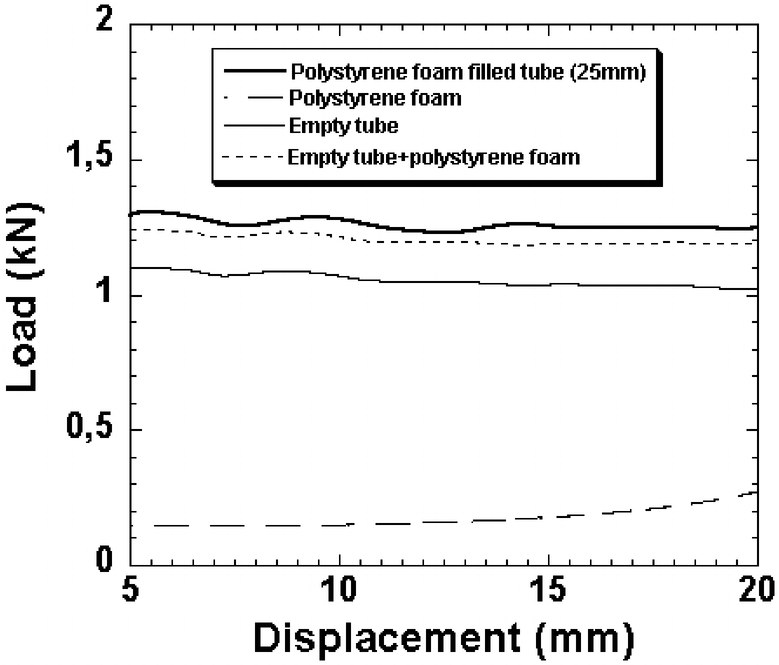

(a)

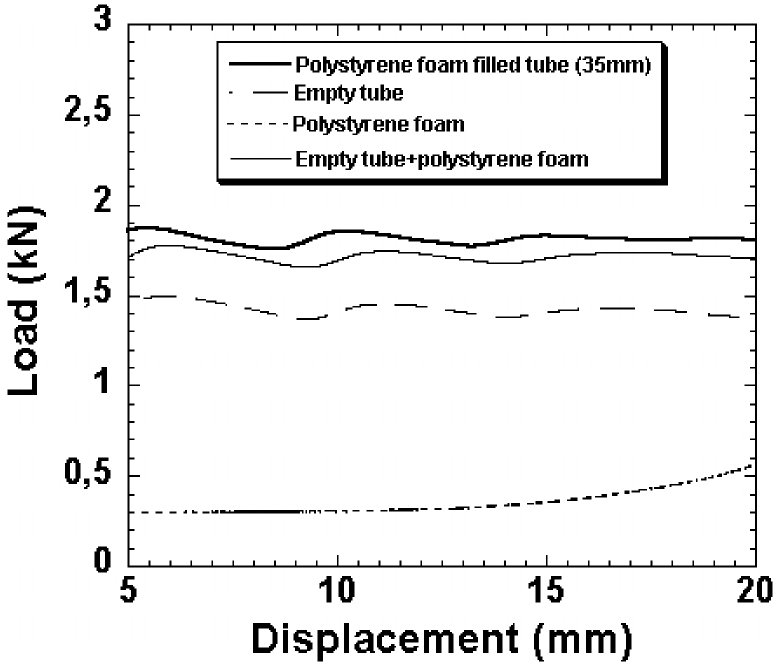

(b)

Figure 6.19 Comparison of average crushing loads of foam-filled, empty and empty tube+foam a) 25 mm and b) 35 mm Al tubes.

Table 6.3 Compression test results of single foam filled tubes

	Extrusion		**Foam**			**Foam filled tube response parameters**			
Test Code	**Tube diameter (mm)**	**Tube thickness (mm)**	**Foam type**	**Foam density (g.cm^{-3})**	**Average plateau stress (MPa)**	**Max force F_{max} (kN)**	**Mean force F_{avg} (kN)**	**Total number of lobes**	**Deformation type**
AFF-1	25	0.29	A	0.288	1.24	2.5516	2.2655	6	Concertina
AFF-2	25	0.29	A	0.2714	1.24	2.4531	2.0409	6	Concertina
AFF-3	25	0.29	A	0.3262	1.96	3.3516	2.699	6	Concertina
AFF-4	25	0.29	A	0.2962	1,24	2.8203	2.4126	6	Concertina
AFF-5	25	0.29	A	0.3633	1.96	3.3672	2.743	6	Concertina
AFF-6	25	0.29	A	0.3836	1.96	3.4297	2.9918	6-7	Concertina
AFF-7	25	0.29	A	0.3469	1.96	3.8359	3.0955	6	Concertina
AFF-8	25	0.29	A	0.2669	1.24	2.0234	1.85	5-6	Concertina
AFF-9	25	0.29	A	0.4353	2.44	3.8125	3.2988	6	Concertina
AFF-10	25	0.29	A	0.4414	2.44	4.6172	3.8594	6	Concertina
AFF-11	25	0.29	A	0.3679	1.96	2.6328	2.1533	6	Concertina
AFF-12	25	0.29	A	0.3882	2.44	3.7187	3.4195	5-6	Concertina
PFF1-1	25	0.29	P	0.0321	0.32	1.7281	1.2462	5-6	Mixed
PFF2-1	25	0.29	P	0.0321	0.32	1.2313	1.0170	4	Mixed
PFF3-1	25	0.29	P	0.0321	0.32	1.6297	1.2609	4	Mixed
PFF4-1	25	0.29	P	0.0321	0.32	1.6263	1.1788	4-5	Mixed
PFF5-1	25	0.29	P	0.0321	0.32	1.4875	1.1694	4	Mixed
PFF6-1	25	0.29	P	0.0321	0.32	1.5297	1.0891	4-5	Mixed
PFF1-2	35	0.35	P	0.0321	0.32	2.3797	1.8544	5	Mixed
PFF2-2	35	0.35	P	0.0321	0.32	2.13	1.5586	4	Mixed
PFF3-2	35	0.35	P	0.0321	0.32	2.6688	1.8368	5	Mixed
PFF4-2	35	0.35	P	0.0321	0.32	2.75	1.7778	5	Mixed
PFF6-2	35	0.35	P	0.0321	0.32	1.4766	1.6681	4	Mixed
PFF7-2	35	0.35	P	0.0321	0.32	2.4687	1.2789	5	Mixed
PFF8-2	35	0.35	P	0.0321	0.32	2.1328	1.8544	4	Mixed

6.5 Compression Behavior of Aluminum and Polystyrene Foam-Filled Bitubal Crush Elements

Three different types of tubular arrangements, composed of two tubes were prepared and tested. These are coded as BPH (interior: empty, exterior: polystyrene foam), BPP (interior: polystyrene foam, exterior: polystyrene foam) and BPA (interior: aluminum foam, exterior: polystyrene foam). Typical load-displacement and average crushing load-displacement curves of BPH samples are shown in Fig. 6.20(a) and (b), respectively. In BPH samples the exterior 35 mm and interior 25 mm tubes deformed in diamond mode as shown in Figure 6.21. The load and average crushing load-displacement curves of BPP samples also show an increase over the empty tube+foam (Fig. 6.22). The deformation mode of exterior 35 mm tube although remained to be diamond, the interior 25 mm tube deformation mode shifted to concertina as depicted in Fig. 6.23. In BPA samples, again the effect of foam-filling was found to be effective in increasing the load and average crushing load values of foam+empty tube (Fig. 6.24(a) and (b). The deformation modes of BPA samples are the same with those of BPP samples, exterior tube deformed in diamond while interior tube deformed in concertina mode (Fig.6.25).

Table 6.4 summarizes the geometrical and crushing parameters of bitubular sections.

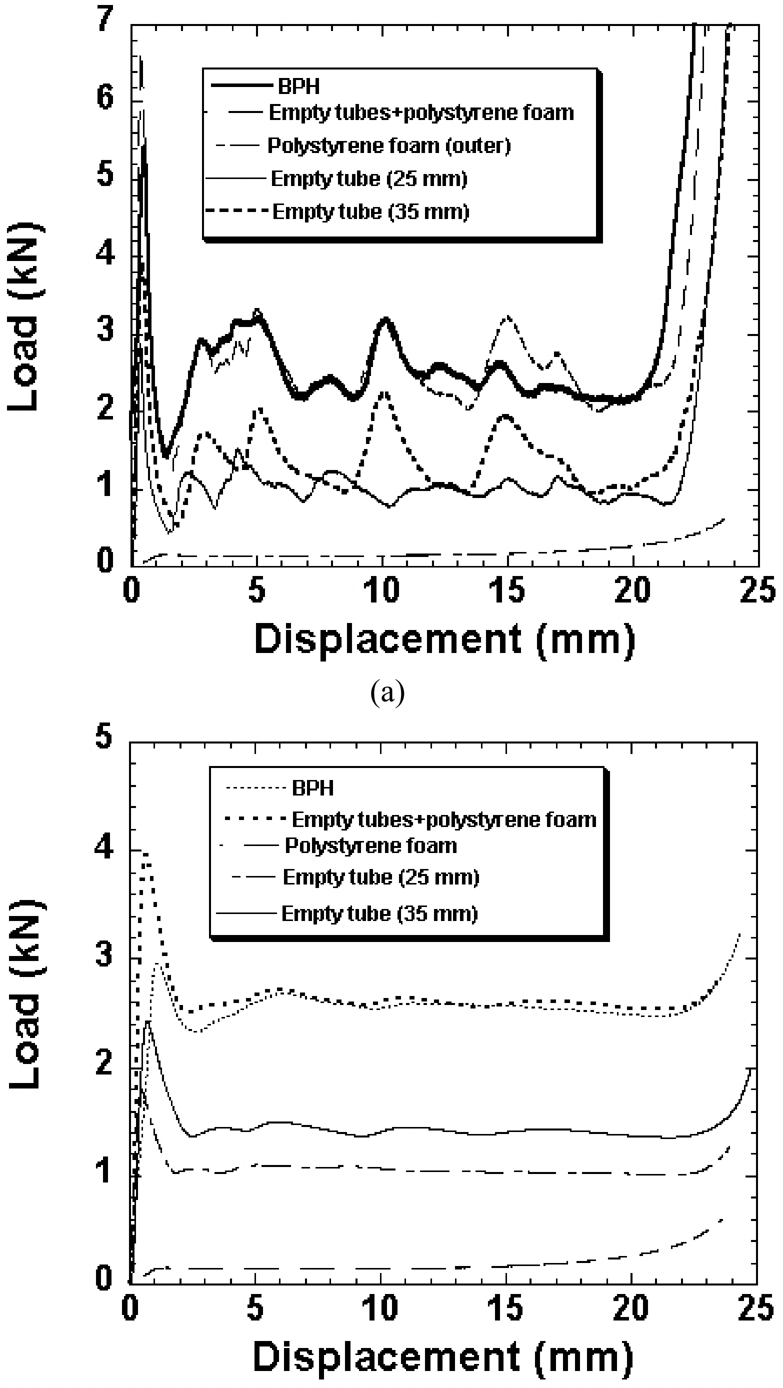

(a)

(b)

Figure 6.20 Typical (a) load-displacement and (b) average crushing load-displacement curves of BPH samples.

Figure 6.21 Crushed BPH series specimen

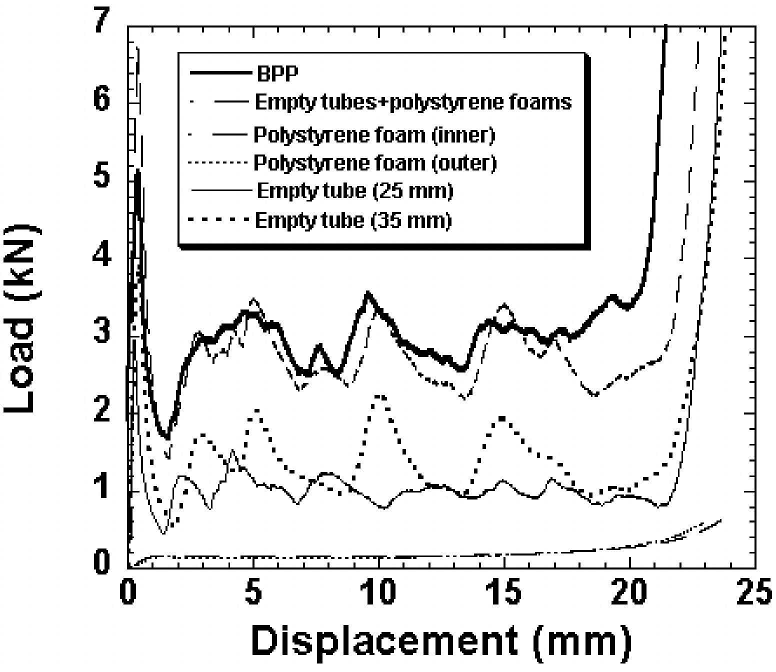

(a)

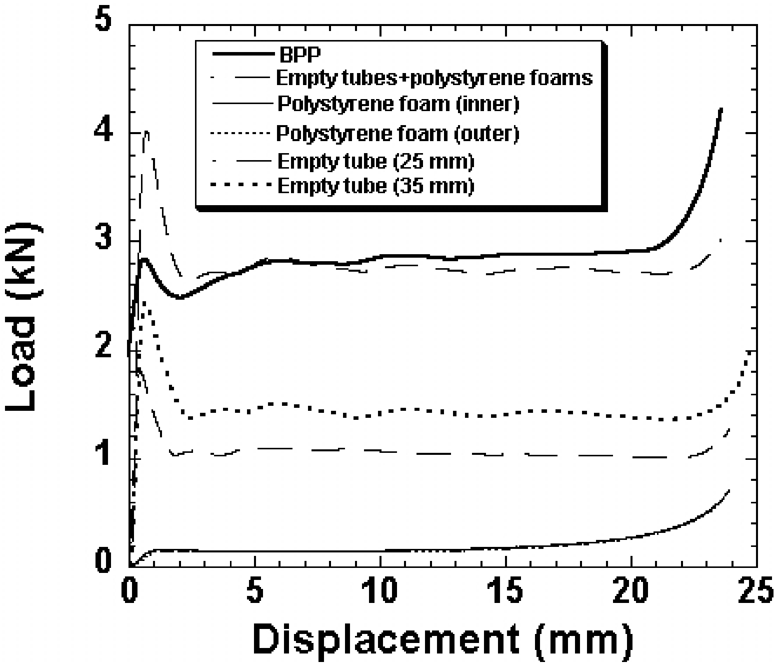

(b)

Figure 6.22 Typical load-displacement and average load-displacement curves of BPP samples.

Figure 6.23 Crushed BPP series specimen.

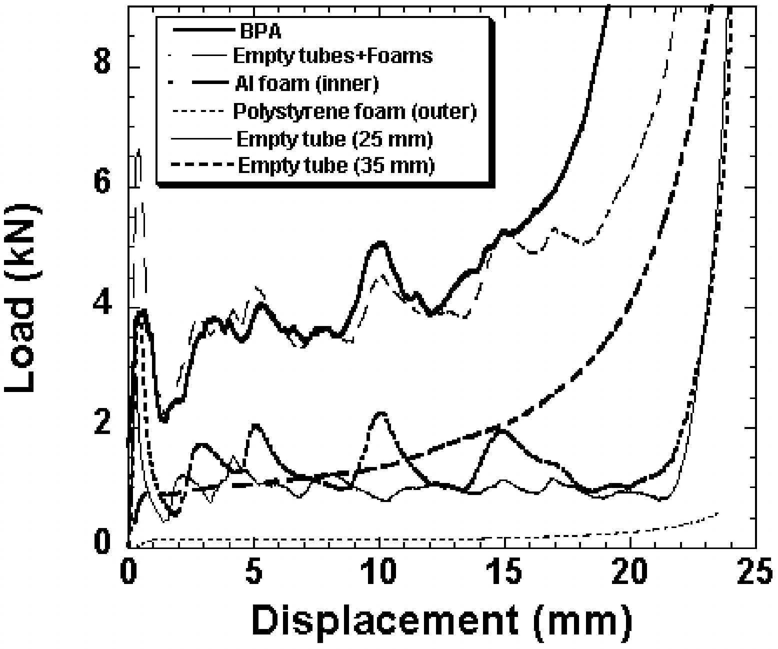

(a)

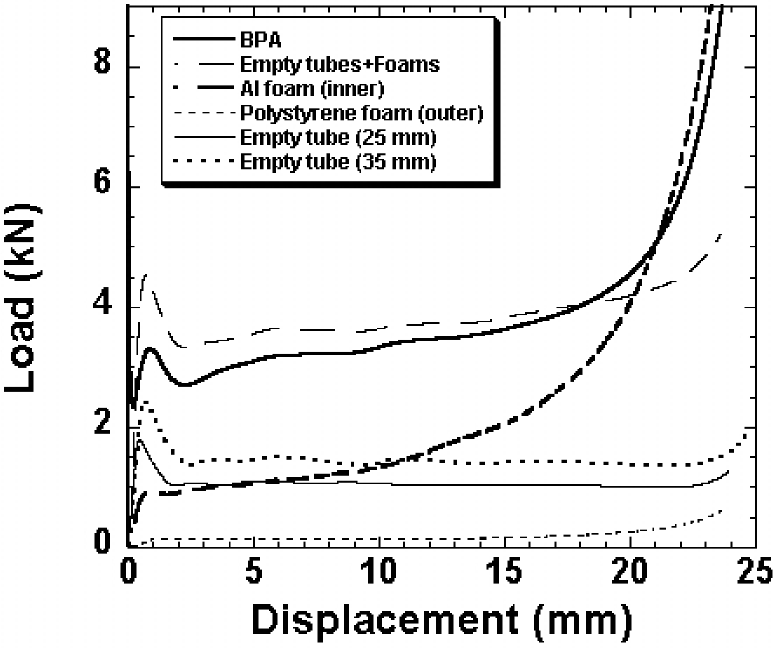

(b)

Figure 6.24 Typical (a) load-displacement and (b) average crushing load-displacement curves of BPA samples.

Figure 6.25 Crushed BPA series specimen.

Table 6.4 Compression test results of bitubal structures

	Extrusion		**Foam**						**Foam filled bitubal structure response parameters**			
				In		**-**	**Out**					
Test Code	**Tube diameter (in/out) (mm)**	**Tube thickness (in/out) (mm)**	**Foam type**	**Foam density (gr.cm^{-3})**	**Average plateau stress (MPa)**	**Foam type**	**Foam density (gr.cm^{-3})**	**Average plateau stress (MPa)**	**Max force F_{max} (kN)**	**Mean force F_{avg} (kN)**	**Total number of lobes (out)**	**Def. Type (in/out)**
BPA1	25 / 35	0.29/0.35	A	0.35	1.96	P	0.0321	0.32	4.5	3.743	4	C/D
BPA3	25 / 35	0.29/0.35	A	0.32	1.96	P	0.0321	0.32	5.17	4.053	4	C/D
BPA4	25 / 35	0.29/0.35	A	0.33	1.96	P	0.0321	0.32	5.27	3.588	4	C/D
BPP2	25 / 35	0.29/0.35	P	0.0321	0.32	P	0.0321	0.32	3.55	2.979	4	C/D
BPP3	25 / 35	0.29/0.35	P	0.0321	0.32	P	0.0321	0.32	3.54	2.973	4-5	C/D
BPP4	25 / 35	0.29/0.35	P	0.0321	0.32	P	0.0321	0.32	3.49	2.944	4	C/D
BPH1	25 / 35	0.29/0.35	-	-	-	P	0.0321	0.32	3.38	2.64	4	D/D
BPH3	25 / 35	0.29/0.35	-	-	-	P	0.0321	0.32	3.21	2.51	4	D/D
BPH4	25 / 35	0.29/0.35	-	-	-	P	0.0321	0.32	3.28	2.535	4	D/D

6.6. Compression Behavior of Hexagonal and Cubic Packed Empty and Aluminum Foam Filled Multi Tubes

Hexagonal and cubic packed empty multi-tubes deformed in diamond mode of deformation, similar to the single empty tubes (Figure 6.26 (a) and (b)). In Al foam-filled multi tube geometries, the deformation mode switched to concertina mode, the same as with that of foam-filled single tube (Figures 6.27 (a, b, c, and d).

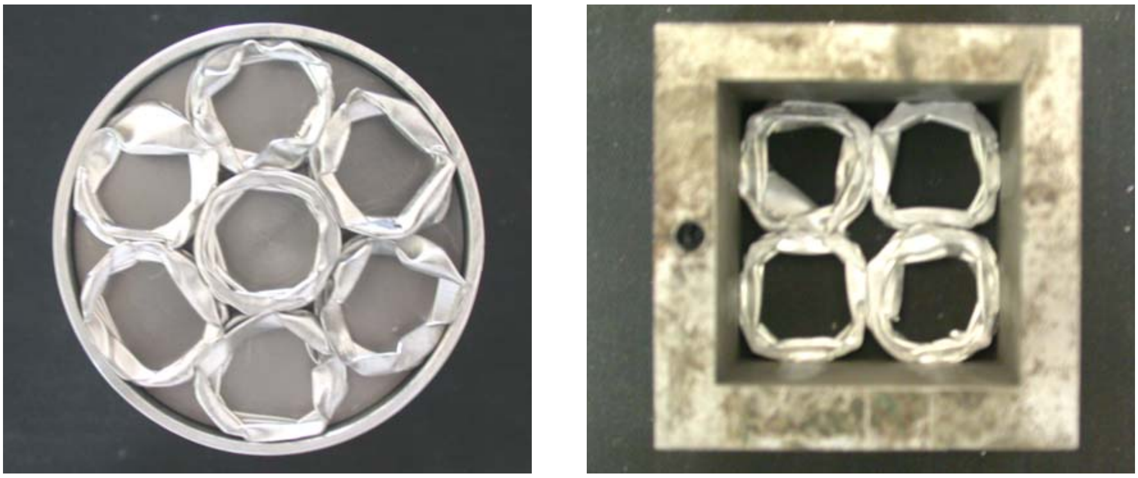

(a) (b)

Figure 6.26 Crushed empty multi-tubes (a) hexagonal packed empty multi tube design (MHE) (b) cubic packed empty multi tube design (MCE)

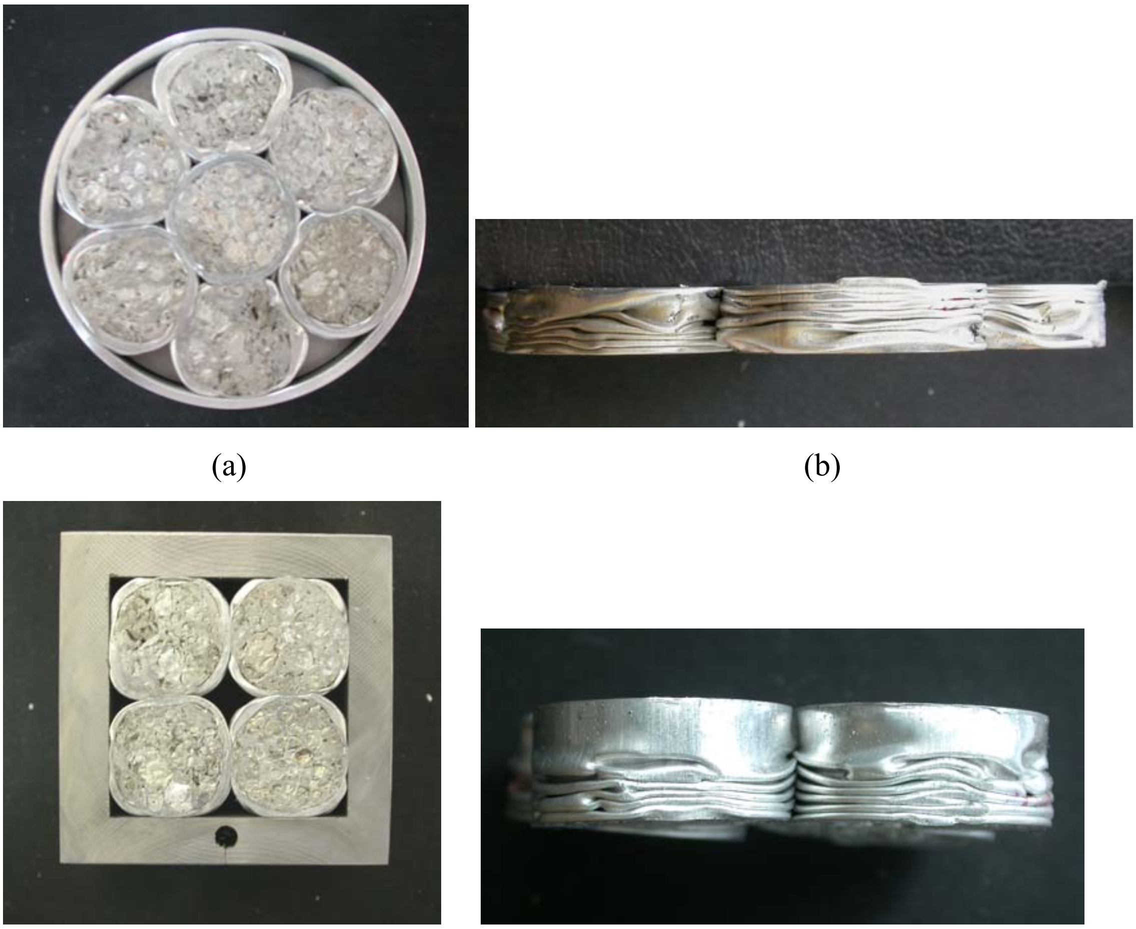

(a) (b)

(c) (d)

Figure 6.27 Crushed Al-foam filled multi tubes (a) MHF top, (b) MHF1 side, (c) MCF top and (d) MCF side views.

Typical load-displacement curves of hexagonal and cubic packed empty and foam-filled tubes are shown sequentially in Figures 6.28 (a) and (b). Dotted lines in these figures show the average crushing loads. As noted in these figures, as the density of Al foam filling increases the load values increase. The average crushing loads for each configuration of multi-tubes were further calculated between 3 and 20 mm displacements for the reason explained before. The crushing properties of foam-filled and empty multi-tube geometries of hexagonal and cubic packing are also tabulated in Table 6.5 and 6.6, respectively. Figure 6.29(a) and (b) compare the load-displacement curves of the sum of the seven empty tubes with empty hexagonal and cubic packed geometries load-displacement curves, respectively. The measured average crushing loads of empty multi-tube designs, both for MHE and MCE, are greater than the expected average crushing loads (number of tube x average crushing load of single empty tube (Figure 6.29 (a), (b)). The increase in average crushing load of multi-tube geometries of empty tubes are 0.92

kN for MHE design and 0.4 kN for MSE design. The increase in average crushing loads of empty multi tube designs simply a result of constraining effect and frictional forces between tubes and tube walls and the die wall. The effect is however greater in MHE design due to a large surface area of tubes touch to each other and to the surfaces of the die wall.

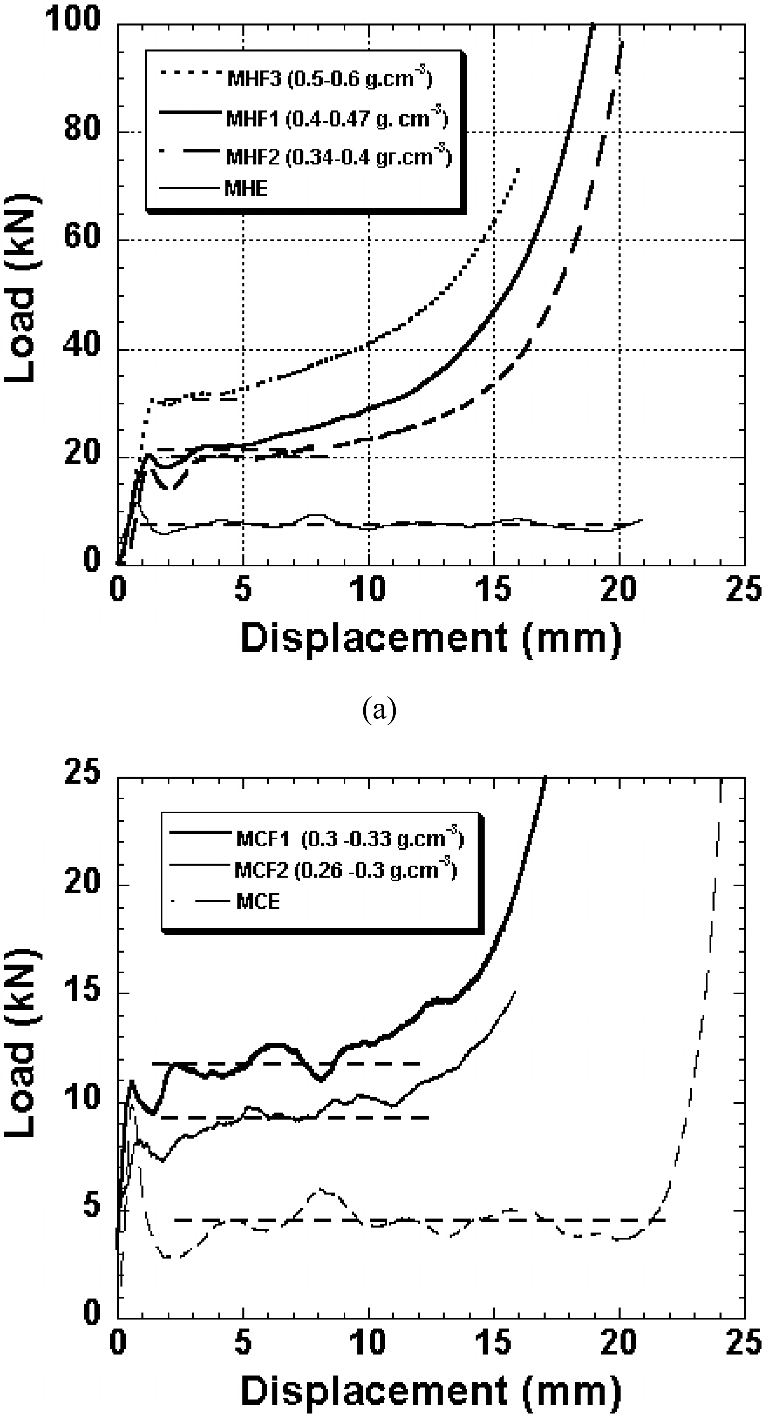

(a)

(b)

Figure 6.28 Load displacement curves (a) empty and al foam filled hexagonal multi tube designs (b) empty and al foam filled cubic multi tube designs.

Table 6.5 Compression test results of hexagonal packed empty end al foam filled multi tubes.

	Extrusion		**Foam**		**Multi tube response parameters**			
Test Code	**Tube diameters (mm)**	**Tube thickness (mm)**	**Foam type**	**Foam density range (g.cm^{-3})**	**Max force F_{max} (kN)**	**Mean force F_{avg} (kN)**	**Total number of lobes**	**Deformation type**
MHF1	25	0.29	A	0.4 - 0.47	30.375	24.818	6-7	Concertina
MHF2	25	0.29	A	0.34 - 0.4	24.508	21.117	6-7	Concertina
MHF3	25	0.29	A	0.5 – 0.6	34.633	31.772	6-7	Concertina
MHE1	25	0.29	-	-	9.1922	8.3278	4-5	Diamond
MHE2	25	0.29	-	-	9.45	7.7298	4-5	Diamond
MHE3	25	0.29	-	-	9.0766	7.5645	4-5	Diamond

A: Aluminum

Table 6.6 Compression test results of cubic packed empty end al foam filled multi tubes.

	Extrusion		**Foam**		**Multi tube response parameters**			
Test Code	**Tube diameters (mm)**	**Tube thickness (mm)**	**Foam type**	**Foam density range (g.cm^{-3})**	**Max force F_{max} (kN)**	**Mean force F_{avg} (kN)**	**Total number of lobes**	**Deformation type**
MCF1	25	0.29	A	0.30 - 0.33	12.914	11.936	7-8	Concertina
MCF2	25	0.29	A	0.28 - 030	10.359	9.4794	6-7	Concertina
MCE1	25	0.29	-	-	6.14	4.4428	4-5	Diamond
MCE2	25	0.29	-	-	6.04	4.4699	5	Diamond
MCE3	25	0.29	-	-	5.71	4.1805	4-5	Diamond

A: Aluminum

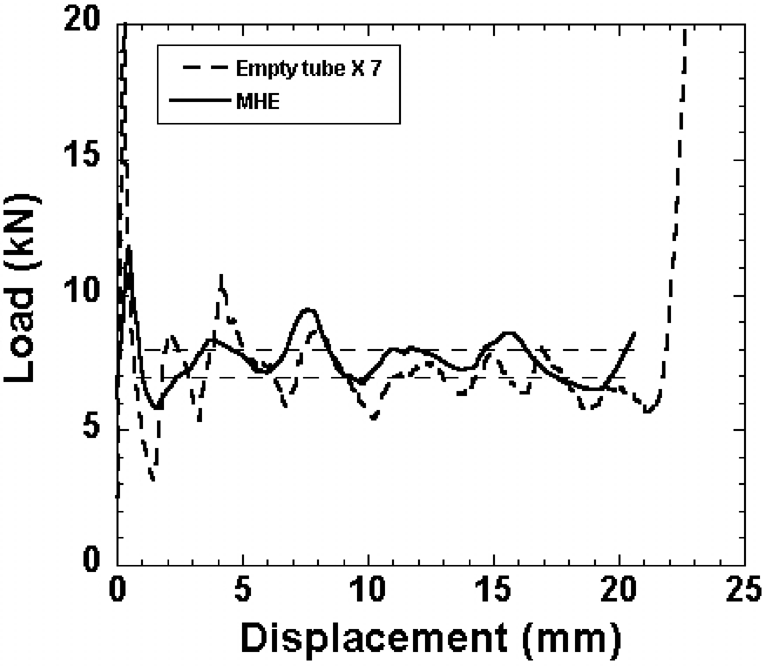

(a)

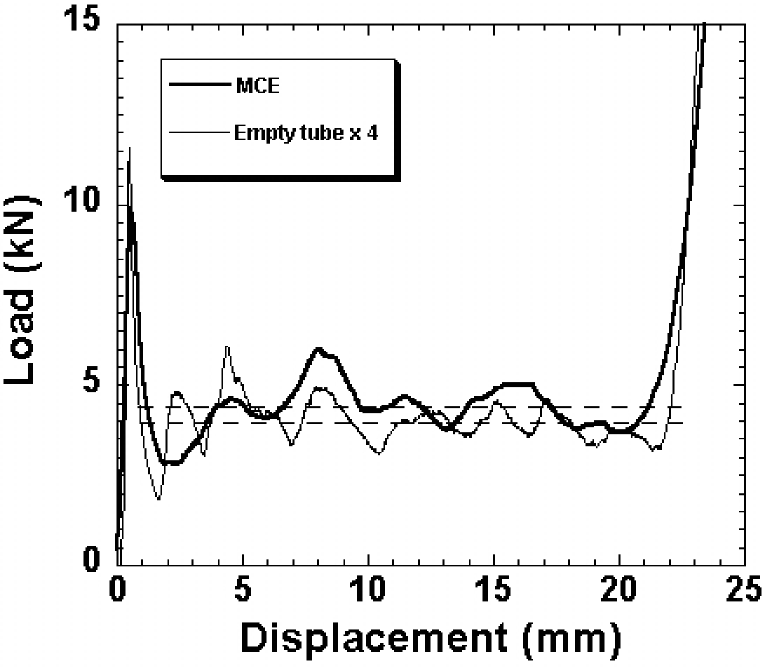

(b)

Figure 6.29 Load displacement curves of (a) MHE and its contributions (b) MCE and its contributions.

In foam-filled multi-tube geometries, the load values are also found to be higher than those of foam+tubes, showing the presence of interaction effect (Figure 6.30(a-d)).

In these foam filled multi-tube geometries the contributions to the crushing loads of the designs include (a) the sum of the empty tube crushing loads (7 multiplied by empty tube average crushing load for MHF design and 4 multiplied by empty tube average crushing load for MCF design), (b) the sum of foam plateau loads (7 multiplied by the plateau load of single foam for MHF design and 4 multiplied by plateau load of single foam for MCF design), (c) the sum of the strengthening load of the foam filled single tubes (7 multiplied by strengthening load of the foam-filled single tube for MHF design and 4 by multiplied by strengthening load of the foam-filled single tube for MCF design) and (d) the frictional loads between tubes, tube walls and die wall and constraining effect of die. The strengthening coefficient of single foam filled tubes is approximately 1.7 times of the foam plateau load (see section 6.5). The frictional loads between tubes and die walls and constraint effect of die itself is calculated by subtracting the contributions of a, b and c from the average crushing loads of filled multi-tube geometries as tabulated in Table 6.7. It is noted in Table 6.7, the frictional and constraining effects increase as the foam density increases for both designs.

Table 6.7 Average force addition of all elements placed in multi tube designs

Geometry	**Test code**	**Sum of the average crushing loads of empty tubes (kN)**	**Sum of the plateau loads of foam fillers (kN)**	**Sum of the strengthening load of the foam filled single tubes (kN)**	**Frictional forces between tubes and tube wall (kN)**	**Average crushing load (kN)**
Hexagonal	MHF1	6.9514	8.8361	7.304	1.7265	24.818
	MHF2	6.9514	7.182	6.0307	0.9529	21.117
	MHE	6.9514	-	-	0.9226	7.874
Cubic	MCF1	3.972	2.856	3.968	1.341	11.936
	MCF2	3.972	2.441	1.795	1.271	9.4794
	MCE	3.972	-	-	0.3924	4.3644

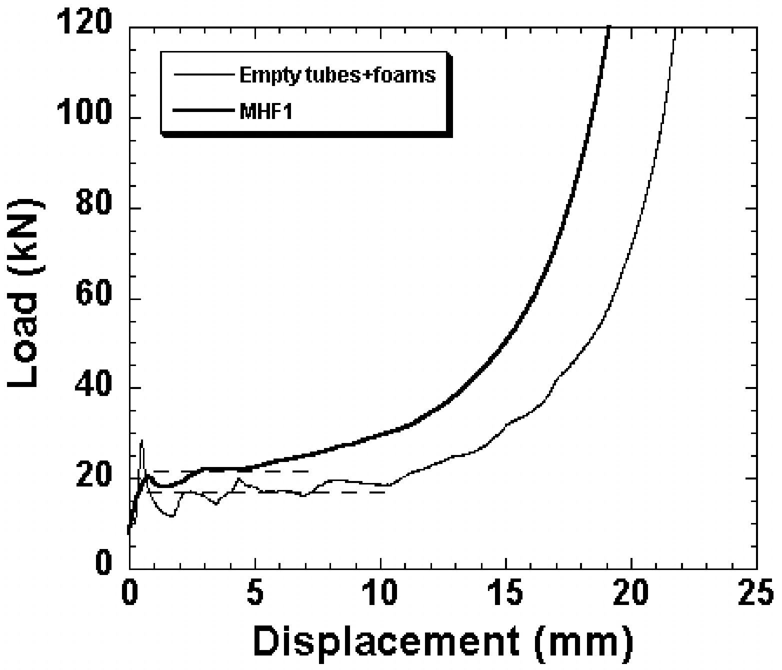
Empty tubes+foams
MHF1
Load (kN)
Displacement (mm)
0
20
40
60
80
100
120
0
5
10
15
20
25

(a)

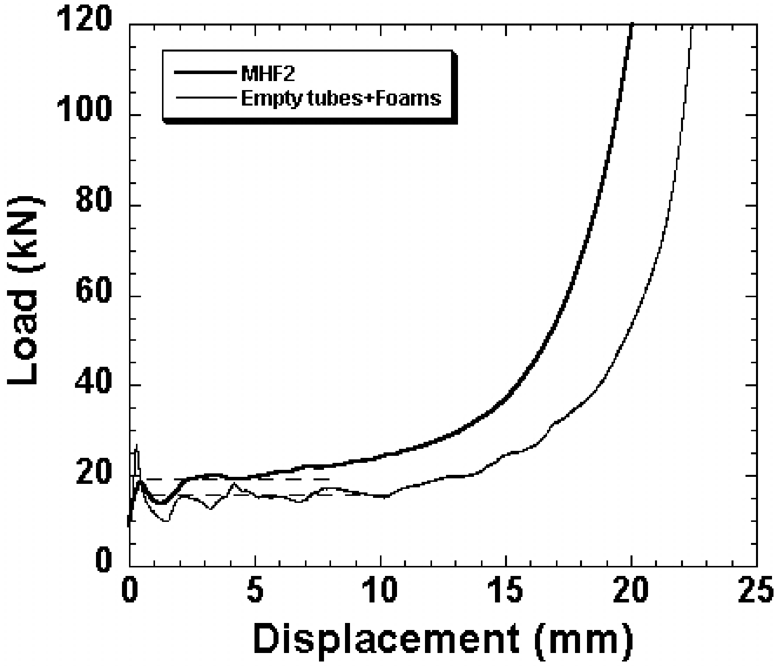
MHF2
Empty tubes+Foams
Load (kN)
Displacement (mm)
0
20
40
60
80
100
120
0
5
10
15
20
25

(b)

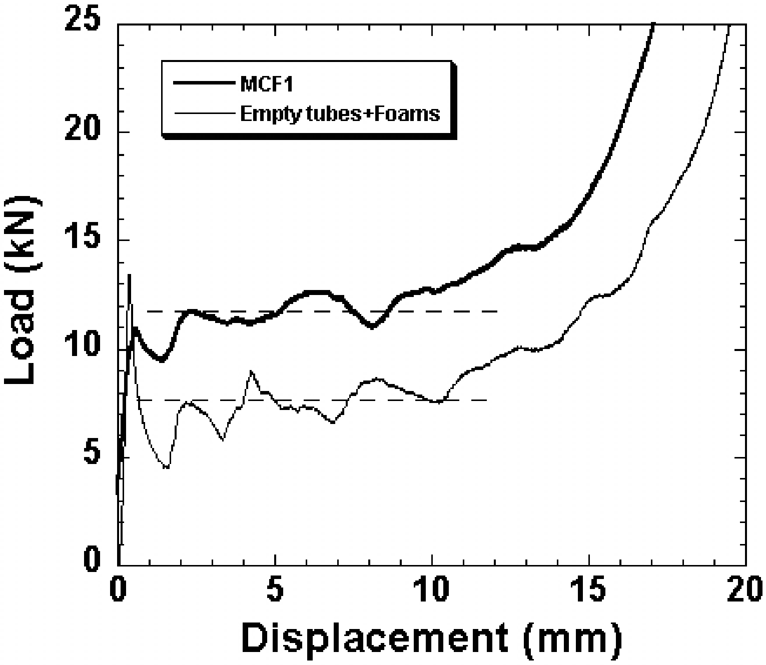

(c)

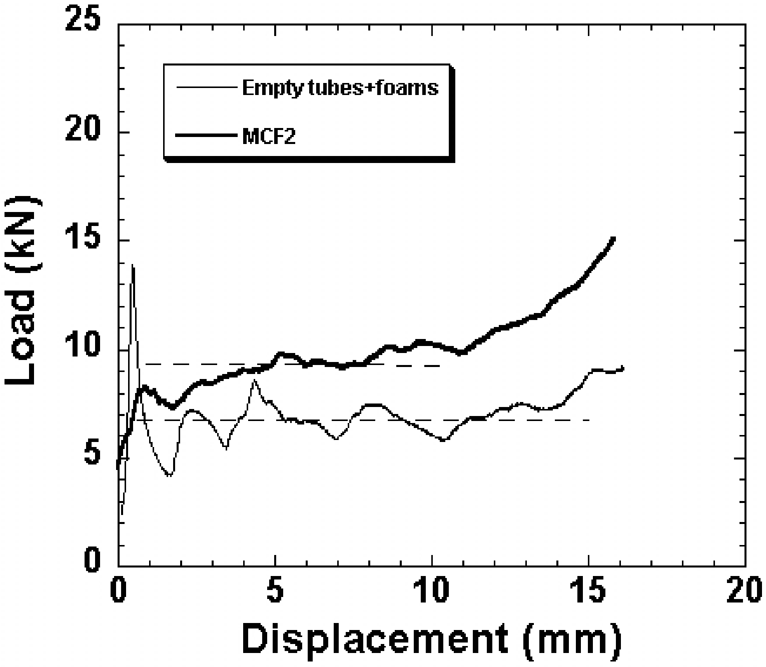

(d)

Figure 6.30 Comparison of load values of multi tube design and the sum of their contributions (a) MFH1 (b) MHF2 (c) MCF1 (d) MCF2.

6.7 Strengthening Coefficient of Foam Filling

The strengthening coefficients of foam filling can be expressed by modifying Equation 3.29 for circular tubes as;

$$C = \frac{P_{sf} - P_{se}}{P_f} \tag{6.4}$$

for single foam filled tubes,

$$C = \frac{P_{bf} - P_{be}}{P_f} \tag{6.5}$$

for bitubular structures and,

$$C = \frac{P_{mf} - P_{me}}{P_f} \tag{6.6}$$

Multi foam filled structures,

where P_{sf} , P_{bf}, P_{mf}, P_{se}, P_{be}, P_{me} and P_f are average crushing loads of foam filled single tube, foam filled bitubular structure, foam filled multi-tube, empty single tube, empty bitubular structure, empty multi tube and foam plateau load respectively.

The strengthening coefficient of single foam-filled tubes is predicted from Figure 6.32, on which increase in average crushing load in foam filled single tubes is drawn as function of foam plateau load. The strengthening coefficient of foam-filled single tubes is predicted to be 1.7 as shown in Figure 6.32 as the slope of the linear curve between the increase of average crushing load vs. foam plateau load. This value of strengthening coefficient is very similar to the previously determined strengthening coefficient value for square Al tubes (1.8) [48]. The strengthening coefficients of foam filling in bitubular and multi-tube geometries are tabulated in Table 6.8 together with empty tube average crushing load and foam plateau load. The strengthening coefficient of bitubular and multi-tube designs are greater than 1, proving the interaction between foam-filler and tube. The strengthening coefficients of bitubular and multi-tube geometries are also found to be greater than that of foam filled single tubes. The increased strengthening coefficient of multi tube designs simply arises from the frictional forces between individual tubes, tube walls and die wall and constraining effect of die. It is also noted the strengthening coefficient of bitubular geometries are also comparable with those of multi-tube geometries. Therefore, both designs can be used to increase the strengthening coefficients of foam-filled tubes. The foam density is found to increase the interaction coefficients in multi-tube designs. This is partly due to the interaction between the deforming individual tubes. In multi tube designs, besides the resistance of the filler to the folding of tube wall, the tube walls itself provides additional resistance to the adjacent deforming tube wall as shown in Figure 6.31 (a), for two adjacent deforming tube walls in hexagonal packed multi tube geometry. Moreover, at the tube wall-die wall contact regions, the folding occurred completely inward, through the filler which also provides additional strengthening in multi tube designs (Figure 6.31 (b)). Compared to single foam filled tubes (see Figure 6.31 (c)), in multi-tube geometries the fold length also reduced. The deformation of multi tube designs are complex and the contributions of several different mechanism to the average crushing load are not known. Further experimentation and microscopic studies will therefore conducted in order to identify the deformation mechanism more clearly and to calculate the extent of contributions of each mechanism to the average crushing load.

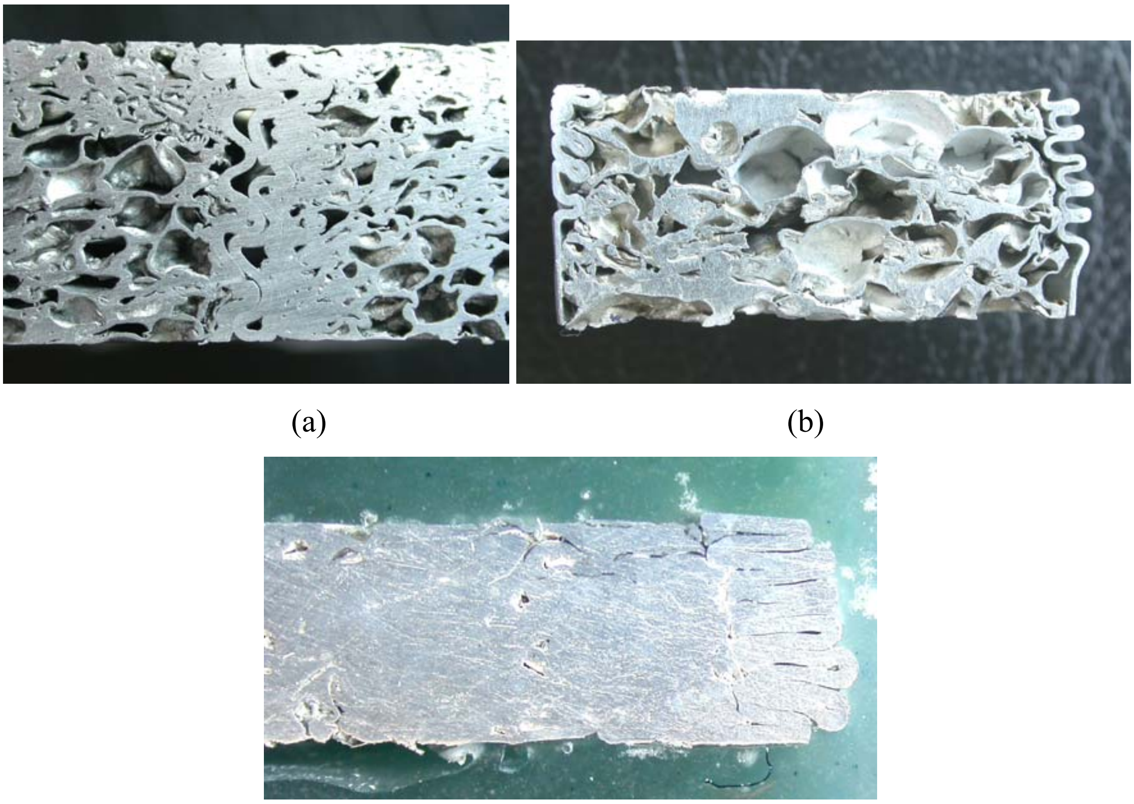

(a) (b)

(c)

Figure 6.31 (a) neighboring tubes in hexagonal packed multi tube geometry (b) al foam filled tube taken from cubic packed design (c) crushed al foam filled single tube

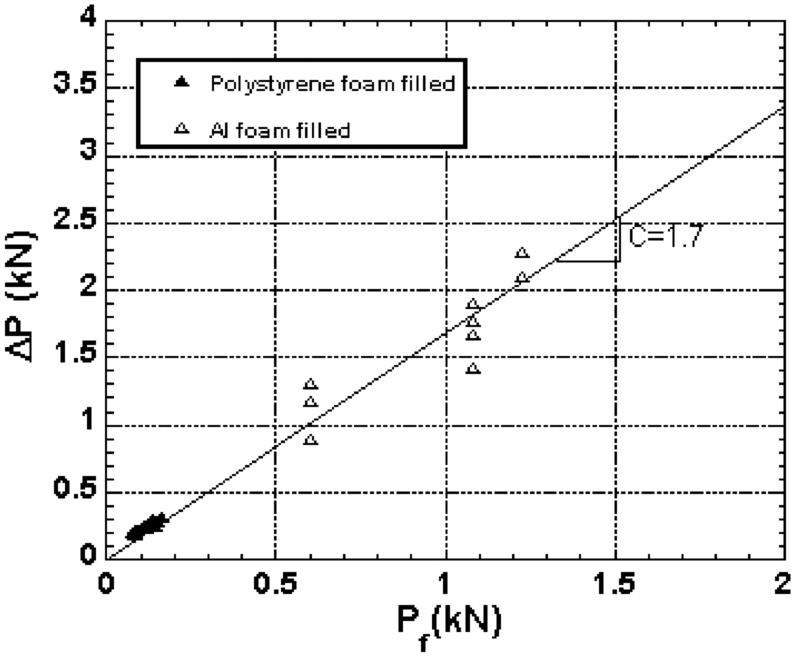

Fig. 6.32 The strengthening load *vs.* foam plateau load of foam filled single tubes.

Table 6.8 Strengthening coefficients of bitubular and multi tube geometries.

Element	Average crushing load (kN)	Empty tube average crushing load (kN)	Average foam plateau load (kN)	Strengthening Coefficient
BPH	2.56	2.243	0.14	2.26
BPP	2.96	2.243	0.29	2.47
BPA	3.79	2.243	0.854	1.81
MHF1 (0.40-0.47 g.cm^{-3})	24.81	7.874	8.836	1.91
MHF2 (0.35-0.40 g.cm^{-3})	21.11	7.874	7.182	1.84
MHF3 (0.5-0.6 g.cm^{-3})	31.77	7.874	10.08	2.37
MCF1 (0.30-0.33 g.cm^{-3})	11.93	4.364	2.856	2.65
MCF2 (0.26-0.30 g.cm^{-3})	9.47	4.364	2.441	2.09

6.9 Specific Absorbed Energy (SAE)

The SAE's of Al-foam filled single tubes are found to be lower than that of empty tube (Figure 6.33 (a-c)) until about the displacements of 20 mm. Thereafter, foam filling becomes more efficient than empty tube. This is mainly due to the increase of the foam density with deformation. It was previously shown that there is a critical total tube mass and the corresponding critical foam density above which the use of foam filling becomes more efficient than empty tube [56, 57]. The critical total mass should be however determined using the tube wall-thickening of empty tube. Three plastic hinge models of Alexander [27], Singace *et al.* [34] and Wierzbicki *et al.* [32] were used to predict the average crushing load of the empty tube as function of the tube wall thickness. These models are given sequentially as:

$$P_a = \sigma_o t^2 \left[8.462 \left(\frac{R}{t} \right)^{1/2} + 1.814 \right] \tag{6.7}$$

$$P_a = \sigma_o t^2 \left[7.874 \left(\frac{R}{t} \right)^{1/2} + 1.408 \right] \tag{6.8}$$

$$P_a = 11.22 \sigma_o t^2 \left(\frac{R}{t} \right)^{1/2} \tag{6.9}$$

where σ_o, t and R are the mean stress from yield point to failure, thickness and mean tube radius, respectively.

The foam plateau stress (σ_{pl}) is found to be well fitted with power-law of strengthening equation,

$$\sigma_{pl} = K\rho^n \text{ (MPa)} \tag{6.10}$$

where K and n are constants and ρ is the foam density in g cm^{-3}. The values of K and n are ~8.63 (MPa) and ~1.47, respectively.

The value of σ_o for the studied tube material was determined from the tension tests and found nearly 141 MPa. In the calculations, the inner radius of the tube was taken as constant (12.21 mm) while the thickness of the tube increased from 0.29 to 6 mm. The calculated specific energy absorption of empty tubes using Eqns. 6.7, 6.8 and 6.9 is shown in Fig. 6.34 as a function of total mass of the tube. For the tested empty tube, Eqn. 6.9 estimates well the specific energy absorption and, therefore, calculations of Al foam filled tube specific energies were based on the average crushing load of the tube estimated by Eqn. 6.9. Foam filling along with an adhesive was previously shown to be used to tailor the specific energy absorption capacity of the filled tubes by increasing the level of interaction effect. The use of adhesive can contribute to the specific energy absorption of the tube by two mechanisms, namely, increased load transfer from tube wall to the foam core and peeling of the adhesive. The value of C in the bonded case (adhesive) was found to be 2.8 [48]. Using Eqn. 3.29 with C values corresponding to bonded and unbonded cases, Eqn. 6.9 for the empty tube average crushing load and Eqn. 6.10 for the Al foam plateau load, the specific energy absorptions of Al foam filled tubes were calculated and also plotted as function of total mass in Figure 6.34. It can be inferred from Fig. 6.34 that within the investigated wall thickness range, for bonded and unbonded cases, there appears no critical total mass (or Al foam density) above which the foam filling is more favorable than thickening of the tube wall. This is partly due to relatively low plateau stresses of Al foam studied. In order to estimate the effect of increasing foam plateau stress on the specific energy absorption, the parameters of Eqn. 6.10 were changed for a stronger Al foam, 6061 Al, (K=22.4 (MPa) and n=1.99), which was previously studied by Toksoy *et. al* [57]. The predicted specific energy absorption of 6061 Al foam filling for unbound case is also shown in Fig. 6.34. In this case, the critical mass and hence foam density (0.6 g cm^{-3}) is clearly seen in Fig. 6.34, proving the effect of foam plateau load on the efficiency of foam filling. A similar critical total mass has been previously found in Al foam filled tubes [56, 57].

The present experimental results and predictions of energy absorptions using the strengthening coefficient of foam filling clearly demonstrate that although foam filling resulted in a higher energy absorption than the sum of the energy absorptions of the tube alone and foam alone, it might be not always more effective in increasing the specific energy than simply thickening the tube walls. Therefore, for efficient foam filling an appropriate foam-tube combination must be selected by considering the magnitude of strengthening coefficient of foam filling and the foam filler plateau load.

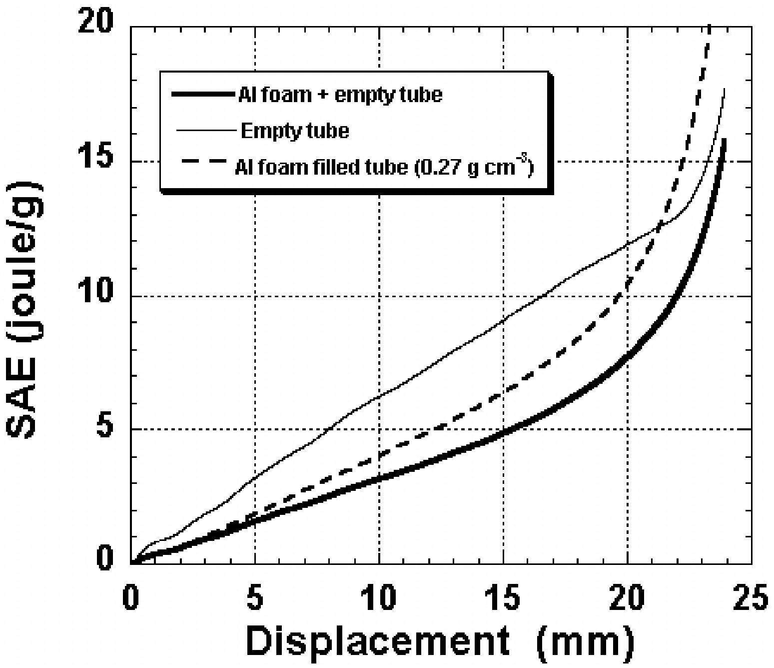
SAE (joule/g)
Displacement (mm)
Al foam + empty tube
Empty tube
Al foam filled tube (0.27 g cm^{-3})
0
5
10
15
20
25

(a)

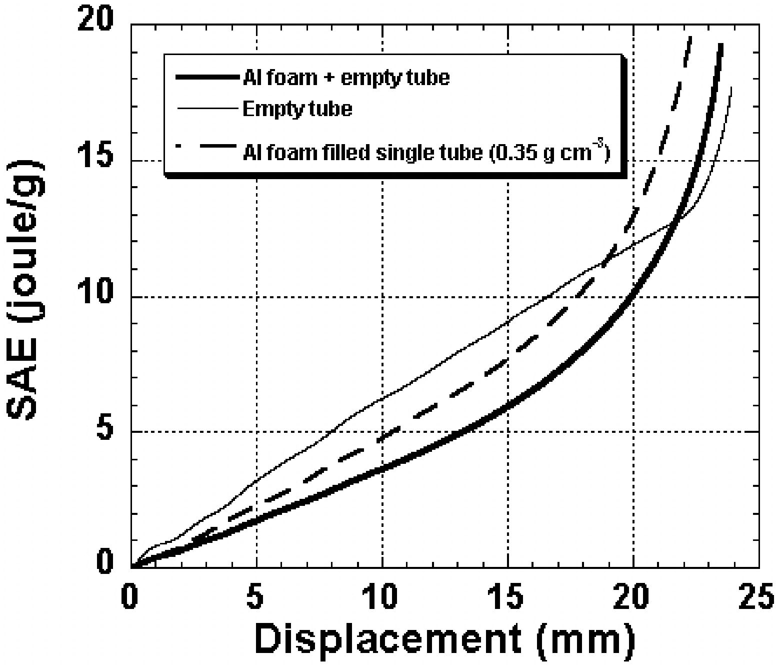
SAE (joule/g)
Displacement (mm)
Al foam + empty tube
Empty tube
Al foam filled single tube (0.35 g cm^{-3})
0
5
10
15
20
25

(b)

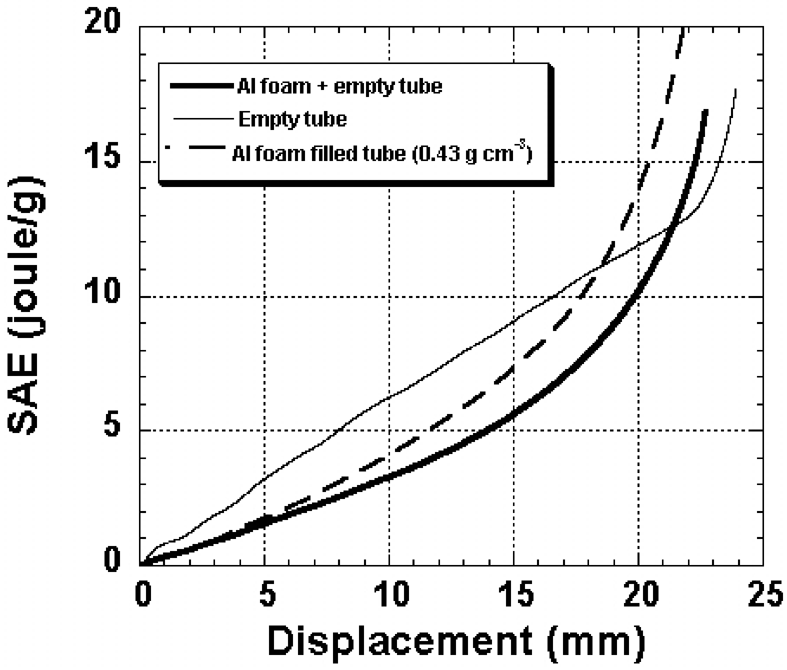

(c)

Figure 6.33 SAE vs. displacement curves of (a) 0.27 g.cm^{-3} al foam filled single tube (b) 0.35 g.cm^{-3} al foam filled single tube (c) 0.43 g.cm^{-3} al foam filled single tube.

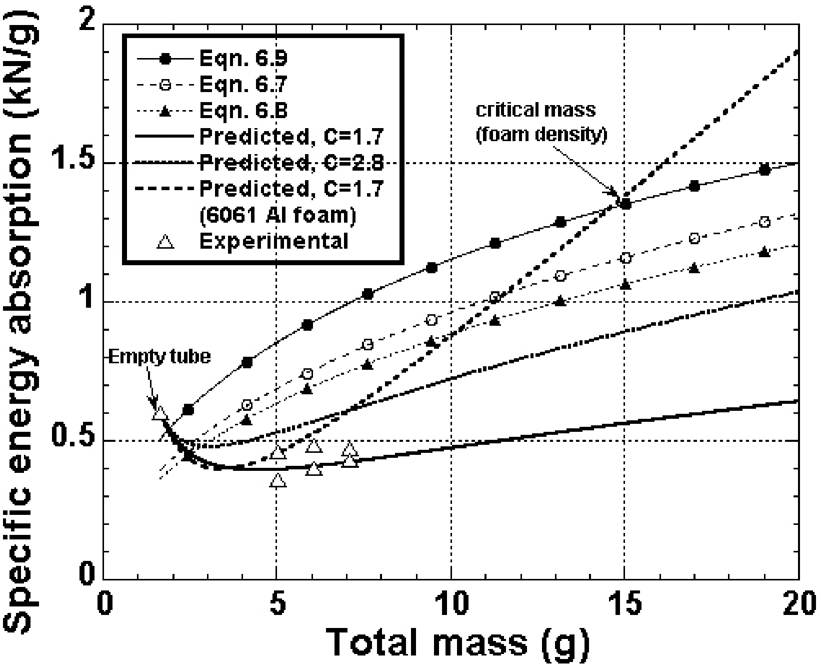

Figure 6.34 Predicted and experimental specific absorbed energy *vs.* mass in empty and Al foam filled tubes.

The SAE's of bitubular tubes are also lower than those of single tube as shown in Figure 6.35. Again the foam density used is not effective in increasing SAE above that of empty tubes. As noted in Figure 6.35, BPA samples show increased energy absorptions at higher displacements due to the densification of the Al-foam filler.

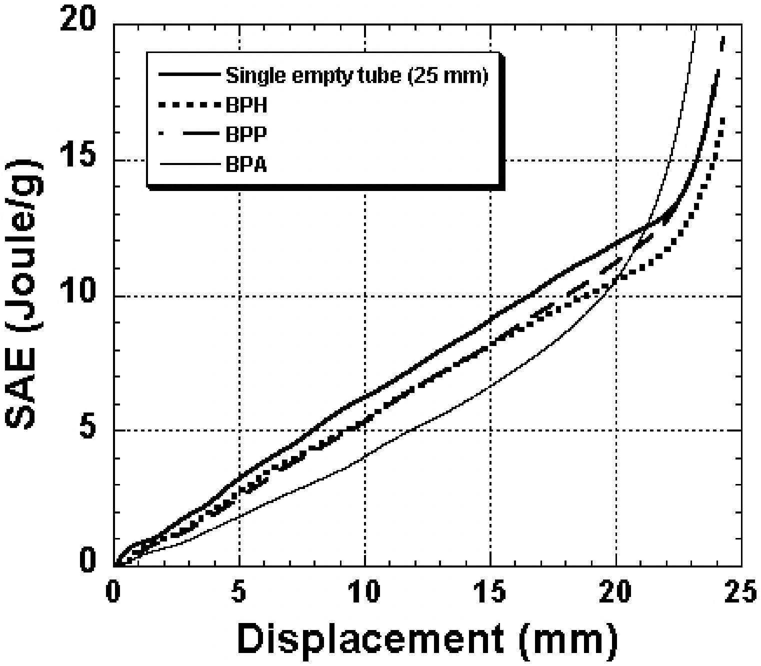

Figure 6.35 Comparison of SAE of empty tube and bitubal structures.

The SAE's of multi-empty tube geometries are however found to be higher than those of empty tubes as shown in Figure 6.36. This is mainly due to frictional effects of die wall and interactions between individuals tubes. The SEA is further found to be higher in MCE designs due to higher contact areas in this design between tubes and die wall. The foam filling of multi tube designs are not effective increasing SAE over the empty tube (Figure 6.37). However at similar foam filler densities multi-tube geometries are more energetically effective than single Al foam filled tubes for both hexagonal and cubic packed geometries. Note that also as the deformation increases, foam filling of multi-tube designs become energetically more efficient as compared with empty and foam–filled single tubes. This is due to increased frictional forces between tube walls and die walls.

The SAE's of multi-filled tube geometries are found to be higher than those of al foam filled single tubes having similar densities as shown in Figure 6.38.

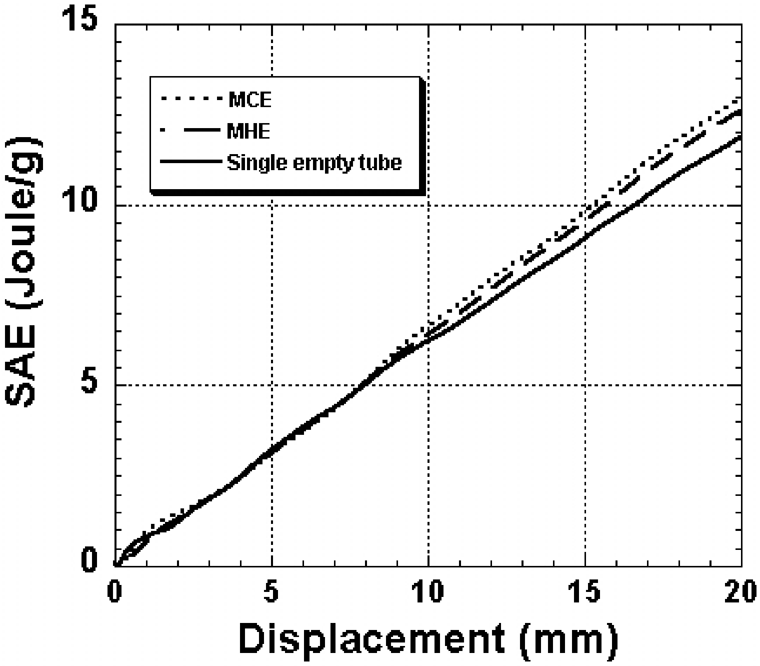

Figure 6.36 Comparison of SAE of empty tube and multi empty tubes.

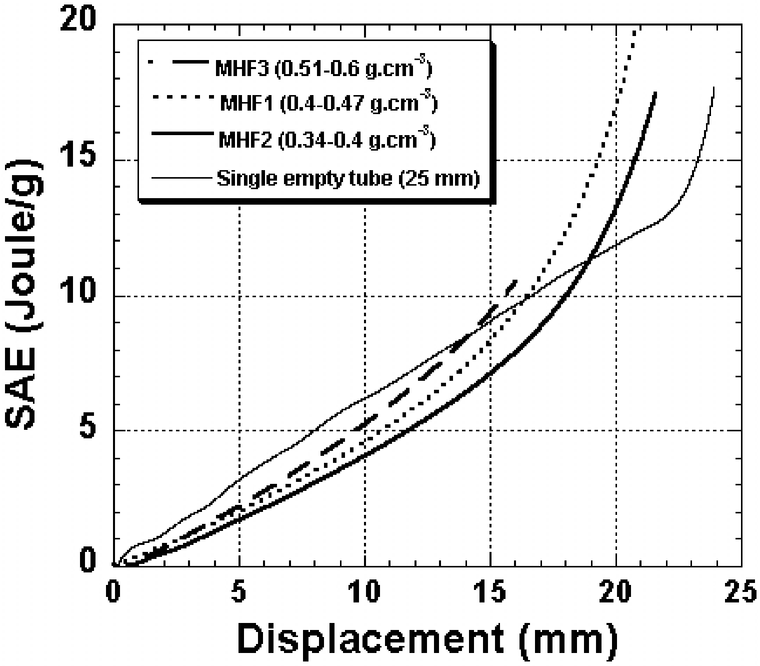

(a)

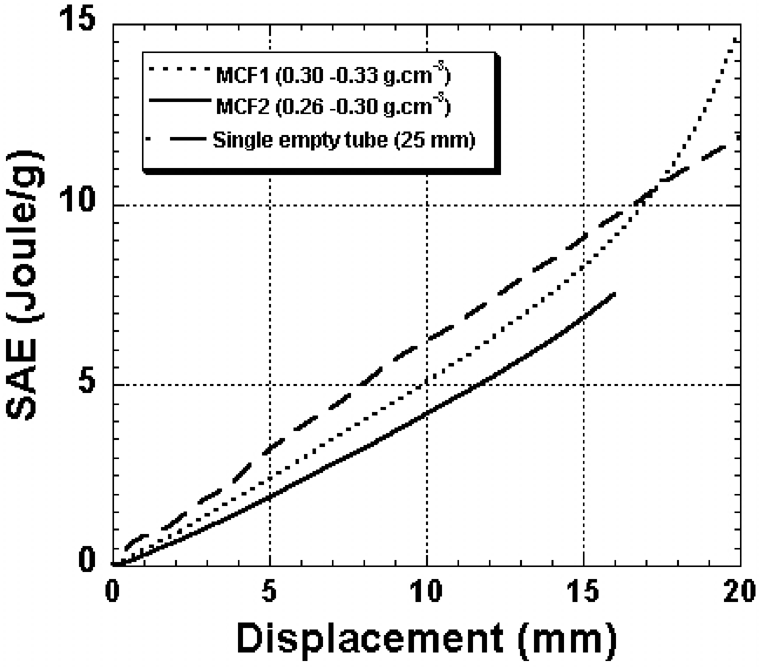

(b)

Figure 6.37 Comparison of SAE (a) empty tube vs. MHF designs (b) empty tube vs. MCF designs.

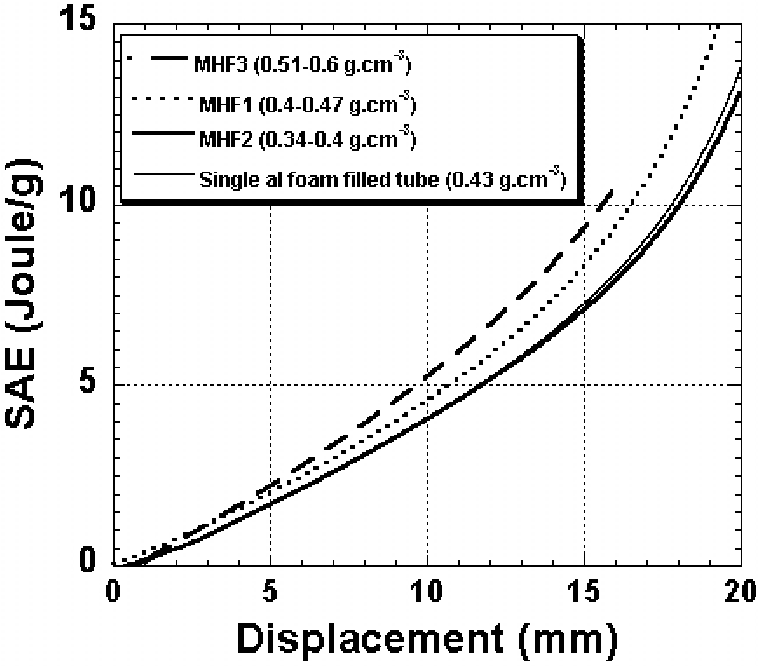

(a)

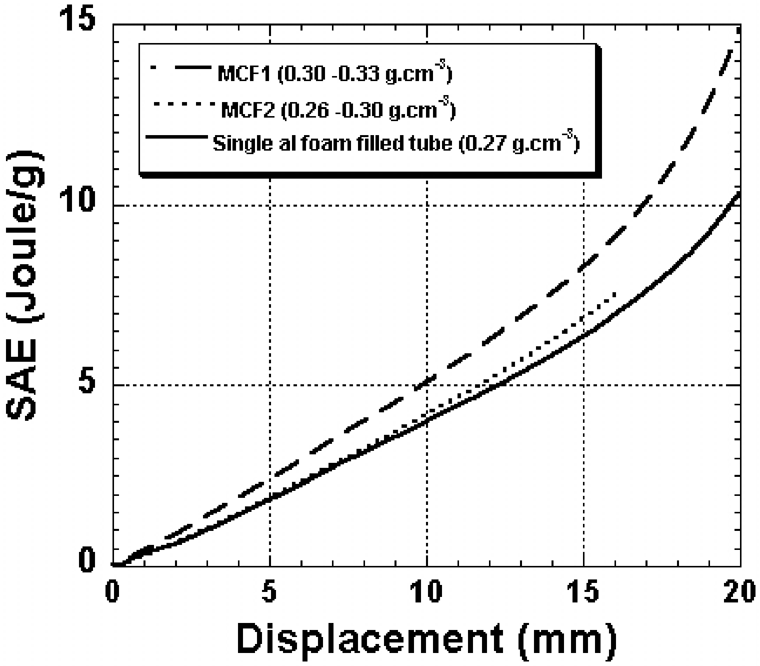

(b)

Figure 6.38 Comparison of SAE (a) single al foam filled tube vs. MHF designs (b) single al foam filled tube e vs. MCF designs.

Chapter 7

CONCLUSIONS

In this study static crushing behavior of Al and polystyrene foam-filled bitubular and multi-tube geometries were investigated through compression testing. Multi-tube designs included hexagonal and cubic packed Al-foam filled tube geometries. The Al-closed-cell foam fillers were prepared in house using the foaming from powder compact process. In order to compare the crushing behavior of bitubular and multi-tube geometries, empty and foam filled single tubes were also prepared and tested under the same conditions. Two different deep drawn Al tubes having 25 and 35 mm outer diameters and similar wall thicknesses were used to construct bitubular tube geometries while 25 mm tubes were used in multi-tube geometries. Based on experimental results and predictions, followings can be concluded;

1. Al empty tubes deformed in diamond mode of deformation while Al foam filling reverted the deformation mode of single tubes from diamond into concertina. In polystyrene foam-filled tubes the deformation mode switched into mixed and/or concertina. The change of deformation mode of tubes when filled with foam was due to the wall thickening effect of foam filling.
2. The effects of foam filling in single tubes were (a) to increase the average crushing load over that of the tube (alone) + foam (alone), known as interaction effect and (b) to decrease the fold length. Similar effects of foam filling were also found in bitubular geometries. structures,
3. Empty multi tube geometries, both hexagonal and cubic packed, deformed in diamond mode of deformation while Al foam filling changed the deformation mode into concertina. In empty multi tube geometries the average crushing load values were however higher than that of the sum of the average crushing loads of equal number of single tubes. The increase in average crushing loads of empty tube geometries was solely due to the frictional forces between adjacent tubes walls, tube walls and die wall and constraining effect of the die itself. The effect was however greater in hexagonal packed design due to more contact

surfaces between adjacent tubes and tube walls and die wall. In foam filled multi-tube geometries, the load values were also found higher than those of foams+tubes, showing the presence of interaction effect. The effect of increasing filler density in these tubes was to increase the crushing loads.

4. The strengthening coefficient of foam filling in single tubes was extracted 1.7. This value of strengthening coefficient was also very similar to the previously determined strengthening coefficient value for square Al tubes (1.8). The strengthening coefficients of bitubular and multi-tube geometries were however shown to be greater than that of foam filled single tubes.
5. The strengthening coefficients of bitubular geometries were comparable with those of multi-tube geometries. Therefore, both designs can be used to increase the strengthening coefficients of foam-filled tubes. The foam density was found to increase the interaction coefficients in multi-tube designs.
6. Although foam filling resulted in higher energy absorption than the sum of the energy absorptions of the tube alone and foam alone, it was found to be not more effective in increasing the specific energy than simply thickening the tube walls. For effective foam filling, an appropriate tube-foam combination must be selected based on the strengthening coefficient of foam filling and the plateau load of foam filler. For efficient foam filling the foam plateau load should be higher than a critical value.
7. The foam filling in multi tube designs were not effective in increasing SAE over the empty tube, however at similar foam filler densities multi-tube geometries were energetically more effective than single Al foam-filled tubes for both hexagonal and cubic packed geometries. This was due to the frictional loads of the multi-tube designs.

REFERENCES

[1] Ş.Akkaya, H.Altıntaş, “Statistical analysis of highways traffic accidents in Turkey: 1989-1999”, V. Ulusal Ekonometri ve İstatistik Sempozyumu, Çukurova University, 19-22 September 2001,Conference Proceeding.

[2] J. T.Wood, "Production and applications of continuously cast foamed aluminum", Fraunhofer USA Metal Foam Symposium, J. Banhart and H. Eifert Edn. Stanton, Delaware, 7-8 Oct. 1997.

[3] US Patent, 4973358.

[4] L. J. Gibson and A. E. Simone, "Aluminum foams: structure and properties", Mechanics and materials seminar, 3 April, 1997.

[5] O. Prakash, H. Sang, J. D. Embury, "Structure and properties of Al-Si foam", Mater. Sci. Eng., A199, 1995, 195-203.

[6] T. Miyoshi, M. Itoh, S. Akiyama, A. Kitahara, "Alporas aluminum foam: production process, properties, and applications", Adv. Eng. Mater., 2, 2000, No:4 179- 183.

[7] J. Banhart, "Metallic foams: challenges and opportunities", Eurofoam 2000, MIT-Verlag, Bremen, 2000, 13-20

[8] J. Banhart, "Production Methods for Metallic Foams", Fraunhofer USA, Metal Foam Symposium, Symposium Proceedings, Delaware, Oct. 7-8, 1997, Verlag Pub. Bremen, 1998.

[9] US Patent, 5151246

[10] F. Baumgartner, I. Duarte, J. Banhart, "Industrialization of powder compact foaming process", Advanced Eng. Mater., 2, 2000, 168-174.

[11] C. Yu, H. Eifert, J. Banhart, J. Baumeister, "Metal foaming by a metallurgy method: production, properties and applications", Journal of Materials Research Innovations, 2 (3) 1998.

[12] "Metal foams near commercialization", Metal Powder Report, April, (1997) 38- 41.

[13] J. Banhart, "Manufacturing routes for metallic foams", JOM, 52 (12) (2000), 22- 27

[14] V. Gergely and B. Clyne, “The Formgrip process: foaming of reinforced metals by gas release in precursors”, Adv. Eng. Mater., 2, 2000 No:4 175-178.

[15] K. Kitazono, E. Sato, K. Kuribayashi, “Novel manufacturing process of closed cell aluminum foam by accumulative roll-bonding”, Scrpt. Mater., 50 ,2004, 495-498.

[16] Y.P. Kathuria, “ Laser assisted aluminum foaming”, Surface and coatings Technology, 142- 144, 2001, 56-60.

[17] L. J. Gibson, M. F. Ashby, “*Cellular Solids: structures and properties, second edition*”, Cambridge University Press, 1997.

[18] M. Avalle, G. Belingardi, R. Montanini, “Characterization of polymeric foam under compressive impact loading by means of energy-absorption diagram”, International Journal of Impact Engineering, 25, 2001, 455-472.

[19] S. K. Maiti, L. J. Gibson, M. F. Ashby, “Deformation and energy absorption diagram for cellular solids”, Acta Metall. , Vol. 32, 11, 1984, 1963-1975.

[20] A. A. A. Alghamdi, “Collapsible impact energy absorbers : an overview”, Thin-Walled structures, 39, 2001, 189-213.

[21] I. W. Hall, O. Ebil, M. Guden, C. J. YU, “Quasi-static and dynamic crushing of empty and foam filled tubes”, Journal of Materials Science, 36, 2001, 5853-5860.

[22] A. A. Singace, “Collapse behavior of plastic tubes filled with wood sawdust”, Thin-Walled Structures, 37, 2000, 163-187.

[23] W. Abramowicz, T. Wierzbicki, “Axial crushing of foam-filled columns”, Journal of Mechanical Science, 30 (3/4), 1988, 263.

[24] A. K. Toksoy, M. Guden, I. W. Hall, “Axial compression of aluminum closed-cell foam filled and empty aluminum tubes”, Automotive Technologies Congress – Bursa, 24-26 June 202, Conference Proceeding, 383-386.

[25] TY. Reddy, STS. Al Hassani, “Axial crushing of wood-filled square metal tubes”, International Journal of Mechanical Science, 35 (3/4), 1993, 231-246.

[26] TY. Reddy, RJ. Wall, “Axial compression of foam filled thin-walled circular tubes”, International Journal of Impact Engineering, 7 (2), 1988,151-166.

[27] J. M. Alexander, “An approximate analysis of the collapse of thin cylindrical shells under axial loading”, Quarterly Journal of Mechanics and Applied Mathematics, 13, 1960, 10-15.

[28] K. R. F. Andrews, G. L. England, E. Ghani, “Classification of the axial collapse of cylindrical tubes under quasi-static loading”, International Journal of Mechanical Science, 25, 1983, No. 9-10, 687-696.

[29]W. Abramowicz, N. Jones, “Dynamic axial crushing of circular tubes”, International Journal of Impact Engineering, 2, 1984, 263-81.

[30] W. Abramowicz, N. Jones, “Dynamic progressive buckling of circular and square tubes”, International Journal of Impact Engineering, 4, 1986, 243-269.

[31] N. Jones, W. Abramowicz, “ Static and dynamic axial crushing of circular and square tubes”, In : Reid SR, editor. Metal Forming and Impact Mechanics. New york: Pergamon Press, 1985, 225-47.

[32] T. Wierzbicki, S.U. Bhat, W. Abramowicz, D. Brodkin, “A two folding elements model of progressive crushing of tubes”, International Journal of Solids and Structures, 29, 1992, 3269-3288.

[33] A.A. Singace, H. Elbosky, “ Further experimental investigation on the eccentricity factor in the progressive crushing of tubes”, International Journal of Solid Structures, 33, 1996, No. 24, 3517-3538.

[34] A.A. Singace, H. Elbosky, “On the eccentricity factor in the progressive crushing of tubes”, International Journal of Solid Structures, 32, 1995, 3589-3602.

[35] A.A. Singace, “Axial crushing analysis of the tubes deforming in the multi-lobe mode”, International Journal of Mechanical Science, 41, 1999, 868-890.

[36] AG. Pugsley., M. Macaulay, “The large scale crumpling of thin cylindrical columns”, Quarterly Journal of Mechanics and Applied Mathematics, 13, 1960, 1, 1-9.

[37] F.C. Bardi, H. D. Yun, S. Kyriakides, “On the axisymmetric progressive crushing of circular tubes under axial compression”, International Journal of Solid Structures, 40, 2003, in press.

[38] H. Abbas, B. L. Tyagi, M. Arif, N. K. Grupta, “Curved fold model analysis for axi-symmetric axial crushing of tubes”, Thin-Walled Structures, 2003, in press.

[39] N. K. Grupta, H. Abbas, “Some considerations in axisymmetric folding of metallic round tubes”, International Journal of Impact Engineering, 25, 2001, 331-344.

[40] T.Wierzbicki , W.Abramowicz , “Axial crushing of multi corner sheet metal columns”, Journal of Applied Mechanics, 50, 1983, 727-734.

[41] T.Wierzbicki , W.Abramowicz , “On the crushing mechanics of thin-walled structures”, Journal of Applied Mechanics, 56, 1989, 113-120.

[42] PH. Thornton, “Energy absorptions by foam filled structures”, SAE paper 800372, 1980.

[43] B.H. Lampinen, R.A. Jeryan., “Effectiveness of polyurethane foam in energy absorbing structures”, SAE paper 820494, 1982.

[44] S.R. Reid, T.Y. Reddy, M.D. Gray, “Static and dynamic axial crushing of foam filled sheet metal tubes”, Int. J. Mech. Sci. 1986; 23:295-322.

[45] S.R. Guillow, G. Lu, R.H. Grezbieta, “Quasi-static compression of thin-walled circular aluminum tubes”, Int. J. Mech. Sci. 2001; 43:2103-23.

[46] M. Seitzberger, F.G. Rammerstorfer, R. Gradinger, H.P. Degischer, M. Blaimschein, C. Walch,“ Experimental studies on the quasi-static axial crushing of steel columns filled with aluminum foam.” Int .J. Solids Struct. 2000; 37:4125-47.

[47] S. Santosa, T. Wierzbicki, “Crash behavior of box columns filled with aluminum honeycomb or foam”, Comput. Stuct. 1998; 68:343-67.

[48] S. Sanatoza, T. Wierzbicki, A. G. Hanssen, M. Langseth, “Experimental and numerical studies of foam-filled sections”, International Journal of Impact Engineering, 24, 2000, 509-534.

[49] A. G. Hanssen, M. Langseth, O.S. Hopperstad, “Static crushing of square aluminum extrusions with aluminum foam filler”, International Journal of Mechanical Science, 41, 1999, No. 8, 967-993.

[50] A. G. Hanssen, M. Langseth, O.S. Hopperstad, “Static and dynamic crushing of square aluminum extrusions with aluminum foam filler”, Int. Journal of Impact Engineering, 24, 2000, 347-383.

[51] A.K.Toksoy, ”Quasi-static compression behavior of empty and polystyrene foam filled aluminum tubes”, Master Thesis, Izmir Institute of Technology, 2003.

[52] S. Elbir, ”Preparation and characterization of aluminum composite closed cell foams”, Master Thesis, Izmir Institute of Technology, 2001.

[53] H.Kavi, S.Yüksel, M.Tanoğlu, M.Güden, Crushing behavior of aluminum foam filled aluminum tubes”, 10th Denizli Material Symposium & Exhibition, 14-16 April 2004, Conference Proceeding, 42-49.

[54] A.G. Hannsen, M.Langseth, O.S. Hopperstad, “Crush behaviour of foam based components: validation of numerical simulations”, Advanced Engineering Materials, 4, 2002, 771-776.

[55] S.R. Guillow, G. Lu, R. H. Grebieta, “Quasi-static axial compression of thin-walled circular aluminum tubes”, International Journal of Mechanical Sciences, 43, 2001, 2103-2123.

[56] S. Santosa, T. Wierzbicki, A. G. Hannsen, M. Langseth, “Crash behavior of box columns filled with aluminum honeycomb or foam”, Computers and Structures, 68, 1998, 347-367.

[57] A. K. Toksoy, M. Tanoğlu, M. Guden, I. W. Hall, “The effect of adhesive on the strengthening of aluminum foam-filled circular tube.”, International Journal of Material Science Letters, accepted.